Jansen, E., Raymo, M.E., Blum, P., et al., 1996
Proceedings of the Ocean Drilling Program, Initial Reports, Vol. 162

3. SITES 980/981[1]

Shipboard Scientific Party[2]

HOLE 980A

Position: 55°29.087′N, 14°42.134′W

Start hole: 0845 hr, 10 July 1995

End hole: 0145 hr, 11 July 1995

Time on hole: 17.00 hr (0.71 days)

Seafloor (drill pipe measurement from rig floor, mbrf): 2182.1

Total depth (drill pipe measurement from rig floor, mbrf): 2296.0

Distance between rig floor and sea level (m): 10.9

Water depth (drill pipe measurement from sea level, m): 2171.2

Penetration (mbsf): 113.9

Coring totals:
Type: APC
Number: 12
Cored: 113.9 m
Recovered: 117.62 m, 103.3%

Formation:
Unit I: 0–113.9 mbsf; Holocene to early Pleistocene; alternating nannofossil ooze and dark gray clay with nannofossils

HOLE 980B

Position: 55°29.094′N, 14°42.137′W

Start hole: 0145 hr, 11 July 1995

End hole: 1300 hr, 11 July 1995

Time on hole: 11.25 hr (0.47 days)

Seafloor (drill pipe measurement from rig floor, mbrf): 2179.3

Total depth (from rig floor, mbrf): 2297.5

Distance between rig floor and sea level (m): 10.9

Water depth (drill pipe measurement from sea level, m): 2168.4

Penetration (mbsf): 118.2

Coring totals:
Type: APC
Number: 13
Cored: 118.2 m
Recovered: 122.48 m, 103.6%

Formation:
Unit I: 0–118.2 mbsf; Holocene to early Pleistocene; alternating nannofossil ooze and dark gray clay with nannofossils

[1] Jansen, E., Raymo, M.E., Blum, P., et al., 1996. *Proc. ODP, Init. Repts.,* 162: College Station, TX (Ocean Drilling Program).

[2] Shipboard Scientific Party is given in the list preceding the Table of Contents.

HOLE 980C

Position: 55°29.103′N, 14°42.128′W

Start hole: 1300 hr, 11 July 1995

End hole: 2200 hr, 11 July 1995

Time on hole: 9.00 hr (0.38 days)

Seafloor (drill pipe measurement from rig floor, mbrf): 2178.9

Total depth (drill pipe measurement from rig floor, mbrf): 2300.5

Distance between rig floor and sea level (m): 10.9

Water depth (drill pipe measurement from sea level, m): 2168.0

Penetration (mbsf): 121.6

Coring totals:
Type: APC
Number: 14
Cored: 121.6 m
Recovered: 126.61 m, 104.1%

Formation:
Unit I: 0–121.6 mbsf; Holocene to early Pleistocene; alternating nannofossil ooze and dark gray clay with nannofossils

HOLE 981A

Position: 55°28.631′N, 14°39.052′W

Start hole: 2200 hr, 11 July 1995

End hole: 0700 hr, 13 July 1995

Time on hole: 33 hr (1.38 days)

Seafloor (drill pipe measurement from rig floor, mbrf): 2184.0

Total depth (drill pipe measurement from rig floor, mbrf): 2504.0

Distance between rig floor and sea level (m): 10.9

Water depth (drill pipe measurement from sea level, m): 2173.1

Penetration (mbsf): 320.0

Coring totals:
Type: APC
Number: 34
Cored: 320.0 m
Recovered: 327.51 m, 102.3%

Formation:
Unit I: 0–160.0 mbsf; Holocene to late Pliocene; alternating nannofossil ooze and clay with nannofossils
Unit II: 160.0–320.0 mbsf; late to early Pliocene; homogenous nannofossil ooze color changes

HOLE 981B

Position: 55°28.642′N, 14°39.049′W

Start hole: 0700 hr, 13 July 1995

End hole: 2300 hr, 13 July 1995

Time on hole: 16.0 hr (0.67 days)

Seafloor (drill pipe measurement from rig floor, mbrf): 2184.1

Total depth (drill pipe measurement from rig floor, mbrf): 2405.0

Distance between rig floor and sea level (m): 11.0

Water depth (drill pipe measurement from sea level, m): 2173.1

Penetration (mbsf): 220.9

Coring totals:
Type: APC
Number: 24
Cored: 220.8 m
Recovered: 227.29 m, 102.9%

Formation:
Unit I: 0–160.0 mbsf; Holocene to late Pliocene; alternating nannofossil ooze and clay with nannofossils
Unit II: 160.0–220.9 mbsf; late to early Pliocene; homogenous nannofossil ooze

HOLE 981C

Position: 55°28.646′N, 14°39.045′W

Start hole: 2300 hr, 13 July 1995

End hole: 0315 hr, 15 July 1995

Time on hole: 28.25 hr (1.18 days)

Seafloor (drill pipe measurement from rig floor, mbrf): 2182.8

Total depth (drill pipe measurement from rig floor, mbrf): 2464.0

Distance between rig floor and sea level (m): 11.0

Water depth (drill pipe measurement from sea level, m): 2171.8

Penetration (meters below seafloor, mbsf): 281.2

Coring totals:
Type: APC
Number: 30
Cored: 281.2 m
Recovered: 293.81 m, 104.5%

Formation:
Unit I: 0–160.0 mbsf; Holocene to late Pliocene; alternating nannofossil ooze and clay with nannofossils
Unit II: 160.0–281.2 mbsf; late to early Pliocene; homogenous nannofossil ooze

Principal results: Sites 980 and 981 are located on the Feni Drift in the northeast Atlantic Ocean, southeast of the Rockall Bank (Fig. 1). The drift is deposited along the northwestern flank of Rockall Trough under the influence of geostrophic currents formed by Norwegian Sea overflow waters flowing across the Iceland-Scotland Ridge as well as deeper waters originating from the south (including Antarctic Bottom Water). The excess deposition of fines on the drift produces expanded sedimentary sections ideally suited for high-resolution paleoceanographic studies. The scientific objective of these sites was to recover expanded sections with sedimentation rates of more than 10 cm/k.y. over the Pliocene-Pleistocene for studies of climate variability and ocean circulation on both Milankovitch and millennial time scales. This will provide information on the emergence of climate instability, linkages between rapid climate change, ocean circulation, and glaciation, and the possible coupling of Milankovitch cyclicity and sub-Milankovitch climate change.

A 6-hr predrilling site survey revealed an area where the upper Pleistocene section was expanded, which was targeted as Site 980, and a second area, where the lower Pliocene sequence was expanded, targeted as Site 981. Since these two sites represent an offset-drilling strategy to obtain the objectives of one "scientific site," they have been combined into one site chapter. Site 981 is approximately 2 nmi southeast of Site 980.

The two sites were thus chosen to enable recovery of sections with maximum sedimentation rates over the whole interval of interest (the Pliocene-Pleistocene). Three APC holes were drilled at each site to ensure recovery of complete (continuous) sections and to recover sufficient sediment for high-resolution studies. Target depths were 110 m and 220 m at Site 980 (FENI-1) and Site 981 (FENI-2), respectively, and were reached or exceeded in all holes. In Hole 981A we recovered early Pliocene sediments by penetrating to a maximum depth of 320 mbsf. All holes had greater than 100% recovery.

The recovered sections consist of rapidly accumulated nannofossil ooze with variable amounts of clays and clayey nannofossil mixed sediments. The main component of lithologic variability occurs on decimeter to meter scales through the section in the form of cyclic changes in color that are mainly related to relative changes in the proportions of biogenic carbonate, detrital clay, and silt. The upper unit (Unit I), partly recovered at Site 980 from 0 to 114 mbsf and at Site 981 from 0 to 160 mbsf, covers the late Pliocene to Holocene and is characterized by alternating dark and light gray clays and oozes. The lower unit (Unit II), 160 to 320 mbsf at Site 981, covers the early to late Pliocene and consists of a more homogenous nannofossil ooze with subtle color changes. Carbonate content is higher and less variable than in Unit I (80%–90% vs. 20%–80%). Going downsection, the boundary between the two units is characterized by a sharp decrease in magnetic susceptibility and natural gamma radiation, and a sharp increase in carbonate content and spectral reflectance.

All core recovered was run through the multisensor track (MST). Correlation of natural gamma radiation, gamma-ray attenuation, and magnetic susceptibility records confirms that we have recovered a complete stratigraphic sequence at Site 980, and down to 250 mcd (about 230 mbsf), or approximately 3.4 Ma, at Site 981. The MST records are easily correlated between the two sites as well as between holes. Below 230 mbsf, small coring gaps may exist; the low amplitude of the MST signals prevents unambiguous correlation between holes in the lowest section of this site.

Age control is from paleomagnetic datums down to the Matuyama/Gauss boundary (where the magnetic signal deteriorates) and from nannofossil and foraminifer biostratigraphy throughout. Site 980 extends to about 1.2 Ma while Site 981 extends beyond 5 Ma. At Site 980, estimated sedimentation rates (in the composite section) are ~135 m/m.y. in the Brunhes, dropping to about 70 m/m.y. in the Matuyama section. Based on color variations, it would appear that interglacial sedimentation rates are significantly higher than glacial rates. At Site 981, sedimentation rates average ~55 m/m.y. in the Pleistocene and ~70 m/m.y. in the Pliocene, although there may be an interval as high as 100 m/m.y. between ~2.4 and 3.0 Ma.

The highest resolution shipboard analyses are from the MST and spectral reflectance data. At Site 980, Heinrich layers from the last glacial interval are clearly identified in spectral reflectance and magnetic susceptibility data. In all intervals, these two proxies correlate extremely well with each other as well as with shipboard measurements of carbonate percentage. On longer time scales, the onset of major Northern Hemisphere glaciation (and ice-rafted-debris input) and the transition from 41-k.y. climate variability to 100-k.y. variability are obvious in these records. As the amplitude of the MST signals (including susceptibility) decreases significantly below 2.5 Ma, we looked to the spectral reflectance record for any evidence of sub-Milankovitch scale lithologic variability in the preglacial Pliocene. Given the 8-cm (or approximately 1000-yr) resolution of the measurements, there appears to be a precessional signal (1–2-m cycle) and a 5–10-k.y. cycle (~50-cm cycle) within this interval. Detailed shore-based sampling is obviously needed.

The extremely high sedimentation rates and strong magnetic signal at Site 980 will permit high-resolution studies of paleomagnetic transitions, as well as secular variation in the intensity of the magnetic field. Likewise,

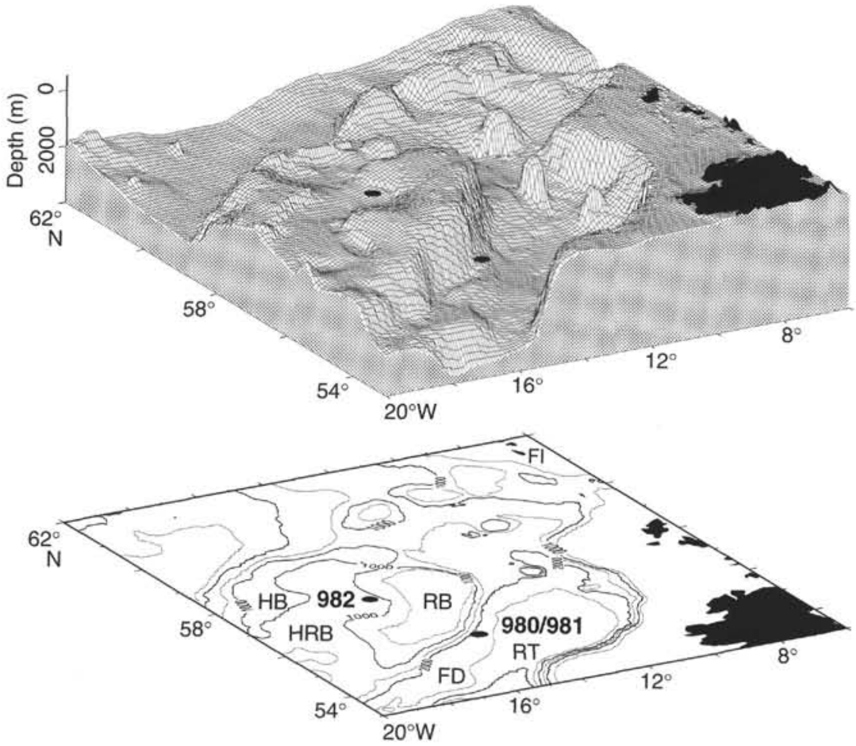

Figure 1. View of the Rockall Trough and the Rockall Plateau showing location of Sites 980, 981, and 982. Flow from northeast is over the Wyville-Thompson Ridge. Land in southeast corner is Ireland. Physiographic features: RB = Rockall Bank, FD = Feni Drift, RT = Rockall Trough, FI = Faeroe Islands, HRB = Hattan-Rockall Basin, HB = Hattan Bank.

these two sites, ~4 km apart, provide a natural laboratory for investigating the effects of sedimentation rate on pore-water chemistry and organic matter preservation. In particular, sulfate reduction appears to be more prevalent in the upper sections of Site 980 vs. 981, with Site 980 having approximately 25% higher accumulation rates. Detailed pore-water sampling for major ion and stable isotopic studies has been carried out. Organic matter is predominantly marine in origin with occasional terrestrial input associated with major glacial cycles.

Major seismic reflectors and the character of three seismic units correlate with the shift from preglacial to glacial mode near the Matuyama/Gauss boundary and with the shift from 41-k.y. cycles to 100-k.y. cycles in the middle Pleistocene.

Lastly, nine successful downhole temperature measurements with the APC temperature tool yielded a linear temperature gradient of 5.1°C/100 m between 70 and 186 mbsf. However, our objective to resolve the geothermal response to Holocene changes in bottom-water temperature could not be met due to the extremely soft nature of the sediment above 70 mbsf (which allowed movement of the tool, causing frictional heat disturbances). An estimated heat flow for the lower section of 0.059 W/m^2 was determined using an average thermal conductivity of 1.15 W/(m·K).

BACKGROUND AND OBJECTIVES

The primary drilling objective at Sites 980 (FENI-1) and 981 (FENI-2) was to recover high-sedimentation-rate pelagic sequences with which to study climate evolution in the North Atlantic region over the last few million years. Recent work in this region has shown that continuous, high-accumulation-rate cores could be recovered from sediment drifts (Bond et al., 1992, 1993; van Weering and de Rijk, 1991; Bond and Lotti, 1995). In fact, the recovery of nearby piston core NA87-22, which had sedimentation rates greater than 10 cm/k.y. (van Weering and de Rijk, 1991), inspired the choice of this drilling target. However, given that sediment drifts are relatively dynamic depositional environments, we were by no means assured that the continuous sedimentation observed in a piston core would continue down a 300-m hole. It was thus with great pleasure that we documented apparently continuous, high-sedimentation-rate sequences extending back to the early Pliocene.

Our scientific objectives for this site are to document ocean-atmosphere climate variability on a range of time scales. Investigations of the late Quaternary in other high-sedimentation-rate cores have demonstrated that rapid century- to millennial-scale oscillations, such as those observed in temperature and dust content in Greenland ice cores (Dansgaard-Oeschger events), also exist in the marine record (e.g., Bond et al., 1993; Bond and Lotti, 1995; Fronval et al., 1995). They can be seen as changes in surface foraminiferal fauna (sea-surface temperature), carbonate content, color, and deep-ocean chemistry. The transitions between cold and warm epochs in ice cores are abrupt: ~6°C warmings occur in as little as 50 years and four-fold drops in dust content in as little as 20 years. Broecker (1994) reviews possible causes for these oscillations and the linkages between deep-sea sedimentation and ice-core records. One possibility is that millennial-scale climate variations in ice cores are related to the strength of the thermohaline "conveyor belt."

Sites 980 and 981 will be used to address a number of questions relating to these "sub-Milankovitch" cycles. In particular, we expect to determine whether these rapid climate oscillations characterized the marine record during earlier, warmer climatic regimes of the past 3 m.y. We will look for variations in color, foraminiferal faunal composition, and lithic concentration. Many of the continuous records of physical properties collected on the ship (e.g., MST and spectral reflectance data) will be used for this purpose, and an early research priority will be to determine how these signals relate to lithologic variations in the sediment (e.g., Robinson and McCave, 1994).

Superimposed on the "Dansgaard-Oeschger" events of the last glacial period are "Heinrich" layers, events with longer characteristic repeat times (~10,000 yr), which may be related to surges of the eastern Laurentian and other major ice sheets (Heinrich, 1988; Bond et al., 1993; MacAyeal, 1993; Broecker, 1994; Fronval et al., 1995). Determining the geographic distribution of these Heinrich events, their long-term character, and the timing of their first occurrence is a main objective of our drilling on the Feni, Gardar, and Bjorn Drifts. Are they restricted to the "100-k.y. world" of the Brunhes Chron, which was characterized by the largest continental ice sheets? Do they occur in warmer intervals characterized by higher frequency variations in smaller ice sheets, or even prior to major Northern Hemisphere glaciation? Do Heinrich events always have a characteristic repeat time of 10,000 years? Sites 980 and 981 are located just north of the zonal axis of the Heinrich layers documented for the last glacial cycle.

By studying deep-water variability using carbon isotopes, Cd/Ca ratios, and other proxies, we will also be able to determine whether millennial-scale variations in surface temperature are associated with variations in thermohaline circulation (Boyle and Keigwin, 1987; Rahmstorf, 1994; Weaver and Hughes, 1994; Oppo and Lehman, 1995). Combining data from Sites 980 and 981 with shallower sites to the northwest (Sites 982, 983, and 984), we will examine if, and how, changes in the vertical nutrient distribution in the North Atlantic occur. In particular, we will examine the behavior of Upper North Atlantic Deep Water (UNADW) relative to production of the denser components of NADW within the different climate regimes of the last 5 m.y. By studying sedimentation patterns, surface-water properties, and deep-water variability on suborbital time scales and relating these observations to ice cores, we hope to better understand the forcing and dynamics of decadal to millennial climate variability in the North Atlantic–Arctic region.

In addition to documenting the character of millennial-scale variability, a major objective is to study how the climate system operates on Milankovitch time scales. It is likely that the sensitivity of the Earth's climate to orbital forcing has increased during the late Cenozoic, with particularly high sensitivity in the last million years. Obtaining climate records from these sensitive latitudes is critical for elucidating how, why, and when enhanced sensitivity evolved and for improving our understanding of the mechanisms by which orbital insolation variations have forced Cenozoic climatic change (e.g., Imbrie et al., 1992, 1993; Saltzman and Verbitsky, 1994). In particular, how has North Atlantic thermohaline circulation evolved over the Pliocene-Pleistocene and what is the role of thermohaline circulation in controlling the exchange of carbon dioxide between the ocean and atmosphere? We will reconstruct water-mass behavior in the North Atlantic on glacial-interglacial time scales of the Pliocene-Pleistocene with special emphasis on the formation of Glacial North Atlantic Intermediate Water (GNAIW) and the links to surface-water conditions (e.g., Raymo et al., 1990; Oppo and Lehman, 1993; McCave et al., 1995).

Sites 980 and 981, at 2157 m water depth, are located downstream of the Wyville-Thomson Ridge, where overflow waters contribute one of the three main components forming modern NADW (the other two being Labrador Sea Water and Denmark Strait Overflow Water) (Fig. 1). At times when NADW is weak, this region may be influenced by the typically deeper Southern Source Water (SSW) and/or by glacial nutrient-depleted intermediate waters (GNAIW) forming at shallower depths (Oppo and Lehman, 1993; Manighetti and McCave, 1995). Along with the other sites drilled north and south of the Greenland-Scotland sill, we hope to unravel the long-term history of deep- and intermediate-water formation in the Nordic Seas and subpolar North Atlantic. Such changes are implicated as a key driving force in conceptual models of atmospheric CO_2 variations and global climate change (Imbrie et al., 1992, 1993; Saltzman and Verbitsky, 1994); however, until now, the lack of high-quality records from high northern latitudes has precluded comprehensive evaluation of these hypotheses.

OPERATIONS

The operational plan for Sites 980 and 981 (FENI-1 and FENI-2) called for three APC holes at each site to approximately 110 and 225 mbsf, respectively.

The vessel left Leith the evening of 7 July 1995. At midnight on 9 July the ship slowed down to 6.0 kt. The seismic gear was deployed and tested for 1.5 hr, and approximately 6 hr were spent surveying the first two drilling Sites 980 and 981 (FENI-1 and FENI-2) near the crest of the Feni sediment drift (see "Seismic Stratigraphy" section, this chapter). Based on the survey results, we located Site 980 (FENI-1) about 1.0 nmi south of the originally proposed site to better target an expanded upper seismic sequence (Pleistocene). Site 981 (FENI-2) was located about 0.8 nmi northeast of the original site in the Leg 162 Prospectus and targeted an expanded lower seismic section (Pliocene). After the site survey was completed, the ship returned to Site 980 and dropped the beacon at 0846 hr on 10 July.

A standard APC/XCB bottom-hole assembly was used for all holes at Sites 980/981, including a nonmagnetic drill collar. At both sites, subsequent (B and C) holes were offset 15 m to the north. The mudline was established for each hole. The APC firing depth was offset by a few meters for subsequent holes to establish continuous sediment sections. Position, depths, and coring totals for each hole are summarized at the top of this chapter. All cores are listed in Table 1.

Coring at Site 980 proceeded smoothly, with only one minor incident. The first APC shot at Hole 980B from 2179 mbrf, 3 m higher than for Hole 980A, recovered a full core, which was discarded. The pipe was raised to 2174 mbrf or a full 8 m higher than where Hole 980A was spudded from, and recovered 4.17 m of core. Target depth was reached in each hole. Core orientation was conducted using the Tensor tool on Cores 980B-3H through 13H, and on Cores 980C-4H through 14H. Operations at Site 980 were terminated when the beacon was recovered at 2300 hr on 11 July.

Site 981 (FENI-2) is approximately 2 nmi southeast of Site 980, so the vessel was maneuvered in dynamic-positioning mode to the global positioning system (GPS) coordinates defined by the site survey. This took about 2.4 hr. The drill string was pulled to a depth of 2059.1 m, or approximately 120 m above the seafloor, during this transit. At 0120 hr, on 12 July, the positioning beacon was dropped. Coring proceeded without incident with two minor exceptions. An incomplete stroke occurred on Core 981A-32H, and the oil-saver unseated when rigging the APC barrel for Core 981A-34H, at which point the sinker bars were laid out and operations were switched to the forward coring line. Coring was suspended in Hole 981A when a maximum overpull of 50,000 lb was experienced on Core 981A-34H. Scientific target depth was reached in all holes.

Core orientation was conducted using the Tensor tool on Cores 981A-3H through 34H and Cores 981C-4H through 14H. In addition, 15 temperature measurements were made using the Adara tool. Eleven consecutive temperature measurements were made on Cores 981C-4H through 14H, and additional measurements were made on Cores 981C-16H, 18H, 20H, and 22H (see "Physical Properties" section, this chapter). Core 981C-22H required washover of 5.0 m and an overpull of 100,000 lb prior to retrieval. Temperature measurements were suspended at that point.

Occupation of Site 981 ended when the vessel was secured for transit and got underway at 0315 hr on 15 July 1995.

COMPOSITE DEPTHS

Based on correlations between magnetic susceptibility, natural gamma radiation (NGR), gamma-ray attenuation porosity (GRAPE), and spectral reflectance data, continuity of the sedimentary sequence was documented for the upper 122 mbsf of the three holes drilled at Site 980, extending from the late Pliocene through the Holocene. Continuity of the sedimentary sequence was also documented for the upper 220 mbsf at Site 981, extending from the middle Pliocene. A composite section was developed, as described in the "Composite Depths" section of the "Explanatory Notes" chapter (this volume). The depth offsets that comprise the composite depth section for Sites 980 and 981 are given in Tables 2 and 3, respectively. The base of the Site 980 composite section is approximately 133 mcd (122 mbsf in

Table 1. Coring summary for Sites 980 and 981.

Core	Date (July 1995)	Time (UTC)	Depth (mbsf)	Length cored (m)	Length recovered (m)	Recovery (%)
162-980A-						
1H	10	1725	0.0–9.4	9.4	9.39	99.9
2H	10	1755	9.4–18.9	9.5	9.58	101.0
3H	10	1835	18.9–28.4	9.5	9.74	102.0
4H	10	1915	28.4–37.9	9.5	9.83	103.0
5H	10	1950	37.9–47.4	9.5	9.79	103.0
6H	10	2025	47.4–56.9	9.5	9.82	103.0
7H	10	2105	56.9–66.4	9.5	9.97	105.0
8H	10	2145	66.4–75.9	9.5	9.84	103.0
9H	10	2230	75.9–85.4	9.5	9.84	103.0
10H	10	2305	85.4–94.9	9.5	9.90	104.0
11H	10	2340	94.9–104.4	9.5	9.88	104.0
12H	11	0025	104.4–113.9	9.5	10.04	105.7
			Coring totals:	113.9	117.60	103.3
162-980B-						
1H	11	0340	0.0–4.2	4.2	4.17	99.3
2H	11	0420	4.2–13.7	9.5	9.62	101.0
3H	11	0505	13.7–23.2	9.5	9.77	102.0
4H	11	0545	23.2–32.7	9.5	9.86	103.0
5H	11	0625	32.7–42.2	9.5	9.98	105.0
6H	11	0715	42.2–51.7	9.5	9.87	104.0
7H	11	0755	51.7–61.2	9.5	9.86	104.0
8H	11	0835	61.2–70.7	9.5	9.88	104.0
9H	11	0920	70.7–80.2	9.5	9.81	103.0
10H	11	1010	80.2–89.7	9.5	9.95	105.0
11H	11	1100	89.7–99.2	9.5	9.99	105.0
12H	11	1140	99.2–108.7	9.5	9.85	103.0
13H	11	1215	108.7–118.2	9.5	9.87	104.0
			Coring totals:	118.2	122.50	103.6
162-980C-						
1H	11	1345	0.0–2.6	2.6	2.61	100.0
2H	11	1410	2.6–12.1	9.5	9.87	104.0
3H	11	1440	12.1–21.6	9.5	9.81	103.0
4H	11	1520	21.6–31.1	9.5	9.98	105.0
5H	11	1555	31.1–40.6	9.5	9.79	103.0
6H	11	1630	40.6–50.1	9.5	9.93	104.0
7H	11	1705	50.1–55.1	5.0	5.89	118.0
8H	11	1740	55.1–64.6	9.5	9.90	104.0
9H	11	1850	64.6–74.1	9.5	9.87	103.0
10H	11	1850	74.1–83.6	9.5	9.78	103.0
11H	11	1925	83.6–93.1	9.5	9.79	103.0
12H	11	2000	93.1–102.6	9.5	9.77	103.0
13H	11	2035	102.6–112.1	9.5	9.82	103.0
14H	11	2110	112.1–121.6	9.5	9.80	103.0
			Coring totals:	121.6	126.60	104.1
162-981A-						
1H	12	0345	0.0–6.5	6.5	6.48	99.7
2H	12	0425	6.5–16.0	9.5	9.77	103.0
3H	12	0510	16.0–25.5	9.5	9.77	103.0
4H	12	0550	25.5–35.0	9.5	9.89	104.0
5H	12	0625	35.0–44.5	9.5	9.62	101.0
6H	12	0725	44.5–54.0	9.5	9.91	104.0
7H	12	0800	54.0–63.5	9.5	9.84	103.0
8H	12	0850	63.5–73.0	9.5	9.96	105.0
9H	12	0935	73.0–82.5	9.5	9.96	105.0
10H	12	1015	82.5–92.0	9.5	6.75	71.0
11H	12	1055	92.0–101.5	9.5	9.70	102.0
12H	12	1140	101.5–111.0	9.5	10.00	105.2
13H	12	1220	111.0–120.5	9.5	9.85	103.0
14H	12	1255	120.5–130.0	9.5	10.01	105.3
15H	12	1330	130.0–139.5	9.5	9.83	103.0
16H	12	1415	139.5–149.0	9.5	9.95	105.0
17H	12	1455	149.0–158.5	9.5	9.84	103.0
18H	12	1530	158.5–168.0	9.5	9.95	105.0
19H	12	1605	168.0–177.5	9.5	9.89	104.0
20H	12	1645	177.5–187.0	9.5	9.82	103.0
21H	12	1720	187.0–196.5	9.5	9.74	102.0
22H	12	1805	196.5–206.5	10.0	9.83	103.0
23H	12	1850	206.0–215.5	9.5	9.66	101.0
24H	12	1930	215.5–225.0	9.5	9.64	101.0
25H	12	2010	225.0–234.5	9.5	9.83	103.0
26H	12	2050	234.5–244.0	9.5	9.72	102.0
27H	12	2125	244.0–253.5	9.5	9.83	103.0
28H	12	2205	253.5–263.0	9.5	9.65	101.0
29H	12	2245	263.0–272.5	9.5	9.84	103.0
30H	12	2325	272.5–282.0	9.5	9.84	103.0
31H	12	0010	282.0–291.5	9.5	9.87	104.0
32H	13	0110	291.5–301.0	9.5	9.77	103.0
33H	13	0220	301.0–310.5	9.5	9.69	102.0
34H	13	0440	310.5–320.0	9.5	9.81	103.0
			Coring totals:	320.5	327.51	102.2
162-981B-						
1H	13	0840	0.0–2.4	2.4	2.35	97.9
2H	13	0925	2.4–11.9	9.5	9.63	101.0
3H	13	1015	11.9–21.4	9.5	9.77	102.0
4H	13	1140	21.4–30.9	9.5	9.94	104.0
5H	13	1210	30.9–40.4	9.5	9.74	102.0
6H	13	1240	40.4–49.9	9.5	9.80	103.0
7H	13	1310	49.9–59.4	9.5	9.84	103.0
8H	13	1335	59.4–68.9	9.5	9.91	104.0
9H	13	1405	68.9–78.4	9.5	9.69	102.0
10H	13	1435	78.4–87.9	9.5	9.83	103.0
11H	13	1505	87.9–97.4	9.5	9.72	102.0
12H	13	1535	97.4–106.9	9.5	9.77	103.0
13H	13	1605	106.9–116.4	9.5	9.83	103.0
14H	13	1640	116.4–125.9	9.5	10.05	105.8
15H	13	1715	125.9–135.4	9.5	9.85	103.0
16H	13	1745	135.4–144.9	9.5	9.74	102.0
17H	13	1815	144.9–154.4	9.5	9.74	102.0
18H	13	1850	154.4–163.9	9.5	9.87	104.0
19H	13	1920	163.9–173.4	9.5	9.73	102.0
20H	13	1955	173.4–182.9	9.5	9.75	102.0
21H	13	2025	182.9–192.4	9.5	9.53	100.0
22H	13	2050	192.4–201.9	9.5	9.81	103.0
23H	13	2125	201.9–211.4	9.5	9.71	102.0
24H	13	2155	211.4–220.9	9.5	9.69	102.0
			Coring totals:	220.9	227.29	102.9
162-981C-						
1H	14	0000	0.0–5.7	5.7	5.70	100.0
2H	14	0040	5.7–15.2	9.5	9.80	103.0
3H	14	0150	15.2–24.7	9.5	9.88	104.0
4H	14	0255	24.7–34.2	9.5	9.80	103.0
5H	14	0340	34.2–43.7	9.5	10.06	105.9
6H	14	0430	43.7–53.2	9.5	9.91	104.0
7H	14	0515	53.2–62.7	9.5	9.95	105.0
8H	14	0600	62.7–72.2	9.5	10.04	105.7
9H	14	0705	72.2–81.7	9.5	9.71	102.0
10H	14	0825	81.7–91.2	9.5	10.05	105.8
11H	14	0910	91.2–100.7	9.5	10.02	105.5
12H	14	0950	100.7–110.2	9.5	10.04	105.7
13H	14	1035	110.2–119.7	9.5	10.15	106.8
14H	14	1120	119.7–129.2	9.5	10.09	106.2
15H	14	1200	129.2–138.7	9.5	9.95	105.0
16H	14	1300	138.7–148.2	9.5	10.27	108.1
17H	14	1330	148.2–157.7	9.5	9.84	103.0
18H	14	1410	157.7–167.2	9.5	10.25	107.9
19H	14	1440	167.2–176.7	9.5	9.98	105.0
20H	14	1520	176.7–186.2	9.5	9.98	105.0
21H	14	1555	186.2–195.7	9.5	9.86	104.0
22H	14	1700	195.7–205.2	9.5	9.85	103.0
23H	14	1730	205.2–214.7	9.5	9.88	104.0
24H	14	1805	214.7–224.2	9.5	9.88	104.0
25H	14	1835	224.2–233.7	9.5	9.73	102.0
26H	14	1910	233.7–243.2	9.5	9.72	102.0
27H	14	1945	243.2–252.7	9.5	9.98	105.0
28H	14	2015	252.7–262.2	9.5	9.89	104.0
29H	14	2050	262.2–271.7	9.5	9.76	103.0
30H	14	2125	271.7–281.2	9.5	9.79	103.0
			Coring totals:	281.2	293.81	104.5

Hole 980C). At Site 981, continuity of the stratigraphic section was confirmed from the mudline to approximately 235 mcd (215 mbsf in Hole 981A, 214 mbsf in Hole 981B, and 216 mbsf in Hole 981C). Below this depth, successive cores from Holes 981A and 981C were placed at their original (mbsf) depth with the accumulated mcd offset added.

Multisensor track (MST) and reflectance records that were useful in correlation are displayed on the composite depth scales in Figures 2 and 3 (see also back pocket). Magnetic susceptibility and GRAPE measurements were the primary parameters used to determine depth offsets for the composite depth section. *P*-wave velocity and natural gamma radiation measurements were also collected over nearly the

Table 2. Site 980 composite depths.

Core, section	Length (cm)	Depth (mbsf)	Depth (mcd)	Offset (mcd – mbsf)
162-980A-				
1H-1	150	0.00	4.11	4.11
1H-2	150	1.50	5.61	4.11
1H-3	150	3.00	7.11	4.11
1H-4	150	4.50	8.61	4.11
1H-5	150	6.00	10.11	4.11
1H-6	150	7.50	11.61	4.11
1H-7	22	9.00	13.11	4.11
1H-CC	17	9.22	13.33	4.11
2H-1	150	9.40	14.54	5.14
2H-2	150	10.90	16.04	5.14
2H-3	150	12.40	17.54	5.14
2H-4	150	13.90	19.04	5.14
2H-5	150	15.40	20.54	5.14
2H-6	150	16.90	22.04	5.14
2H-7	40	18.40	23.54	5.14
2H-CC	18	18.80	23.94	5.14
3H-1	150	18.90	25.62	6.72
3H-2	150	20.40	27.12	6.72
3H-3	150	21.90	28.62	6.72
3H-4	150	23.40	30.12	6.72
3H-5	150	24.90	31.62	6.72
3H-6	150	26.40	33.12	6.72
3H-7	56	27.90	34.62	6.72
3H-CC	18	28.46	35.18	6.72
4H-1	150	28.40	36.31	7.91
4H-2	150	29.90	37.81	7.91
4H-3	150	31.40	39.31	7.91
4H-4	150	32.90	40.81	7.91
4H-5	150	34.40	42.31	7.91
4H-6	150	35.90	43.81	7.91
4H-7	65	37.40	45.31	7.91
4H-CC	18	38.05	45.96	7.91
5H-1	150	37.90	47.13	9.23
5H-2	150	39.40	48.63	9.23
5H-3	150	40.90	50.13	9.23
5H-4	150	42.40	51.63	9.23
5H-5	150	43.90	53.13	9.23
5H-6	150	45.40	54.63	9.23
5H-7	64	46.90	56.13	9.23
5H-CC	15	47.54	56.77	9.23
6H-1	150	47.40	57.47	10.07
6H-2	150	48.90	58.97	10.07
6H-3	150	50.40	60.47	10.07
6H-4	150	51.90	61.97	10.07
6H-5	150	53.40	63.47	10.07
6H-6	150	54.90	64.97	10.07
6H-7	61	56.40	66.47	10.07
6H-CC	21	57.01	67.08	10.07
7H-1	150	56.90	68.45	11.55
7H-2	150	58.40	69.95	11.55
7H-3	150	59.90	71.45	11.55
7H-4	150	61.40	72.95	11.55
7H-5	150	62.90	74.45	11.55
7H-6	150	64.40	75.95	11.55
7H-7	72	65.90	77.45	11.55
7H-CC	25	66.62	78.17	11.55
8H-1	150	66.40	78.71	12.31
8H-2	150	67.90	80.21	12.31
8H-3	150	69.40	81.71	12.31
8H-4	150	70.90	83.21	12.31
8H-5	150	72.40	84.71	12.31
8H-6	150	73.90	86.21	12.31
8H-7	66	75.40	87.71	12.31
8H-CC	18	76.06	88.37	12.31
9H-1	150	75.90	89.09	13.19
9H-2	150	77.40	90.59	13.19
9H-3	150	78.90	92.09	13.19
9H-4	150	80.40	93.59	13.19
9H-5	150	81.90	95.09	13.19
9H-6	150	83.40	96.59	13.19
9H-7	68	84.90	98.09	13.19
9H-CC	16	85.58	98.77	13.19
10H-1	150	85.40	99.63	14.23
10H-2	150	86.90	101.13	14.23
10H-3	150	88.40	102.63	14.23
10H-4	150	89.90	104.13	14.23
10H-5	150	91.40	105.63	14.23
10H-6	150	92.90	107.13	14.23
10H-7	68	94.40	108.63	14.23
10H-CC	22	95.08	109.31	14.23
11H-1	150	94.90	108.77	13.87
11H-2	150	96.40	110.27	13.87
11H-3	150	97.90	111.77	13.87
11H-4	150	99.40	113.27	13.87
11H-5	150	100.90	114.77	13.87
11H-6	150	102.40	116.27	13.87
11H-7	59	103.90	117.77	13.87
11H-CC	29	104.49	118.36	13.87
12H-1	150	104.40	119.36	14.96
12H-2	150	105.90	120.86	14.96
12H-3	150	107.40	122.36	14.96
12H-4	150	108.90	123.86	14.96
12H-5	150	110.40	125.36	14.96
12H-6	150	111.90	126.86	14.96
12H-7	77	113.40	128.36	14.96
12H-CC	27	114.17	129.13	14.96
162-980B-				
1H-1	150	0.00	0.00	0.00
1H-2	150	1.50	1.50	0.00
1H-3	107	3.00	3.00	0.00
1H-CC	10	4.07	4.07	0.00
2H-1	150	4.20	5.41	1.21
2H-2	150	5.70	6.91	1.21
2H-3	150	7.20	8.41	1.21
2H-4	150	8.70	9.91	1.21
2H-5	150	10.20	11.41	1.21
2H-6	150	11.70	12.91	1.21
2H-7	44	13.20	14.41	1.21
2H-CC	18	13.64	14.85	1.21
3H-1	150	13.70	16.14	2.44
3H-2	150	15.20	17.64	2.44
3H-3	150	16.70	19.14	2.44
3H-4	150	18.20	20.64	2.44
3H-5	150	19.70	22.14	2.44
3H-6	150	21.20	23.64	2.44
3H-7	65	22.70	25.14	2.44
3H-CC	12	23.35	25.79	2.44
4H-1	150	23.20	26.57	3.37
4H-2	150	24.70	28.07	3.37
4H-3	150	26.20	29.57	3.37
4H-4	150	27.70	31.07	3.37
4H-5	150	29.20	32.57	3.37
4H-6	150	30.70	34.07	3.37
4H-7	63	32.20	35.57	3.37
4H-CC	23	32.83	36.20	3.37
5H-1	150	32.70	37.15	4.45
5H-2	150	34.20	38.65	4.45
5H-3	150	35.70	40.15	4.45
5H-4	150	37.20	41.65	4.45
5H-5	150	38.70	43.15	4.45
5H-6	150	40.20	44.65	4.45
5H-7	73	41.70	46.15	4.45
5H-CC	25	42.43	46.88	4.45
6H-1	139	42.20	47.96	5.76
6H-2	150	43.59	49.35	5.76
6H-3	150	45.09	50.85	5.76
6H-4	150	46.59	52.35	5.76
6H-5	150	48.09	53.85	5.76
6H-6	150	49.59	55.35	5.76
6H-7	71	51.09	56.85	5.76
6H-CC	27	51.80	57.56	5.76
7H-1	150	51.70	58.48	6.78
7H-2	150	53.20	59.98	6.78
7H-3	150	54.70	61.48	6.78
7H-4	150	56.20	62.98	6.78
7H-5	150	57.70	64.48	6.78
7H-6	150	59.20	65.98	6.78
7H-7	67	60.70	67.48	6.78
7H-CC	19	61.37	68.15	6.78
8H-1	150	61.20	69.17	7.97
8H-2	150	62.70	70.67	7.97
8H-3	150	64.20	72.17	7.97
8H-4	150	65.70	73.67	7.97
8H-5	150	67.20	75.17	7.97
8H-6	150	68.70	76.67	7.97
8H-7	65	70.20	78.17	7.97
8H-CC	23	70.85	78.82	7.97
9H-1	150	70.70	80.40	9.70
9H-2	150	72.20	81.90	9.70
9H-3	150	73.70	83.40	9.70
9H-4	150	75.20	84.90	9.70
9H-5	150	76.70	86.40	9.70
9H-6	150	78.20	87.90	9.70
9H-7	61	79.70	89.40	9.70
9H-CC	20	80.31	90.01	9.70
10H-1	150	80.20	91.63	11.43
10H-2	150	81.70	93.13	11.43
10H-3	150	83.20	94.63	11.43
10H-4	150	84.70	96.13	11.43
10H-5	150	86.20	97.63	11.43
10H-6	150	87.70	99.13	11.43
10H-7	67	89.20	100.63	11.43
10H-CC	28	89.87	101.30	11.43
11H-1	150	89.70	101.99	12.29
11H-2	150	91.20	103.49	12.29
11H-3	150	92.70	104.99	12.29
11H-4	150	94.20	106.49	12.29
11H-5	150	95.70	107.99	12.29
11H-6	150	97.20	109.49	12.29
11H-7	73	98.70	110.99	12.29
11H-CC	26	99.43	111.72	12.29
12H-1	150	99.20	111.92	12.72
12H-2	150	100.70	113.42	12.72
12H-3	150	102.20	114.92	12.72
12H-4	150	103.70	116.42	12.72
12H-5	150	105.20	117.92	12.72
12H-6	150	106.70	119.42	12.72
12H-7	59	108.20	120.92	12.72
12H-CC	26	108.79	121.51	12.72
13H-1	150	108.70	120.67	11.97
13H-2	150	110.20	122.17	11.97
13H-3	150	111.70	123.67	11.97
13H-4	150	113.20	125.17	11.97
13H-5	150	114.70	126.67	11.97
13H-6	150	116.20	128.17	11.97
13H-7	61	117.70	129.67	11.97
13H-CC	26	118.31	130.28	11.97
162-980C-				
1H-1	150	0.00	0.00	0.00
1H-2	87	1.50	1.50	0.00
1H-CC	24	2.37	2.37	0.00
2H-1	150	2.60	3.57	0.97
2H-2	150	4.10	5.07	0.97
2H-3	150	5.60	6.57	0.97
2H-4	150	7.10	8.07	0.97
2H-5	150	8.60	9.57	0.97
2H-6	150	10.10	11.07	0.97
2H-7	62	11.60	12.57	0.97
2H-CC	25	12.22	13.19	0.97
3H-1	150	12.10	13.89	1.79
3H-2	150	13.60	15.39	1.79
3H-3	150	15.10	16.89	1.79
3H-4	150	16.60	18.39	1.79
3H-5	150	18.10	19.89	1.79
3H-6	150	19.60	21.39	1.79
3H-7	53	21.10	22.89	1.79
3H-CC	28	21.63	23.42	1.79
4H-1	150	21.60	23.76	2.16
4H-2	150	23.10	25.26	2.16
4H-3	150	24.60	26.76	2.16
4H-4	150	26.10	28.26	2.16
4H-5	150	27.60	29.76	2.16
4H-6	150	29.10	31.26	2.16
4H-7	75	30.60	32.76	2.16
4H-CC	23	31.35	33.51	2.16
5H-1	150	31.10	34.22	3.12
5H-2	150	32.60	35.72	3.12
5H-3	150	34.10	37.22	3.12
5H-4	150	35.60	38.72	3.12
5H-5	150	37.10	40.22	3.12
5H-6	150	38.60	41.72	3.12
5H-7	58	40.10	43.22	3.12
5H-CC	21	40.68	43.80	3.12
6H-1	150	40.60	44.38	3.78
6H-2	150	42.10	45.88	3.78
6H-3	150	43.60	47.38	3.78
6H-4	150	45.10	48.88	3.78
6H-5	150	46.60	50.38	3.78
6H-6	150	48.10	51.88	3.78
6H-7	72	49.60	53.38	3.78
6H-CC	21	50.32	54.10	3.78
7H-1	150	50.10	54.11	4.01
7H-2	150	51.60	55.61	4.01
7H-3	150	53.10	57.11	4.01
7H-4	108	54.60	58.61	4.01
7H-CC	31	55.68	59.69	4.01
8H-1	150	55.10	59.57	4.47
8H-2	150	56.60	61.07	4.47
8H-3	150	58.10	62.57	4.47
8H-4	150	59.60	64.07	4.47
8H-5	150	61.10	65.57	4.47
8H-6	150	62.60	67.07	4.47
8H-7	65	64.10	68.57	4.47
8H-CC	25	64.75	69.22	4.47
9H-1	150	64.60	71.10	6.50
9H-2	150	66.10	72.60	6.50
9H-3	150	67.60	74.10	6.50
9H-4	150	69.10	75.60	6.50

Table 2 (continued).

Core, section	Length (cm)	Depth (mbsf)	Depth (mcd)	Offset (mcd – mbsf)
9H-5	150	70.60	77.10	6.50
9H-6	150	72.10	78.60	6.50
9H-7	60	73.60	80.10	6.50
9H-CC	27	74.20	80.70	6.50
10H-1	150	74.10	81.25	7.15
10H-2	150	75.60	82.75	7.15
10H-3	150	77.10	84.25	7.15
10H-4	150	78.60	85.75	7.15
10H-5	150	80.10	87.25	7.15
10H-6	150	81.60	88.75	7.15
10H-7	63	83.10	90.25	7.15
10H-CC	15	83.73	90.88	7.15
11H-1	150	83.60	91.93	8.33
11H-2	150	85.10	93.43	8.33
11H-3	150	86.60	94.93	8.33
11H-4	150	88.10	96.43	8.33
11H-5	150	89.60	97.93	8.33
11H-6	150	91.10	99.43	8.33
11H-7	61	92.60	100.93	8.33
11H-CC	18	93.21	101.54	8.33
12H-1	150	93.10	102.69	9.59
12H-2	150	94.60	104.19	9.59
12H-3	150	96.10	105.69	9.59
12H-4	150	97.60	107.19	9.59
12H-5	150	99.10	108.69	9.59
12H-6	150	100.60	110.19	9.59
12H-7	64	102.10	111.69	9.59
12H-CC	13	102.74	112.33	9.59
13H-1	150	102.60	113.46	10.86
13H-2	150	104.10	114.96	10.86
13H-3	150	105.60	116.46	10.86
13H-4	150	107.10	117.96	10.86
13H-5	150	108.60	119.46	10.86
13H-6	150	110.10	120.96	10.86
13H-7	60	111.60	122.46	10.86
13H-CC	22	112.20	123.06	10.86
14H-1	150	112.10	123.52	11.42
14H-2	150	113.60	125.02	11.42
14H-3	150	115.10	126.52	11.42
14H-4	150	116.60	128.02	11.42
14H-5	150	118.10	129.52	11.42
14H-6	150	119.60	131.02	11.42
14H-7	54	121.10	132.52	11.42
14H-CC	26	121.64	133.06	11.42

Note: Depths are from the top of each section.

entire cored sequence of all holes at both sites. These measurements, combined with percent spectral reflectance measurements (see "Lithostratigraphy" section, this chapter), were useful in confirming the hole-to-hole correlations. Natural gamma radiation variations generally follow a similar pattern to magnetic susceptibility, although NGR variations remained strong below approximately 175 mcd at Site 981, while the magnetic susceptibility signal decreased to nearly zero. Although variations in color reflectance at Sites 980 and 981 were generally inversely correlated to susceptibility, they were not a "mirror image" and thus provided another constraint for hole-to-hole correlations. These records on the Site 980 composite depth scale are shown in Figure 2, and the Site 981 records are shown in Figure 3 (see also back pocket).

At each site, overlap between adjacent holes was documented throughout the composite depth section. Although the relative agreement of sedimentary features in adjacent holes was excellent, stretching and compression of the cored sequence occurred over most intervals. Because much of this distortion occurred on scales of less than 9 m, it was not possible to align every sedimentary feature using only composite depth scale adjustments. Within-core, decimeter to centimeter depth scale adjustments would be required to align all sedimentary features simultaneously.

The expansion of the composite depth section relative to the mbsf depth scale results from physical expansion of the cores after recovery as well as stretching of the sequence during the coring process. This expansion is illustrated in Figures 4 and 5 for Sites 980 and 981, respectively. Growth of the mcd scale relative to the mbsf scale is about 10% or greater in all holes from Sites 980 and 981.

Following construction of the composite depth sections for Sites 980 and 981, single spliced records were assembled from the aligned cores as described in the "Explanatory Notes" chapter. The tie points for the Site 980 splice are given in Table 4. At Site 981, although overlap between adjacent holes and continuity of the sedimentary sequence was confirmed through 235 mcd, the exact alignment of events between holes was obscure below Core 981B-19H at 189 mcd (173 mbsf). Therefore, a spliced record for Site 981 was developed only to this depth. The tie points for the Site 981 splice are given in Table 5. Plots of spliced reflectance, magnetic susceptibility and GRAPE data are shown in Figures 6 and 7.

LITHOSTRATIGRAPHY

The sediments at Sites 980/981 have an average calcium carbonate content of around 54% and are predominantly composed of rapidly accumulated nannofossil oozes with variable amounts of clay, clayey nannofossil mixed sediments, and clays with variable amounts of nannofossils and silt. Minor ubiquitous authigenic components include iron sulfides primarily in the form of disseminated pyrite. The main component of lithologic variability occurs at meter (at Site 980) and decimeter to meter (at Site 981) scales throughout the entire sediment section in the form of distinct cyclic changes in color that are mainly related to relative changes in the proportions of biogenic carbonate, detrital clay minerals, and to a lesser extent, detrital silt.

The primary lithostratigraphic units for the sedimentary sequence at Sites 980/981 are defined on the basis of data obtained from seven sources: (1) visual observation of color, (2) smear slide examination, (3) bulk calcium carbonate measurements, (4) spectral reflectance measurements, (5) magnetic susceptibility measurements, (6) natural gamma-ray measurements, and (7) X-ray diffraction (XRD) analysis. A distinct boundary dividing the section into two units occurs at the 159 mbsf level at Site 981, where rather abrupt and distinct changes in the above data are observed. The boundary is marked by sharp downcore decreases in magnetic susceptibility and natural gamma radiation and sharp downcore increases in calcium carbonate content and spectral reflectance. A more gradual but discernible increase in biogenic silica occurs within an interval that encompasses this sharp lithologic change (Fig. 8). More subtle, but distinct changes in the above data occur at 195 mbsf at Site 981 and are used to divide Unit II into two subunits. Lithostratigraphic Units I and Subunits IIA and IIB are described in detail in the following section.

Description of Lithostratigraphic Units

Unit I

Intervals:
- Cores 162-980A-1H through 12H
- Cores 162-980B-1H through 13H
- Cores 162-980C-1H through 14H
- Core 162-981A-1H through Section 18H-1, 50 cm
- Core 162-981B-1H through Section 18H-4, 10 cm
- Core 162-981C-1H through Section 18H-1, 130 cm

Age: Holocene to late Pliocene
Depth: 0 to 159 mbsf

Unit I sediments are dominated by variable amounts of calcareous nannofossils, clay, and, to a lesser extent, silt and foraminifers. Specifically, the unit consists of alternating intervals of three sets of lithofacies: (1) very light gray, light gray, and gray nannofossil oozes, nannofossil oozes with clay, and clayey nannofossil oozes, (2) dark gray to gray clayey nannofossil mixed sediment, and (3) dark gray to dark grayish brown nannofossil clay and clay with nannofossils. XRD and smear slide analyses reveal that quartz, inorganic calcite,

Table 3. Site 981 composite depths.

Core, section	Length (cm)	Depth (mbsf)	Depth (mcd)	Offset (mcd – mbsf)
162-981A-				
1H-1	150	0.00	1.07	1.07
1H-2	150	1.50	2.57	1.07
1H-3	150	3.00	4.07	1.07
1H-4	150	4.50	5.57	1.07
1H-5	28	6.00	7.07	1.07
1H-CC	20	6.28	7.35	1.07
2H-1	150	6.50	7.69	1.19
2H-2	150	8.00	9.19	1.19
2H-3	150	9.50	10.69	1.19
2H-4	150	11.00	12.19	1.19
2H-5	150	12.50	13.69	1.19
2H-6	150	14.00	15.19	1.19
2H-7	61	15.50	16.69	1.19
2H-CC	16	16.11	17.30	1.19
3H-1	150	16.00	17.90	1.90
3H-2	150	17.50	19.40	1.90
3H-3	150	19.00	20.90	1.90
3H-4	150	20.50	22.40	1.90
3H-5	150	22.00	23.90	1.90
3H-6	150	23.50	25.40	1.90
3H-7	55	25.00	26.90	1.90
3H-CC	22	25.55	27.45	1.90
4H-1	150	25.50	28.73	3.23
4H-2	150	27.00	30.23	3.23
4H-3	150	28.50	31.73	3.23
4H-4	150	30.00	33.23	3.23
4H-5	150	31.50	34.73	3.23
4H-6	150	33.00	36.23	3.23
4H-7	71	34.50	37.73	3.23
4H-CC	18	35.21	38.44	3.23
5H-1	150	35.00	39.11	4.11
5H-2	150	36.50	40.61	4.11
5H-3	150	38.00	42.11	4.11
5H-4	47	39.50	43.61	4.11
5H-5	150	39.97	44.08	4.11
5H-6	150	41.47	45.58	4.11
5H-7	90	42.97	47.08	4.11
5H-CC	75	43.87	47.98	4.11
6H-1	150	44.50	50.02	5.52
6H-2	150	46.00	51.52	5.52
6H-3	150	47.50	53.02	5.52
6H-4	150	49.00	54.52	5.52
6H-5	150	50.50	56.02	5.52
6H-6	150	52.00	57.52	5.52
6H-7	65	53.50	59.02	5.52
6H-CC	26	54.15	59.67	5.52
7H-1	150	54.00	61.11	7.10
7H-2	150	55.50	62.60	7.10
7H-3	150	57.00	64.10	7.10
7H-4	150	58.50	65.60	7.10
7H-5	150	60.00	67.10	7.10
7H-6	150	61.50	68.60	7.10
7H-7	65	63.00	70.10	7.10
7H-CC	19	63.65	70.75	7.10
8H-1	150	63.50	71.30	7.80
8H-2	150	65.00	72.80	7.80
8H-3	150	66.50	74.30	7.80
8H-4	150	68.00	75.80	7.80
8H-5	150	69.50	77.30	7.80
8H-6	150	71.00	78.80	7.80
8H-7	72	72.50	80.30	7.80
8H-CC	24	73.22	81.02	7.80
9H-1	150	73.00	82.76	9.76
9H-2	150	74.50	84.26	9.76
9H-3	150	76.00	85.76	9.76
9H-4	150	77.50	87.26	9.76
9H-5	150	79.00	88.76	9.76
9H-6	150	80.50	90.26	9.76
9H-7	69	82.00	91.76	9.76
9H-CC	27	82.69	92.45	9.76
10H-1	150	82.50	93.43	10.93
10H-2	150	84.00	94.93	10.93
10H-3	150	85.50	96.43	10.93
10H-4	150	87.00	97.93	10.93
10H-5	46	88.50	99.43	10.93
10H-CC	29	88.96	99.89	10.93
11H-1	150	92.00	103.56	11.56
11H-2	150	93.50	105.06	11.56
11H-3	150	95.00	106.56	11.56
11H-4	150	96.50	108.06	11.56
11H-5	150	98.00	109.56	11.56
11H-6	150	99.50	111.06	11.56
11H-7	48	101.00	112.56	11.56
11H-CC	22	101.48	113.04	11.56
12H-1	150	101.50	113.60	12.10
12H-2	150	103.00	115.10	12.10
12H-3	150	104.50	116.60	12.10
12H-4	150	106.00	118.10	12.10
12H-5	150	107.50	119.60	12.10
12H-6	150	109.00	121.10	12.10
12H-7	73	110.50	122.60	12.10
12H-CC	27	111.23	123.33	12.10
13H-1	150	111.00	124.36	13.36
13H-2	150	112.50	125.86	13.36
13H-3	150	114.00	127.36	13.36
13H-4	150	115.50	128.86	13.36
13H-5	150	117.00	130.36	13.36
13H-6	150	118.50	131.86	13.36
13H-7	68	120.00	133.36	13.36
13H-CC	17	120.68	134.04	13.36
14H-1	150	120.50	134.52	14.02
14H-2	150	122.00	136.02	14.02
14H-3	150	123.50	137.52	14.02
14H-4	150	125.00	139.02	14.02
14H-5	150	126.50	140.52	14.02
14H-6	150	128.00	142.02	14.02
14H-7	73	129.50	143.52	14.02
14H-CC	28	130.23	144.25	14.02
15H-1	150	130.00	144.76	14.76
15H-2	150	131.50	146.26	14.76
15H-3	150	133.00	147.76	14.76
15H-4	150	134.50	149.26	14.76
15H-5	150	136.00	150.76	14.76
15H-6	150	137.50	152.26	14.76
15H-7	62	139.00	153.76	14.76
15H-CC	21	139.62	154.38	14.76
16H-1	150	139.50	154.56	15.06
16H-2	150	141.00	155.06	15.06
16H-3	150	142.50	159.06	15.06
16H-4	150	144.00	159.06	15.06
16H-5	150	145.50	160.56	15.06
16H-6	150	147.00	162.06	15.06
16H-7	72	148.50	163.56	15.06
16H-CC	23	149.22	164.28	15.06
17H-1	150	149.00	163.96	14.96
17H-2	150	150.50	165.46	14.96
17H-3	150	152.00	166.96	14.96
17H-4	150	153.50	168.46	14.96
17H-5	150	155.00	169.96	14.96
17H-6	150	156.50	171.46	14.96
17H-7	60	158.00	172.96	14.96
17H-CC	24	158.60	173.56	14.96
18H-1	150	158.50	174.28	15.78
18H-2	150	160.00	175.78	15.78
18H-3	150	161.50	177.28	15.78
18H-4	150	163.00	178.78	15.78
18H-5	150	164.50	180.28	15.78
18H-6	150	166.00	181.78	15.78
18H-7	64	167.50	183.28	15.78
18H-CC	31	168.14	183.92	15.78
19H-1	150	168.00	184.46	16.46
19H-2	150	169.50	185.96	16.46
19H-3	150	171.00	187.46	16.46
19H-4	150	172.50	188.96	16.46
19H-5	150	174.00	190.46	16.46
19H-6	150	175.50	191.96	16.46
19H-7	61	177.00	193.46	16.46
19H-CC	28	177.61	194.07	16.46
20H-1	150	177.50	194.89	17.39
20H-2	150	179.00	196.39	17.39
20H-3	150	180.50	197.89	17.39
20H-4	150	182.00	199.39	17.39
20H-5	150	183.50	200.89	17.39
20H-6	150	185.00	202.39	17.39
20H-7	64	186.50	203.89	17.39
20H-CC	18	187.14	204.53	17.39
21H-1	150	187.00	204.73	17.73
21H-2	150	188.50	206.23	17.73
21H-3	150	190.00	207.73	17.73
21H-4	150	191.50	209.02	17.73
21H-5	150	193.00	210.73	17.73
21H-6	140	194.50	212.23	17.73
21H-7	64	195.90	213.63	17.73
21H-CC	20	196.54	214.27	17.73
22H-1	150	196.50	215.69	19.19
22H-2	150	198.00	217.19	19.19
22H-3	150	199.50	218.69	19.19
22H-4	150	201.00	220.19	19.19
22H-5	150	202.50	221.69	19.19
22H-6	150	204.00	223.19	19.19
22H-7	66	205.50	224.69	19.19
22H-CC	17	206.16	225.35	19.19
23H-1	150	206.00	226.17	20.17
23H-2	150	207.50	227.67	20.17
23H-3	150	209.00	229.17	20.17
23H-4	150	210.50	230.67	20.17
23H-5	150	212.00	232.18	20.17
23H-6	150	213.50	233.67	20.17
23H-7	54	215.00	235.17	20.17
23H-CC	12	215.54	235.71	20.17
24H-1	150	215.50	235.67	20.17
24H-2	150	217.00	237.17	20.17
24H-3	150	218.50	238.67	20.17
24H-4	150	220.00	240.17	20.17
24H-5	150	221.50	241.67	20.17
24H-6	150	223.00	243.17	20.17
24H-7	53	224.50	244.67	20.17
24H-CC	11	225.03	245.20	20.17
25H-1	150	225.00	245.17	20.17
25H-2	150	226.50	246.67	20.17
25H-3	150	228.00	248.17	20.17
25H-4	150	229.50	249.67	20.17
25H-5	150	231.00	251.17	20.17
25H-6	150	232.50	252.67	20.17
25H-7	73	234.00	254.17	20.17
25H-CC	10	234.73	254.90	20.17
26H-1	150	234.50	254.67	20.17
26H-2	150	236.00	256.17	20.17
26H-3	150	237.50	257.67	20.17
26H-4	150	239.00	259.17	20.17
26H-5	150	240.50	260.67	20.17
26H-6	150	242.00	262.17	20.17
26H-7	54	243.50	263.67	20.17
26H-CC	18	244.04	264.21	20.17
27H-1	150	244.00	262.17	20.17
27H-2	150	245.50	265.67	20.17
27H-3	150	247.00	267.17	20.17
27H-4	150	248.50	268.67	20.17
27H-5	150	250.00	270.17	20.17
27H-6	150	251.50	271.67	20.17
27H-7	57	253.00	273.17	20.17
27H-CC	26	253.57	273.74	20.17
28H-1	150	253.50	273.67	20.17
28H-2	150	255.00	275.17	20.17
28H-3	150	256.50	276.67	20.17
28H-4	150	258.00	278.17	20.17
28H-5	150	259.50	279.67	20.17
28H-6	130	261.00	281.17	20.17
28H-7	74	262.30	282.47	20.17
28H-CC	11	263.04	283.21	20.17
29H-1	150	263.00	283.17	20.17
29H-2	150	264.50	284.67	20.17
29H-3	150	266.00	286.17	20.17
29H-4	150	267.50	287.67	20.17
29H-5	150	269.00	289.17	20.17
29H-6	150	270.50	290.67	20.17
29H-7	62	272.00	292.17	20.17
29H-CC	22	272.62	292.79	20.17
30H-1	150	272.50	292.67	20.17
30H-2	150	274.00	294.17	20.17
30H-3	150	275.50	295.67	20.17
30H-4	150	277.00	297.17	20.17
30H-5	150	278.50	298.67	20.17
30H-6	150	280.00	300.17	20.17
30H-7	70	281.50	301.67	20.17
30H-CC	14	282.20	302.37	20.17
31H-1	150	282.00	302.17	20.17
31H-2	150	283.50	303.67	20.17
31H-3	150	285.00	305.17	20.17
31H-4	150	286.50	306.67	20.17
31H-5	150	288.00	308.17	20.17
31H-6	150	289.50	309.67	20.17
31H-7	64	291.00	311.17	20.17
31H-CC	23	291.64	311.81	20.17
32H-1	150	291.50	311.67	20.17
32H-2	150	293.00	313.17	20.17
32H-3	150	294.50	314.67	20.17
32H-4	150	296.00	316.17	20.17
32H-5	150	297.50	317.67	20.17
32H-6	150	299.00	319.17	20.17
32H-7	60	300.50	320.67	20.17
32H-CC	17	301.10	321.27	20.17
33H-1	150	301.00	321.17	20.17
33H-2	150	302.50	322.67	20.17
33H-3	150	304.00	324.17	20.17
33H-4	150	305.50	325.67	20.17
33H-5	150	307.00	327.17	20.17
33H-6	150	308.50	328.67	20.17
33H-7	54	310.00	330.17	20.17
33H-CC	15	310.54	330.71	20.17
34H-1	150	310.50	330.67	20.17
34H-2	150	312.00	332.17	20.17
34H-3	63	313.50	333.67	20.17
34H-4	150	314.13	334.30	20.17
34H-5	150	315.63	335.80	20.17
34H-6	150	317.13	335.54	20.17

Table 3 (continued).

Core, section	Length (cm)	Depth (mbsf)	Depth (mcd)	Offset (mcd – mbsf)
34H-7	128	318.63	338.80	20.17
34H-CC	40	319.91	340.08	20.17
162-981B-				
1H-1	150	0.00	0.00	0.00
1H-2	63	1.50	1.50	0.00
1H-CC	22	2.13	2.13	0.00
2H-1	150	2.40	4.02	1.62
2H-2	150	3.90	5.52	1.62
2H-3	150	5.40	7.02	1.62
2H-4	150	6.90	8.52	1.62
2H-5	150	8.40	10.02	1.62
2H-6	150	9.90	11.52	1.62
2H-7	43	11.40	13.02	1.62
2H-CC	20	11.83	13.45	1.62
3H-1	150	11.90	14.68	2.78
3H-2	150	13.40	16.18	2.78
3H-3	150	14.90	17.68	2.78
3H-4	150	16.40	19.18	2.78
3H-5	150	17.90	20.68	2.78
3H-6	150	19.40	22.18	2.78
3H-7	58	20.90	23.68	2.78
3H-CC	19	21.48	24.26	2.78
4H-1	150	21.40	26.18	4.78
4H-2	150	22.90	27.68	4.78
4H-3	150	24.40	29.18	4.78
4H-4	150	25.90	30.68	4.78
4H-5	150	27.40	32.18	4.78
4H-6	150	28.90	33.68	4.78
4H-7	67	30.40	35.18	4.78
4H-CC	27	31.07	35.85	4.78
5H-1	150	30.90	37.16	6.26
5H-2	150	32.40	38.66	6.26
5H-3	150	33.90	40.16	6.26
5H-4	150	35.40	41.66	6.26
5H-5	150	36.90	43.16	6.26
5H-6	150	38.40	44.66	6.26
5H-7	58	39.90	46.16	6.26
5H-CC	16	40.48	46.74	6.26
6H-1	150	40.40	47.16	6.76
6H-2	150	41.90	48.66	6.76
6H-3	150	43.40	50.16	6.76
6H-4	150	44.90	51.66	6.76
6H-5	150	46.40	53.16	6.76
6H-6	150	47.90	54.66	6.76
6H-7	61	49.40	56.16	6.76
6H-CC	19	50.01	56.77	6.76
7H-1	150	49.90	57.34	7.44
7H-2	150	51.40	58.84	7.44
7H-3	150	52.90	60.34	7.44
7H-4	150	54.40	61.84	7.44
7H-5	150	55.90	63.34	7.44
7H-6	150	57.40	64.84	7.44
7H-7	59	58.90	66.34	7.44
7H-CC	25	59.49	66.93	7.44
8H-1	150	59.40	68.67	9.27
8H-2	150	60.90	70.17	9.27
8H-3	150	62.40	71.67	9.27
8H-4	150	63.90	73.17	9.27
8H-5	150	65.40	74.67	9.27
8H-6	150	66.90	76.17	9.27
8H-7	66	68.40	77.67	9.27
8H-CC	25	69.06	78.33	9.27
9H-1	150	68.90	78.25	9.35
9H-2	150	70.40	79.75	9.35
9H-3	150	71.90	81.25	9.35
9H-4	150	73.40	82.75	9.35
9H-5	150	74.90	84.25	9.35
9H-6	150	76.40	85.75	9.35
9H-7	50	77.90	87.25	9.35
9H-CC	19	78.40	87.75	9.35
10H-1	150	78.40	88.09	9.69
10H-2	150	79.90	89.59	9.69
10H-3	150	81.40	91.09	9.69
10H-4	150	82.90	92.59	9.69
10H-5	150	84.40	94.09	9.69
10H-6	150	85.90	95.59	9.69
10H-7	61	87.40	97.09	9.69
10H-CC	22	88.01	97.70	9.69
11H-1	150	87.90	98.20	10.30
11H-2	150	89.40	99.70	10.30
11H-3	150	90.90	101.20	10.30
11H-4	150	92.40	102.70	10.30
11H-5	150	93.90	104.20	10.30
11H-6	150	95.40	105.70	10.30
11H-7	57	96.90	107.20	10.30
11H-CC	15	97.47	107.77	10.30
12H-1	150	97.40	108.09	10.69
12H-2	150	98.90	109.59	10.69
12H-3	150	100.40	111.09	10.69
12H-4	150	101.90	112.59	10.69
12H-5	150	103.40	114.09	10.69
12H-6	150	104.90	115.59	10.69
12H-7	61	106.40	117.09	10.69
12H-CC	16	107.01	117.70	10.69
13H-1	150	106.90	118.05	11.15
13H-2	150	108.40	119.55	11.15
13H-3	150	109.90	121.05	11.15
13H-4	150	111.40	122.55	11.15
13H-5	150	112.90	124.05	11.15
13H-6	90	114.40	125.55	11.15
13H-7	120	115.30	126.45	11.15
13H-CC	23	116.50	127.65	11.15
14H-1	150	116.40	127.82	11.42
14H-2	150	117.90	129.32	11.42
14H-3	150	119.40	130.82	11.42
14H-4	150	120.90	132.32	11.42
14H-5	150	122.40	133.82	11.42
14H-6	150	123.90	135.32	11.42
14H-7	78	125.40	136.82	11.42
14H-CC	27	126.18	137.60	11.42
15H-1	150	125.90	137.72	11.82
15H-2	150	127.40	139.22	11.82
15H-3	150	128.90	140.72	11.82
15H-4	150	130.40	142.22	11.82
15H-5	150	131.90	143.72	11.82
15H-6	140	133.40	145.22	11.82
15H-7	72	134.80	146.62	11.82
15H-CC	23	135.52	147.34	11.82
16H-1	150	135.40	147.85	12.45
16H-2	150	136.90	149.35	12.45
16H-3	150	138.40	150.85	12.45
16H-4	150	139.90	152.35	12.45
16H-5	150	141.40	153.85	12.45
16H-6	150	142.90	155.35	12.45
16H-7	55	144.40	156.85	12.45
16H-CC	19	144.95	157.40	12.45
17H-1	150	144.90	158.07	13.17
17H-2	150	146.40	159.57	13.17
17H-3	150	147.90	161.07	13.17
17H-4	150	149.40	162.57	13.17
17H-5	150	150.90	164.07	13.17
17H-6	150	152.40	165.57	13.17
17H-7	57	153.90	167.07	13.17
17H-CC	17	154.47	167.64	13.17
18H-1	150	154.40	168.68	14.28
18H-2	150	155.90	170.18	14.28
18H-3	150	157.40	171.68	14.28
18H-4	150	158.90	173.18	14.28
18H-5	150	160.40	174.68	14.28
18H-6	150	161.90	176.18	14.28
18H-7	72	163.40	177.68	14.28
18H-CC	15	164.12	178.40	14.28
19H-1	150	163.90	179.44	15.54
19H-2	150	165.40	180.94	15.54
19H-3	150	166.90	182.44	15.54
19H-4	150	168.40	183.94	15.54
19H-5	150	169.90	185.44	15.54
19H-6	150	171.40	186.94	15.54
19H-7	61	172.90	188.44	15.54
19H-CC	12	173.51	189.05	15.54
20H-1	150	173.40	190.18	16.78
20H-2	150	174.90	191.68	16.78
20H-3	150	176.40	193.18	16.78
20H-4	150	177.90	194.68	16.78
20H-5	150	179.40	196.18	16.78
20H-6	150	180.90	197.68	16.78
20H-7	60	182.40	199.18	16.78
20H-CC	15	183.00	199.78	16.78
21H-1	150	182.90	200.60	17.70
21H-2	150	182.90	200.60	17.70
21H-3	150	182.90	200.60	17.70
21H-4	150	182.90	200.60	17.70
21H-5	150	182.90	200.60	17.70
21H-6	150	182.90	200.60	17.70
21H-7	38	182.90	200.60	17.70
21H-CC	15	182.90	200.60	17.70
22H-1	150	192.40	211.19	18.79
22H-2	150	193.90	212.69	18.79
22H-3	150	195.40	214.19	18.79
22H-4	150	196.90	215.69	18.79
22H-5	150	198.40	217.19	18.79
22H-6	150	199.90	218.69	18.79
22H-7	60	201.40	220.19	18.79
22H-CC	21	202.00	220.79	18.79
23H-1	150	201.90	222.08	20.18
23H-2	150	203.40	223.58	20.18
23H-3	150	204.90	225.08	20.18
23H-4	150	206.40	226.58	20.18
23H-5	150	207.90	228.08	20.18
23H-6	150	209.40	229.58	20.18
23H-7	55	210.90	231.08	20.18
23H-CC	16	211.45	231.63	20.18
24H-1	150	211.40	232.69	21.29
24H-2	150	212.90	234.19	21.29
24H-3	150	214.40	235.69	21.29
24H-4	150	215.90	237.19	21.29
24H-5	150	217.40	238.69	21.29
24H-6	150	218.90	240.19	21.29
24H-7	52	220.40	241.69	21.29
24H-CC	17	220.92	242.21	21.29
162-981C-				
1H-1	150	0.00	0.91	0.91
1H-2	150	1.50	2.41	0.91
1H-3	150	3.00	3.91	0.91
1H-4	103	4.50	5.41	0.91
1H-CC	17	5.53	6.44	0.91
2H-1	150	5.70	7.69	1.99
2H-2	150	7.20	9.19	1.99
2H-3	150	8.70	10.69	1.99
2H-4	150	10.20	12.19	1.99
2H-5	150	11.70	13.69	1.99
2H-6	150	13.20	15.19	1.99
2H-7	62	14.70	16.69	1.99
2H-CC	18	15.32	17.31	1.99
3H-1	150	15.20	18.79	3.59
3H-2	150	16.70	20.29	3.59
3H-3	150	18.20	21.79	3.59
3H-4	150	19.70	23.29	3.59
3H-5	150	21.20	24.79	3.59
3H-6	150	22.70	26.29	3.59
3H-7	68	24.20	27.79	3.59
3H-CC	20	24.88	28.47	3.59
4H-1	150	24.70	28.76	4.06
4H-2	150	26.20	30.26	4.06
4H-3	150	27.70	31.76	4.06
4H-4	150	29.20	33.26	4.06
4H-5	150	30.70	34.76	4.06
4H-6	150	32.20	36.26	4.06
4H-7	69	33.70	37.76	4.06
4H-CC	11	34.39	38.45	4.06
5H-1	150	34.20	38.50	4.30
5H-2	150	35.70	40.00	4.30
5H-3	150	37.20	41.50	4.30
5H-4	150	38.70	43.00	4.30
5H-5	150	40.20	44.50	4.30
5H-6	150	41.70	46.00	4.30
5H-7	78	43.20	47.50	4.30
5H-CC	28	43.98	48.28	4.30
6H-1	150	43.70	48.07	4.37
6H-2	150	45.20	49.57	4.37
6H-3	150	46.70	51.07	4.37
6H-4	150	48.20	52.57	4.37
6H-5	150	49.70	54.07	4.37
6H-6	150	51.20	55.57	4.37
6H-7	72	52.70	57.07	4.37
6H-CC	19	53.42	57.79	4.37
7H-1	150	53.20	58.61	5.41
7H-2	150	54.70	60.11	5.41
7H-3	150	56.20	61.61	5.41
7H-4	150	57.70	63.11	5.41
7H-5	150	59.20	64.61	5.41
7H-6	150	60.70	66.11	5.41
7H-7	70	62.20	67.61	5.41
7H-CC	25	62.90	68.31	5.41
8H-1	150	62.70	68.24	5.54
8H-2	150	64.20	69.74	5.54
8H-3	150	65.70	71.24	5.54
8H-4	150	67.20	72.74	5.54
8H-5	150	68.70	74.24	5.54
8H-6	150	70.20	75.74	5.54
8H-7	66	71.70	77.24	5.54
8H-CC	38	72.36	77.90	5.54
9H-1	150	72.20	78.35	6.15
9H-2	150	73.70	79.85	6.15
9H-3	150	75.20	81.35	6.15
9H-4	150	76.70	82.85	6.15
9H-5	150	78.20	84.35	6.15
9H-6	150	79.70	85.85	6.15
9H-7	56	81.20	87.34	6.15
9H-CC	15	81.76	87.91	6.15
10H-1	150	81.70	88.94	7.24
10H-2	150	83.20	90.44	7.24

Table 3 (continued).

Core, section	Length (cm)	Depth (mbsf)	Depth (mcd)	Offset (mcd – mbsf)
10H-3	150	84.70	91.94	7.24
10H-4	150	86.20	93.44	7.24
10H-5	150	87.70	94.94	7.24
10H-6	150	89.20	96.44	7.24
10H-7	66	90.70	97.94	7.24
10H-CC	39	91.36	98.60	7.24
11H-1	150	91.20	99.40	8.20
11H-2	150	92.70	100.90	8.20
11H-3	150	94.20	102.40	8.20
11H-4	150	95.70	103.90	8.20
11H-5	150	97.20	105.40	8.20
11H-6	150	98.70	106.90	8.20
11H-7	66	100.20	108.40	8.20
11H-CC	36	100.86	109.06	8.20
12H-1	150	100.70	111.00	10.30
12H-2	150	102.20	112.50	10.30
12H-3	150	103.70	114.00	10.30
12H-4	150	105.20	115.50	10.30
12H-5	150	106.70	117.00	10.30
12H-6	150	108.20	118.50	10.30
12H-7	69	109.70	120.00	10.30
12H-CC	35	110.39	120.69	10.30
13H-1	150	110.20	121.24	11.04
13H-2	150	111.70	122.74	11.04
13H-3	150	113.20	124.24	11.04
13H-4	150	114.70	125.74	11.04
13H-5	150	116.20	127.24	11.04
13H-6	150	117.70	128.74	11.04
13H-7	80	119.20	130.24	11.04
13H-CC	35	120.00	131.04	11.04
14H-1	150	119.70	132.14	12.44
14H-2	150	121.20	133.64	12.44
14H-3	150	122.70	135.14	12.44
14H-4	150	124.20	136.64	12.44
14H-5	150	125.70	138.14	12.44
14H-6	150	127.20	139.64	12.44
14H-7	70	128.70	141.44	12.44
14H-CC	39	129.40	141.84	12.44
15H-1	150	129.20	142.61	13.41
15H-2	150	130.70	144.11	13.41
15H-3	150	132.20	145.61	13.41
15H-4	150	133.70	147.11	13.41
15H-5	150	135.20	148.61	13.41
15H-6	150	136.70	150.11	13.41
15H-7	66	138.20	151.61	13.41
15H-CC	29	138.86	152.27	13.41
16H-1	150	138.70	153.59	14.89
16H-2	150	140.20	155.09	14.89
16H-3	150	141.70	156.59	14.89
16H-4	150	143.20	158.09	14.89
16H-5	150	144.70	159.20	14.89
16H-6	150	146.20	161.09	14.89
16H-7	79	147.70	162.69	14.89
16H-CC	48	148.49	163.38	14.89
17H-1	150	148.20	163.54	15.34
17H-2	150	149.70	165.04	15.34
17H-3	150	151.20	166.54	15.34
17H-4	150	152.70	167.04	15.34
17H-5	150	154.20	169.54	15.34
17H-6	150	155.70	171.04	15.34
17H-7	68	157.20	172.54	15.34
17H-CC	16	157.88	173.22	15.34
18H-1	150	157.70	174.10	16.40
18H-2	150	159.20	175.60	16.40
18H-3	150	160.70	177.10	16.40
18H-4	150	162.20	178.60	16.40
18H-5	150	163.70	180.10	16.40
18H-6	150	165.20	181.60	16.40
18H-7	87	166.70	183.10	16.40
18H-CC	38	167.57	183.97	16.40
19H-1	150	167.20	184.37	17.17
19H-2	150	168.70	185.87	17.17
19H-3	150	170.20	187.37	17.17
19H-4	150	171.70	188.87	17.17
19H-5	150	173.20	190.37	17.17
19H-6	150	174.70	191.87	17.17
19H-7	73	176.20	193.37	17.17
19H-CC	25	176.93	194.67	17.74
20H-1	150	176.70	194.44	17.74
20H-2	150	178.20	195.94	17.74
20H-3	150	179.70	197.44	17.74
20H-4	150	181.20	198.94	17.74
20H-5	150	182.70	200.44	17.74
20H-6	150	184.20	201.94	17.74
20H-7	66	185.70	203.44	17.74
20H-CC	32	186.36	204.10	17.74
21H-1	150	186.20	204.05	17.85
21H-2	150	187.70	205.55	17.85
21H-3	150	189.20	207.05	17.85
21H-4	150	190.70	208.55	17.85
21H-5	150	192.20	210.05	17.85
21H-6	100	193.70	211.55	17.85
21H-7	117	194.70	212.55	17.85
21H-CC	19	195.87	213.72	17.85
22H-1	150	195.70	214.58	18.88
22H-2	150	197.20	216.08	18.88
22H-3	150	198.70	217.58	18.88
22H-4	150	200.20	219.08	18.88
22H-5	150	201.70	220.58	18.88
22H-6	150	203.20	222.08	18.88
22H-7	73	204.70	223.58	18.88
22H-CC	12	205.43	224.31	18.88
23H-1	150	205.20	223.56	18.36
23H-2	150	206.70	225.06	18.36
23H-3	150	208.20	226.56	18.36
23H-4	150	209.70	228.06	18.36
23H-5	150	211.20	229.56	18.36
23H-6	150	212.70	231.06	18.36
23H-7	69	214.20	232.56	18.36
23H-CC	19	214.89	233.25	18.36
24H-1	150	214.70	233.96	19.26
24H-2	150	216.20	235.46	19.26
24H-3	150	217.70	239.96	19.26
24H-4	150	219.20	238.46	19.26
24H-5	150	220.70	239.96	19.26
24H-6	150	222.20	241.46	19.26
24H-7	69	223.70	242.96	19.26
24H-CC	19	224.39	243.65	19.26
25H-1	150	224.20	243.46	19.26
25H-2	150	225.70	244.96	19.26
25H-3	150	227.20	246.46	19.26
25H-4	150	228.70	247.96	19.26
25H-5	150	230.20	249.46	19.26
25H-6	150	231.70	250.96	19.26
25H-7	58	233.20	252.46	19.26
25H-CC	15	233.78	253.04	19.26
26H-1	150	233.70	252.96	19.26
26H-2	150	235.20	254.46	19.26
26H-3	150	236.70	255.96	19.26
26H-4	150	238.20	257.46	19.26
26H-5	150	239.70	258.96	19.26
26H-6	150	241.20	260.46	19.26
26H-7	56	242.70	261.96	19.26
26H-CC	16	243.26	262.52	19.26
27H-1	150	243.20	262.46	19.26
27H-2	150	244.70	263.96	19.26
27H-3	150	246.20	265.46	19.26
27H-4	150	247.70	266.96	19.26
27H-5	150	249.20	268.46	19.26
27H-6	150	250.70	269.96	19.26
27H-7	72	252.20	271.46	19.26
27H-CC	26	252.92	272.18	19.26
28H-1	150	252.70	271.96	19.26
28H-2	150	254.20	273.46	19.26
28H-3	150	255.70	274.96	19.26
28H-4	150	257.20	276.46	19.26
28H-5	150	258.70	277.96	19.26
28H-6	150	260.20	279.46	19.26
28H-7	74	261.70	280.96	19.26
28H-CC	15	262.44	281.70	19.26
29H-1	150	262.20	281.46	19.26
29H-2	150	263.70	282.96	19.26
29H-3	150	265.20	284.46	19.26
29H-4	150	266.70	285.96	19.26
29H-5	150	268.20	287.46	19.26
29H-6	150	269.70	288.96	19.26
29H-7	61	271.20	290.46	19.26
29H-CC	15	271.81	291.07	19.26
30H-1	150	271.70	290.96	19.26
30H-2	150	273.20	292.46	19.26
30H-3	150	274.70	293.96	19.26
30H-4	150	276.20	295.46	19.26
30H-5	150	277.70	296.96	19.26
30H-6	150	279.20	298.46	19.26
30H-7	67	280.70	299.96	19.26
30H-CC	12	281.37	300.63	19.26

Note: Depths are from the top of each section.

and feldspar dominate the detrital silt component found in the silty dark gray clay layers.

The mean carbonate content of Unit I is 44.8%. Values fluctuate from 2.3% at 83.88 mbsf (Hole 981A) to 84.5% at 53.77 mbsf (Hole 981A) and are indicative of the considerable color contrast observed between the oozes and clays within the unit, particularly when compared with Unit II (see below). High-amplitude meter-scale variations in the percentage of carbonate persist throughout Unit I.

In all of Unit I, particularly at Site 980 where rates of sedimentation are high (see "Sedimentation Rates" section, this chapter), cyclic dark (low carbonate) to light (high carbonate) color changes occur at meter and decimeter to meter scales, with color boundaries ranging from gradational to sharp and bioturbated (see Fig. 9). These smaller-scale distinct color changes are superimposed upon larger 5- to 10-m-scale changes that are readily observed in plots of the percentage of spectral reflectance (Figs. 8, 10).

All dropstones observed at Sites 980/981 occur in Unit I. In all, 24 dropstones greater than 1 cm in size were identified throughout the unit (see Figs. 8, 10, 11). They generally occur in the dark-colored intervals within the unit, suggesting that these darker sediments accumulated under the influence of ice-rafting. The distribution, texture, and composition of all dropstones greater than 1 cm in size are summarized in Table 6.

In Unit I, near the bottom of Site 980, a series of foraminifer-rich fine sand intervals are found (Fig. 10). These coarser layers are generally less than 10 cm thick. They are found between 93 and 107 mbsf in all three holes and may indicate short periods of winnowing.

Unit II

Intervals:
- Section 162 981A-18H-1, 50 cm, through Core 34H
- Section 162 981B-18H-4, 60 cm, through Core 24H
- Core 162-981C-18H through Section 30H-1, 130 cm

Age: late Pliocene to early Pliocene
Depth: 158 to 321 mbsf

Unit II sediments are dominated by biogenic carbonate with only minor amounts of clay, and, to an even lesser extent, biogenic silica. The mean carbonate content of Unit II, at 80.1%, is considerably higher than that of Unit I. Subunit IIA occupies the upper 35 m of Unit II (160–195 mbsf). It is predominantly composed of greenish

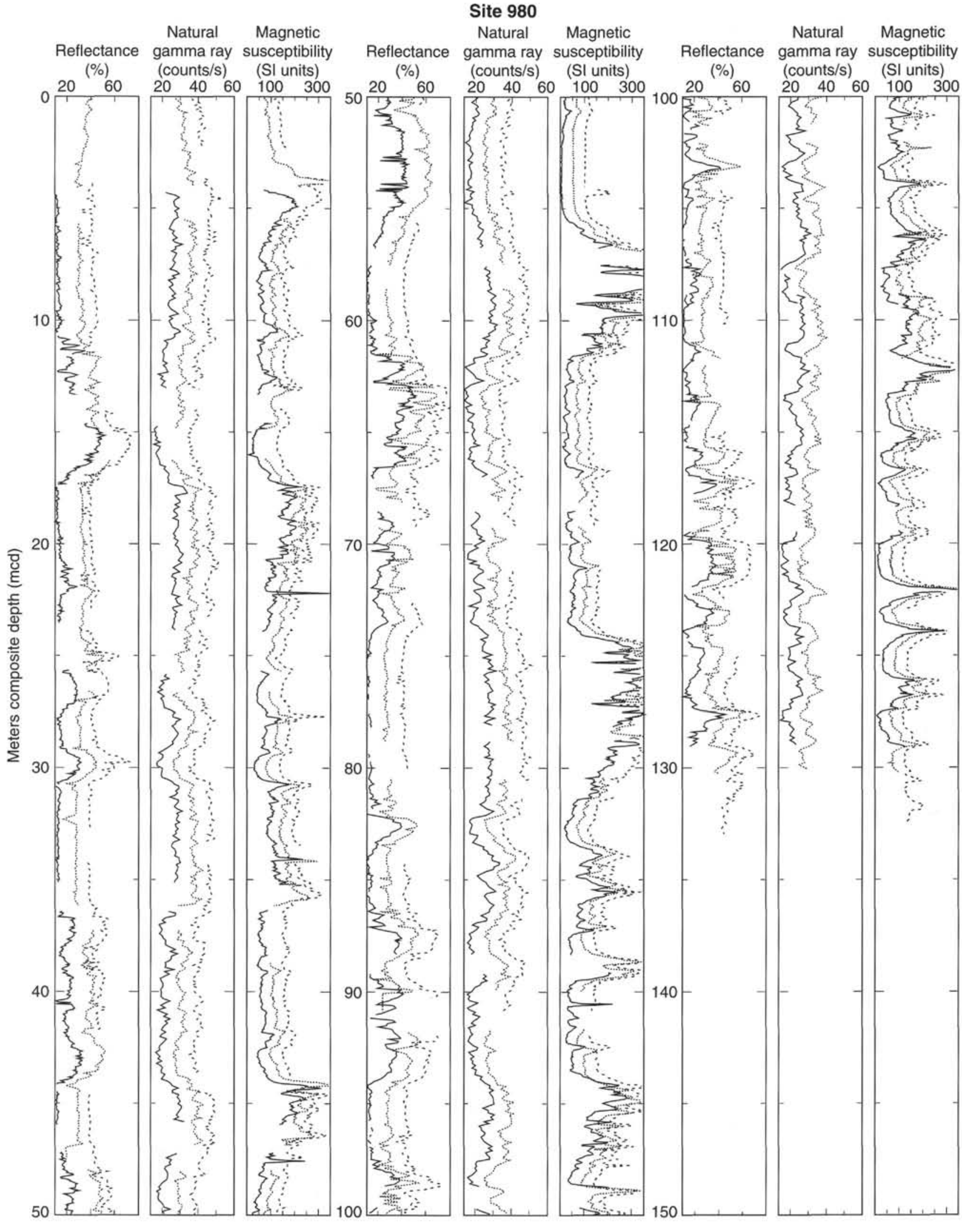

Figure 2. Spectral reflectance (650–700 nm), natural gamma radiation, and magnetic susceptibility data from Site 980 on the mcd (meters composite depth) scale. Lines for Holes 980B (dotted) and 980C (dashed) have been horizontally offset from line for Hole 980A (solid) for better display; therefore, values given on horizontal scale are the true values only for Hole 980A. (See also back pocket.)

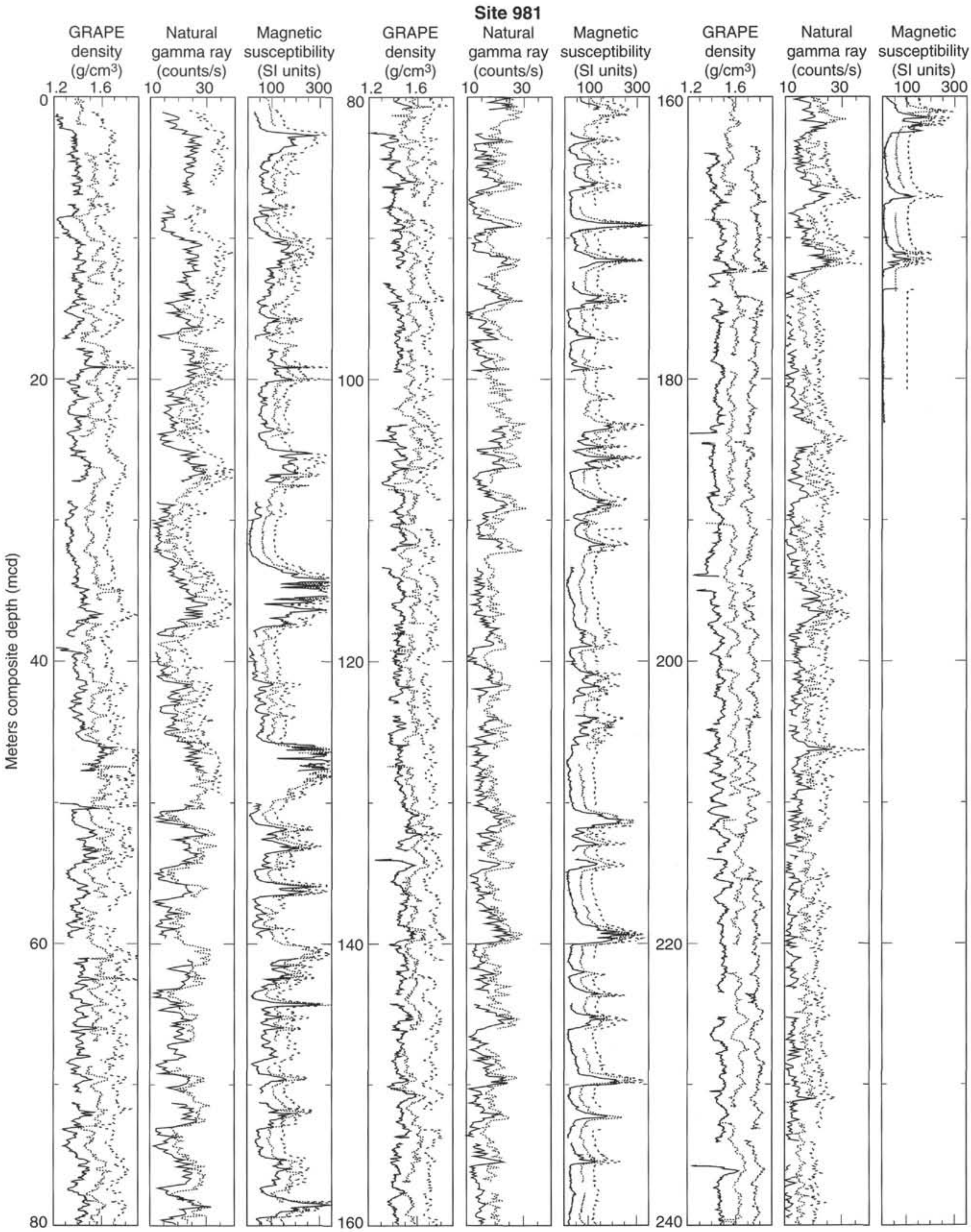

Figure 3. GRAPE density, natural gamma radiation, and magnetic susceptibility data from Site 981 on the mcd (meters composite depth) scale. Lines for Holes 981B (dotted) and 981C (dashed) have been horizontally offset from line for Hole 981A (solid) for better display; therefore, values given on horizontal scale are the true values only for Hole 980A. (See also back pocket.)

Table 4. Site 980 splice tie points.

Hole, core, section (cm)	Depth (mbsf)	Depth (mcd)		Hole, core, section (cm)	Depth (mbsf)	Depth (mcd)
162-980-				162-980-		
B-1H-3, 92	3.92	3.92	tie to	C-2H-1, 35	2.95	3.92
C-2H-5, 65	9.25	10.22	tie to	B-2H-4, 31	9.01	10.22
B-2H-6, 122	12.92	14.13	tie to	C-3H-1, 26	12.36	14.13
C-3H-6, 8	19.68	21.45	tie to	B-3H-4, 80	19.00	21.45
B-3H-6, 88	22.08	24.53	tie to	C-4H-1, 77	22.36	24.53
C-4H-6, 23	29.33	31.49	tie to	B-4H-4, 43	28.13	31.49
B-4H-6, 65	31.35	34.71	tie to	C-5H-1, 49	31.59	34.71
C-5H-5, 85	37.95	41.07	tie to	B-5H-3, 92	36.62	41.07
B-5H-6, 61	40.81	45.26	tie to	C-6H-1, 88	41.48	45.26
C-6H-4, 101	46.10	49.88	tie to	B-6H-2, 53	44.12	49.88
B-6H-7, 22	51.31	57.07	tie to	C-7H-2, 146	53.06	57.07
C-7H-4, 58	55.18	59.19	tie to	B-7H-1, 71	52.41	59.19
B-7H-3, 140	56.10	62.88	tie to	C-8H-3, 32	58.41	62.88
C-8H-7, 32	64.42	68.89	tie to	A-7H-1, 44	57.34	68.89
A-7H-3, 140	61.30	72.85	tie to	C-9H-2, 26	66.35	72.85
C-9H-6, 49	72.59	79.09	tie to	A-8H-1, 38	66.78	79.09
A-8H-4, 115	72.05	84.36	tie to	C-10H-3, 11	77.21	84.36
C-10H-6, 110	82.70	89.85	tie to	A-9H-1, 76	76.66	89.85
A-9H-3, 82	79.72	92.91	tie to	C-11H-1, 98	84.58	92.91
C-11H-6, 82	91.92	100.25	tie to	A-10H-1, 62	86.02	100.25
A-10H-4, 46	90.36	104.59	tie to	C-12H-2, 41	95.00	104.59
C-12H-6, 119	101.78	111.37	tie to	A-11H-2, 110	97.50	111.37
A-11H-5, 128	102.18	116.05	tie to	C-13H-2, 110	105.19	116.05
C-13H-6, 133	111.43	122.29	tie to	A-12H-2, 143	107.33	122.29
A-12H-5, 37	110.77	125.73	tie to	C-14H-2, 71	114.31	125.73
C-14H-6, 143	121.03	132.45				

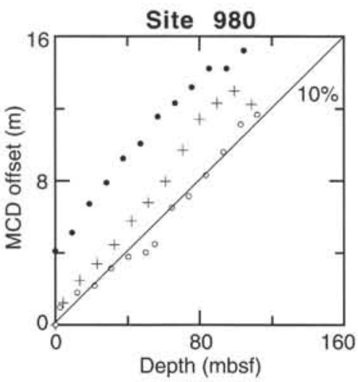

Figure 4. Depth offsets of the Site 980 meters composite depth scale relative to mbsf depth, illustrating the "growth" of the composite depth scale. Solid circles = Hole 980A, crosses = Hole 980B, open circles = Hole 980C.

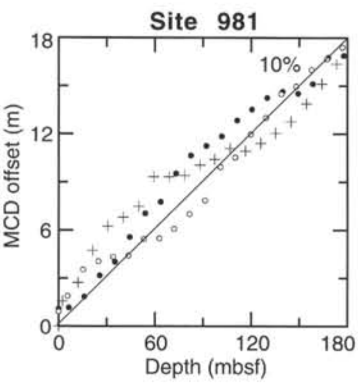

Figure 5. Depth offsets of the Site 981 meters composite depth scale relative to mbsf depth, illustrating the "growth" of the composite depth scale. Solid circles = Hole 981A, crosses = Hole 981B, open circles = Hole 981C.

Table 5. Site 981 splice tie points.

Hole, core, section (cm)	Depth (mbsf)	Depth (mcd)		Hole, core, section (cm)	Depth (mbsf)	Depth (mcd)
162-981-						
B-1H-2, 38	1.88	1.88	tie to	C-1H-1, 97	0.97	1.88
C-1H-4, 8	4.57	5.48	tie to	B-2H-1, 146	3.86	5.48
B-2H-3, 143	6.83	8.45	tie to	C-2H-1, 77	6.46	8.45
C-2H-6, 67	13.87	15.86	tie to	B-3H-1, 118	13.08	15.86
B-3H-4, 62	17.01	19.79	tie to	C-3H-1, 101	16.20	19.79
C-3H-6, 89	23.59	27.18	tie to	B-4H-1, 101	22.40	27.18
B-4H-3, 38	24.77	29.55	tie to	C-4H-1, 79	25.49	29.55
C-4H-7, 14	33.83	37.89	tie to	B-5H-1, 73	31.63	37.89
B-5H-4, 58	35.98	42.24	tie to	C-5H-3, 74	37.94	42.24
C-5H-7, 5	43.24	47.54	tie to	B-6H-1, 38	40.78	47.54
B-6H-6, 146	49.36	56.12	tie to	A-6H-5, 10	50.60	56.12
A-6H-6, 146	53.46	58.98	tie to	C-7H-1, 37	53.57	58.98
C-7H-6, 95	61.65	67.06	tie to	A-7H-4, 146	59.96	67.06
A-7H-6, 5	61.54	68.64	tie to	C-8H-1, 40	63.10	68.64
C-8H-6, 109	71.29	76.83	tie to	A-8H-4, 103	69.03	76.83
A-8H-6, 13	71.13	78.93	tie to	C-9H-1, 58	72.78	78.93
C-9H-6, 82	80.52	86.67	tie to	A-9H-3, 91	76.91	86.67
A-9H-5, 104	80.04	89.80	tie to	C-10H-1, 86	82.56	89.80
C-10H-6, 101	90.20	97.44	tie to	A-10H-3, 101	86.51	97.44
A-10H-5, 18	88.67	99.60	tie to	C-11H-1, 20	91.40	99.60
C-11H-5, 58	97.78	105.98	tie to	A-11H-2, 92	94.42	105.98
A-11H-6, 107	100.57	112.13	tie to	C-12H-1, 113	101.83	112.13
C-12H-6, 70	108.90	119.20	tie to	B-13H-1, 115	108.05	119.20
B-13H-5, 116	114.06	125.21	tie to	A-13H-1, 85	111.85	125.21
A-13H-6, 5	118.55	131.91	tie to	B-14H-3, 109	120.49	131.91
B-14H-5, 116	123.56	134.98	tie to	C-14H-2, 134	122.54	134.98
C-14H-6, 16	127.36	139.80	tie to	B-15H-2, 58	127.98	139.80
B-15H-6, 50	133.89	145.71	tie to	C-15H-3, 11	132.30	145.71
C-15H-6, 8	136.77	150.18	tie to	B-16H-2, 83	137.73	150.18
B-16H-6, 40	143.30	155.75	tie to	C-16H-2, 66	140.86	155.75
C-16H-6, 137	147.57	162.46	tie to	B-17H-3, 139	149.29	162.46
B-17H-6, 32	152.71	165.88	tie to	C-17H-2, 84	150.54	165.88
C-17H-6, 116	156.86	172.20	tie to	B-18H-3, 52	157.92	172.20
B-18H-5, 51	160.91	175.19	tie to	C-18H-1, 109	158.79	175.19
C-18H-6, 51	165.71	182.11	tie to	B-19H-2, 117	166.57	182.11
B-19H-3, 70	170.90	188.07	tie to	A-19H-3, 61	171.61	188.07
A-34H-7, 119	319.82	339.99				

gray nannofossil ooze with clay. Below, Subunit IIB (195–320 mbsf) is composed of light gray and light greenish gray nannofossil ooze. The somewhat higher clay content of Subunit IIB is reflected in its lower mean carbonate content of 66.7% compared to a mean of 83.7% for the lighter colored nannofossil-rich sediments of Subunit IIB, where only one carbonate value falls below 77%. In addition to a distinct difference in calcium carbonate content, Subunit IIA exhibits slightly higher natural gamma-ray counts, a more distinct lower frequency mode of variability in percentage spectral reflectance than does Subunit IIB (see Fig. 8), and a small but distinct component of biogenic silica (diatoms, sponge spicules, and silicoflagellates). Despite its persistent high carbonate content, Unit II also exhibits subtle, cyclic variations in color at scales similar to that found in Unit I at Site 980.

The only evidence of sediment disturbed by natural processes occurs in the lower part of Subunit IIB. Contorted beds in Core 27H in both Holes 981A and 981C lie between beds that dip steeply in opposite directions (Section 981A-27H-2 through 27H-3 and Section 981C-27H-5 through 27H-6; see Site 981 core photographs and Fig. 12). These features, found just above and below 248 mbsf, respectively, are interpreted as slumps. A similar slump structure is found slightly deeper, in Core 981C-30H (Sections 981C-30H-1 through 30H-5), at 272 to 279 mbsf.

Interpretation

The most prominent lithologic feature at Sites 980/981 is the persistent meter-scale, and in some cases, decimeter-scale changes in color that were observed during the visual descriptions of the six holes. While the color hues change at much larger scales, throughout the sequence there are always at least faint, but usually very distinct intervals alternating between darker and lighter color. These changes are precisely recorded by the percentage spectral reflectance data col-

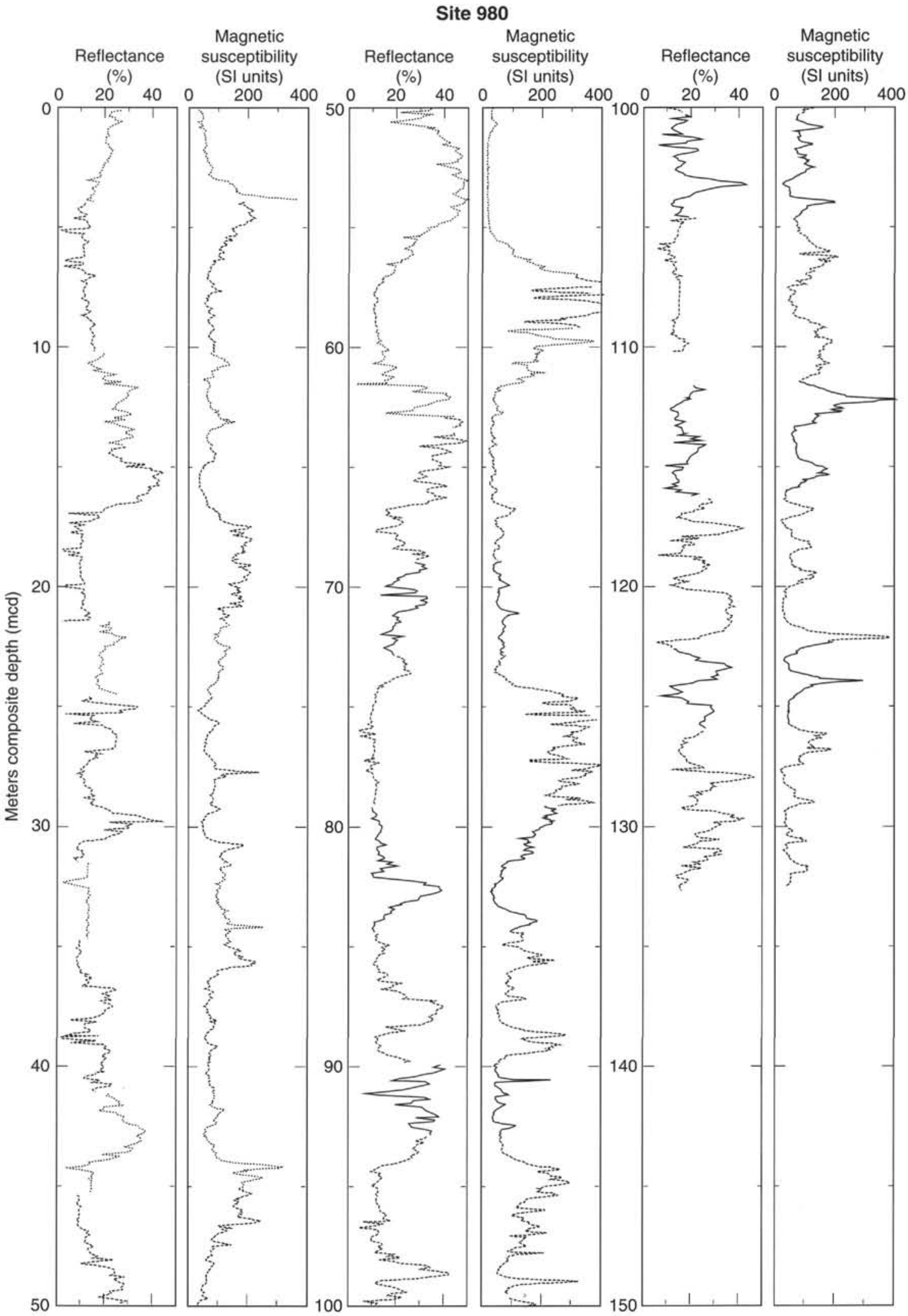

Figure 6. Spliced records of spectral reflectance and magnetic susceptibility data from Site 980. Tie points for forming the splice are given in Table 4. Holes are 980A (solid), 980B (dotted), and 980C (dashed).

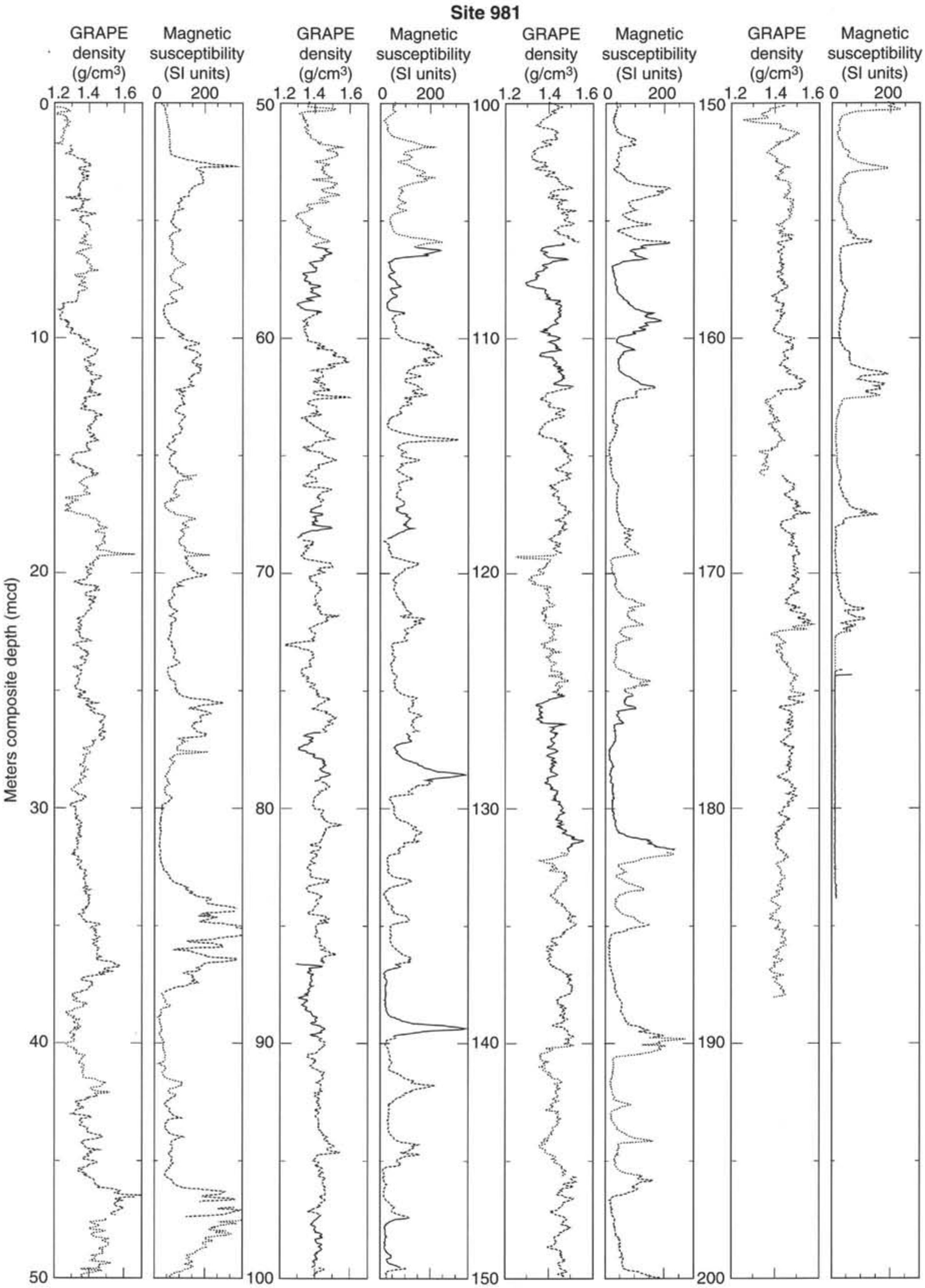

Figure 7. Spliced records of GRAPE density and magnetic susceptibility data from Site 981. Tie points for forming the splice are given in Table 5. Holes are 981A (solid), 981B (dotted), and 981C (dashed).

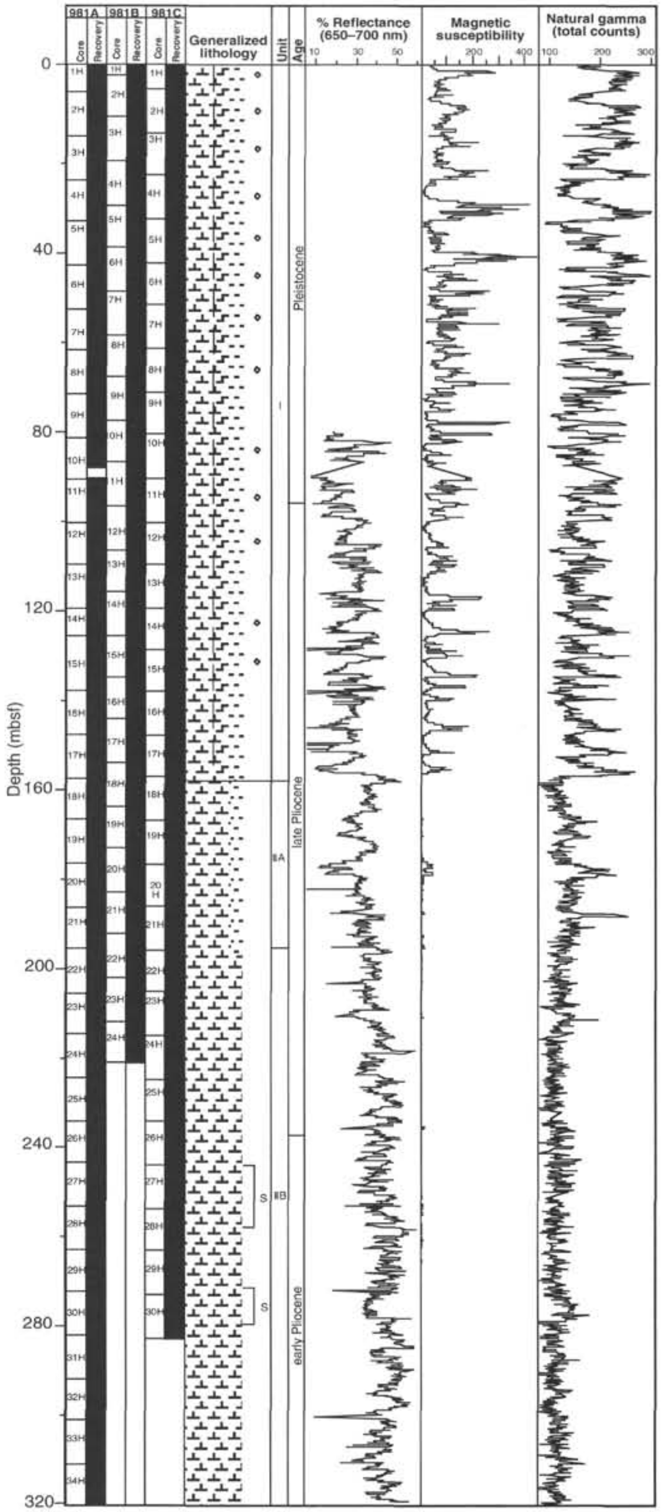

Figure 8. Core recovery, lithostratigraphy, age, percentage reflectance (red band), magnetic susceptibility, and natural gamma radiation of sediments recovered in Holes 981A through 981C. Locations of dropstones (open diamonds) and slumps (S) are shown in the column adjacent to the lithostratigraphy. Percentage reflectance, magnetic susceptibility, and natural gamma radiation records are from Hole 981A. (Key to symbols used in the "Generalized Lithology" column can be found in fig. 4, "Explanatory Notes" chapter, this volume.)

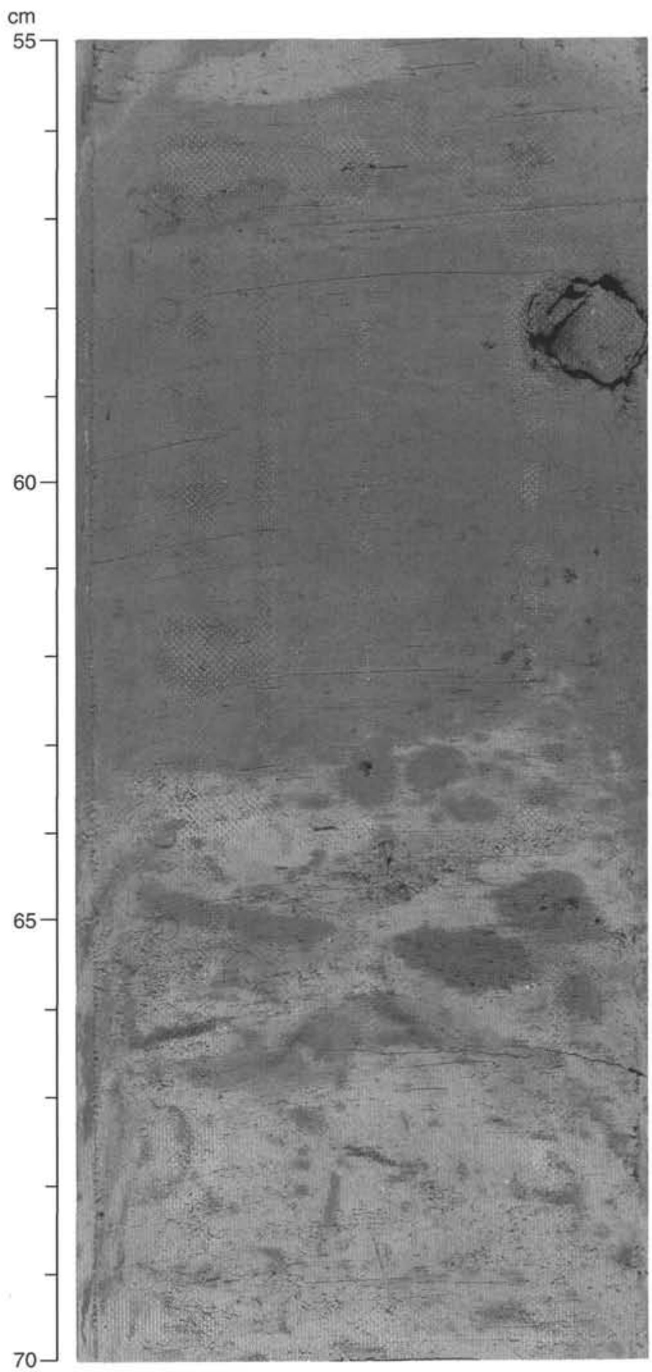

Figure 9. Photograph showing a typical bioturbated color contact in Site 980/981 sediments (Section 162-980A-8H-6, 55–70 cm). Note dropstone 6 cm above bioturbated interval.

lected at 4-cm intervals (0–60 mbsf, Hole 980A) and 8-cm intervals (all other Site 980/981 measurements) throughout the sequence (Fig. 13).

A large component of the percentage reflectance variability seems to be controlled by variations in the calcium carbonate content of the sediment in both Units I and II. The tight curvilinear relationship observed between the percentage carbonate and the percentage reflectance in Figure 14 suggests that reflectance can be used as a first-order proxy for calcium content at Sites 980/981. Slightly more scat-

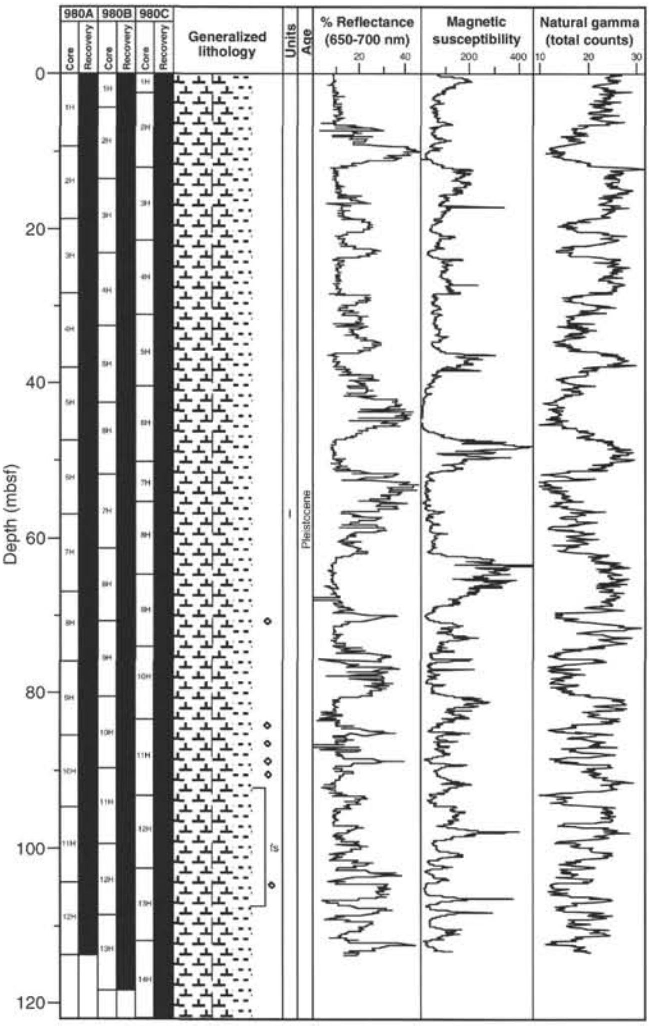

Figure 10. Core recovery, lithostratigraphy, age, percentage reflectance (red band), magnetic susceptibility, and natural gamma radiation of sediments recovered from Holes 980A, 980B, and 980C. Locations of dropstones (open diamonds) and interval containing foraminifer-rich fine sands (bracket labeled "fs") are shown in column adjacent to the lithostratigraphy. Percentage reflectance, magnetic susceptibility, and natural gamma radiation records are from Hole 980A. (Key to symbols used in the "Generalized Lithology" column can be found in fig. 4, "Explanatory Notes" chapter, this volume.)

ter is observed for the lower carbonate "darker" colored intervals of Unit I and is likely related to variations in the composition of the noncarbonate fraction.

The bedding-scale reflectance within the blue band (450–500 nm) oscillates at various amplitudes between 10% and 55% (Fig. 13). When the regularity and scale of these oscillations are considered within the context of estimated sedimentation rates for Sites 980/981 (see "Sedimentation Rates" section, this chapter), it is apparent that these cyclic changes occur well within Milankovitch time scales. Closer examination of the Site 980 record in particular suggests that the reflectance data is recording cyclic variations at even shorter time scales (see Core 980A-5H in Fig. 13). Thus, it seems that lithologic variability at Sites 980/981 occurs cyclically at a number of different depth scales and may record changes at both orbital and suborbital time scales.

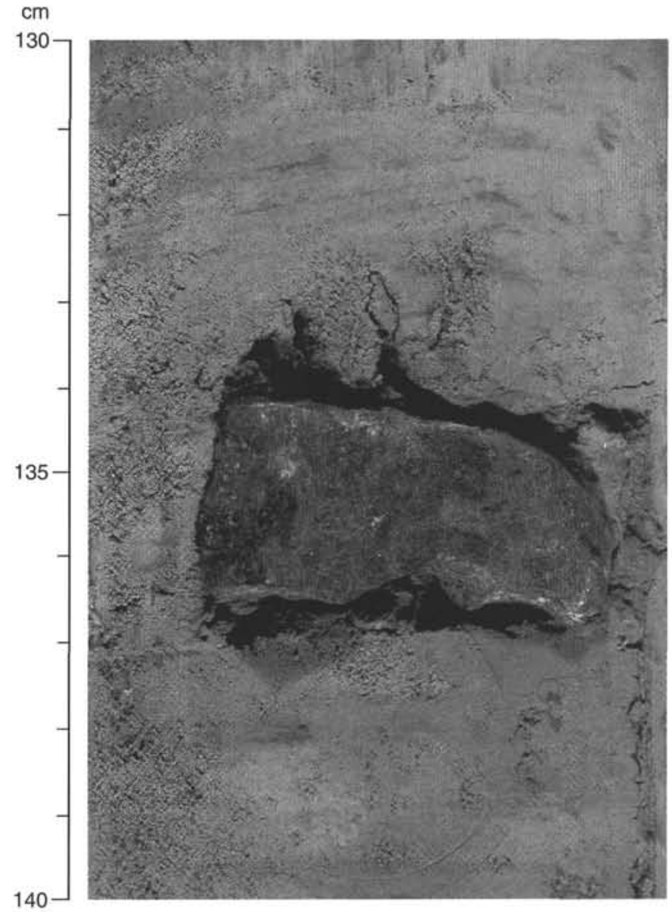

Figure 11. Photograph of a 5-cm angular crystalline dropstone found in Section 162-980C-11H-4, 130–140 cm (89.44–89.46 mbsf).

Table 6. Summary table of dropstones greater than 1 cm in size found in lithostratigraphic Unit I at Sites 980/981.

Core, section, interval top (cm)	Depth (mbsf)	Size (cm)	Composition	Shape
162-980A-				
8H-5, 77	73.17	2.0	Basalt	Subrounded
10H-3, 132	84.52	1.0	Siltstone	Well rounded
10H-5, 127	87.47	2.5	Layered mudstone	Subrounded
12H-5, 17	105.4	1.1	Granitic	Subangular
11H-4, 134	89.44	5.0	Dark, igneous/metamorphic	Angular
11H-5, 29	89.89	1.8	Serpentinite	Subangular
162-981A-				
3H-5, 136	23.36	1.5	Light, igneous/metamorphic	Rounded
4H-4, 125	31.25	1.0	Gray, igneous/metamorphic	Angular
5H-5, 142	41.39	2.2	Black, mudstone	Subrounded
7H-1, 131	55.31	1.0	Black, vesicular basalt	Subangular
8H-2, 3	65.03	1.5	Dark, igneous/metamorphic	
8H-6, 12	71.12	1.0	Reddish, igneous	
11H-1, 18	92.18	1.5	Basalt	Subrounded
14H-4, 111	126.10	2.0	Black, mudstone	Subrounded
162-981B-				
6H-4, 24	45.14	4.0	Gneiss	Subangular
7H-3, 82	53.72	1.5	Sandstone	Subangular
7H-3, 83	53.73	1.1	Dark, igneous/metamorphic	Subrounded
11H-3, 30	91.20	1.0	Black, basalt	Subangular
162-981C-				
1H-3, 94	3.94	1.5	Black, vesicular basalt	Subrounded
2H-4, 10	10.30	2.5	Black, amphibolite	Subangular
4H-5, 97	31.67	2.2	Granite	Subangular
6H-1, 123	44.93	1.0	Coal	Subangular
12H-6, 66	108.90	1.0	Quartz	Subangular
15H-7, 20	138.40	1.5	Igneous	Subangular

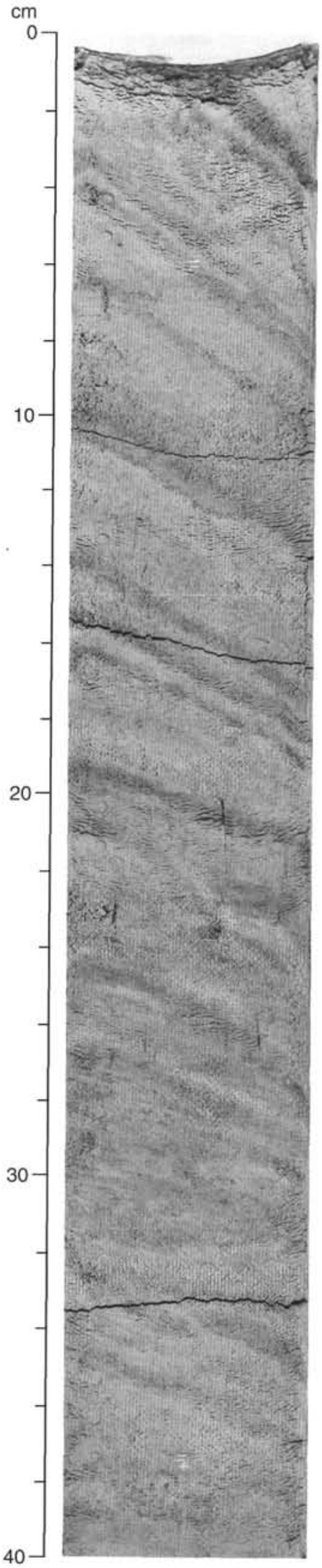

Figure 12. Photograph showing steeply inclined bedding interpreted as part of slump in Section 162-981A-27H-3, 0–40 cm (247.00–247.40 mbsf).

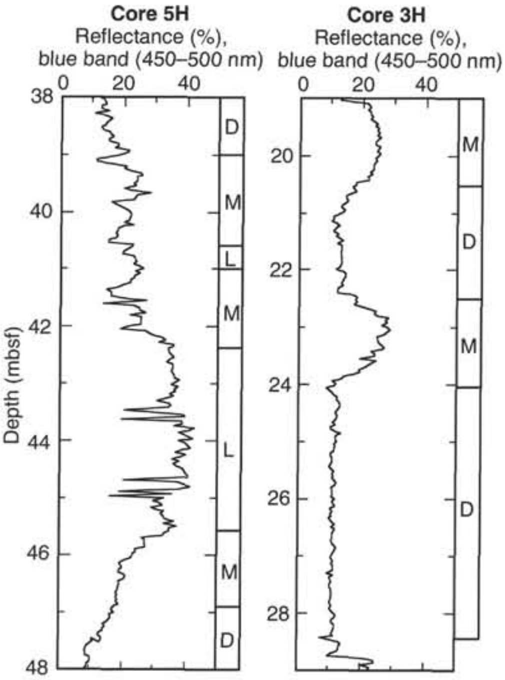

Figure 13. Percentage reflectance and visual color changes for the predominantly "dark-colored" Core 162-980A-3H and predominantly "light-colored" Core 162-980A-5H from the rapidly accumulated sediments in Hole 980A. Color changes in the cores are represented as follows: L = very light gray and light gray; M = gray; and D = dark gray and dark greenish gray. Note that cyclic reflectance changes occur at smaller scales than the visual color changes, particularly in Core 5H.

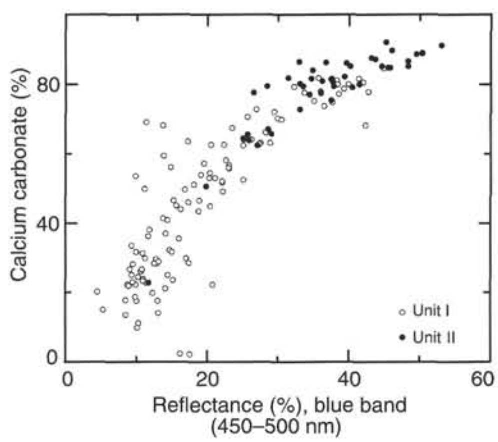

Figure 14. Percentage carbonate content vs. percentage reflectance for Units I and II in Holes 980A and 981A.

BIOSTRATIGRAPHY

Site 980 yielded a continuous calcareous sequence of early Pleistocene to Holocene age, with generally abundant and well-preserved calcareous microfossils that provide the primary biostratigraphic information for this site. Nannofossil zones, together with planktonic foraminiferal and diatom zones, are summarized in Table 7 and Figure 15. Graphic presentation of the these data vs. depth is provided in the "Sedimentation Rates" section (this chapter).

Table 7. Depth range of biostratigraphic datums, Hole 980A.

Datum	Age (Ma)	Core, section, interval (cm)	Depth (mbsf)	Depth (mcd)
		162-980A-		
FO *E. huxleyi* (N)	0.26	3H-CC, 14–18	28.60	35.32
		4H-1, 10	28.50	36.41
LO *P. lacunosa* (N)	0.46	6H-4, 10	52.00	62.07
		6H-5, 10	53.50	63.57
LO *N. reinholdii* (D)	0.65	7H-CC, 20–25	66.82	78.37
		8H-CC, 13–18	76.19	88.50
LO *N. fossilis* (N)	0.92	9H-CC, 13–18	85.71	98.90
		10H-3, 55	88.95	103.18
FO *Gephyrocapsa* spp. C/D (N)	1.03	8H-CC, 13–18	76.19	88.50
		9H-1, 10	76.00	89.19
LO *H. sellii* (N)	1.22	11H-5, 10	101.00	114.87
		11H-6, 10	102.50	116.37
LO *Gephyrocapsa* spp. A/B (N)	1.23	11H-2, 70	97.10	110.97
		11H-3, 18	98.08	111.95

Notes: FO = first occurrence; LO = last occurrence. In parentheses: N = calcareous nannofossil; D = diatom.

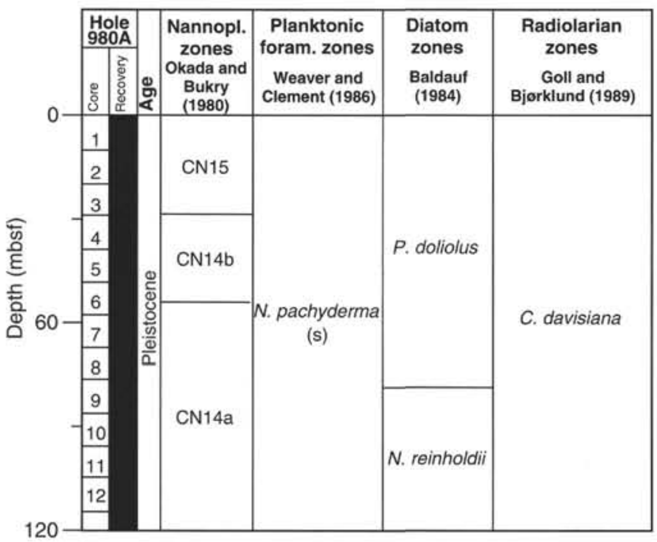

Figure 15. Biostratigraphic summary, Hole 980A.

Table 8. Depth range of biostratigraphic datums, Hole 981A.

Datum	Age (Ma)	Core, section, interval (cm)	Depth (mbsf)	Depth (mcd)
		162-981A-		
FO *E. huxleyi* (N)	0.26	3H-3, 109	20.09	21.93
		3H-4, 49	20.99	22.83
LO *P. lacunosa* (N)	0.46	4H-CC, 14–18	35.35	38.52
		5H-1, 70	35.70	39.70
FO *Gephyrocapsa* spp. C/D (N)	0.78	6H-1, 19	44.69	50.26
		6H-2, 140	47.40	52.97
LO *M. quadrangula* (S)	0.90	5H-CC, 73–75	44.60	48.60
		6H-CC, 23–26	54.38	59.95
LO *H. sellii* (N)	1.22	9H-1, 44	73.44	82.98
		9H-2, 130	75.80	85.34
LO *Gephyrocapsa* spp. A/B (N)	1.23	8H-4, 99	68.99	76.75
		8H-5, 100	70.50	78.26
LO *C. macintyrei* (N)	1.59	10H-CC, 26–29	89.22	99.85
		11H-1, 49	92.49	103.74
FO *Gephyrocapsa* spp. A/B (N)	1.70	11H-1, 49	92.49	103.74
		11H-2, 49	93.99	105.24
S, acme *N. pachyderma* s. (F)	1.80	10H-CC, 26–29	89.22	99.85
		11H-CC, 19–22	101.67	112.92
FO *P. doliolus* (D)	1.89	10H-2, 90–92	84.90	95.53
		10H-4, 90–92	87.90	98.53
LO *A. serotinum* (E)	2.00	13H-CC, 14–17	120.82	133.68
		14H-CC, 25–28	130.48	144.00
FO *Gr. inflata* (F)	2.09	13H-CC, 14–17	120.82	133.68
		14H-2, 49	122.49	136.01
LO *T. convexa* (D)	2.19	14H-5, 49–51	126.99	140.51
		14H-CC, 25–28	130.48	144.00
LO *N. atlantica* (F)	2.41	16H-2, 19	141.19	155.83
		16H-5, 19	145.69	160.33
LO *Gr. puncticulata* (F)	2.41	16H-5, 19	145.69	160.33
		16H-CC, 20–23	149.42	164.06
LO *D. surculus* (N)	2.59	19H-3, 60	171.60	188.37
		19H-4, 50	173.00	189.77
LO *E. cornuta* (E)	2.61	16H-CC, 20–23	149.42	164.06
		17H-CC, 20–24	158.80	173.34
LO *D. tamalis* (N)	2.78	21H-5, 10	193.10	210.62
		21H-6, 10	194.60	212.12
LO *Gr. crassula* (F)	3.30	22H-CC, 12–17	206.28	223.49
		23H-2, 30	207.80	226.98
FO *P. lacunosa* (N)	3.70	27H-1, 10	244.10	262.51
		27H-2, 10	245.60	264.01
FO *T. convexa* (D)	3.85	26H-CC, 13–18	244.17	262.58
		29H-CC, 17–22	272.79	291.20
FO *Gr. puncticulata* (F)	4.50	29H-CC, 17–22	272.79	291.20
		30H-CC, 9–14	282.29	300.70
LO *A. primus* (N)	4.70	32H-5, 10	297.60	316.01
		32H-6, 10	299.10	317.51

Notes: FO = first occurrence; LO = last occurrence; S = start. In parentheses: N = calcareous nannofossil, F = planktonic foraminifer, D = diatom, S = silicoflagellate, and E = ebridian.

Site 981 also yields abundant, generally well-preserved calcareous microfossils, which allow a reasonably detailed biostratigraphy to be developed (Table 8; Fig. 16). Siliceous microfossils occur mainly in the upper Pliocene, where they provide useful stratigraphic information. Most ages obtained from different fossil groups are consistent (Tables 7, 8). The biostratigraphic information summarized in Figure 16, plus that presented in the "Sedimentation Rate" section (this chapter), indicates that the sedimentary sequence recovered at Site 981 is continuous without any significant hiatuses.

Calcareous Nannofossils

Site 980

All core-catcher samples plus one sample per section from several cores in Hole 980A have been examined to locate nannofossil datums. Nannofossils are generally abundant and well preserved throughout the sequence. Reworked nannofossils are very rare or absent, except in intervals of probable glacial periods where the abundance of in situ nannofossils is low, and reworked Cretaceous nannofossils are frequently observed.

Emiliania huxleyi is common to abundant in the first three cores. The first occurrence of this species, which generally correlates with oxygen isotope stage 8 (0.26 Ma), is located between Samples 162-980A-3H-CC and 4H-1, 10 cm. Rare specimens of *Pseudoemiliania lacunosa* were first encountered in Sample 162-980A-6H-5, 10 cm. An age of about 0.46 Ma can be assigned to this sample. The first occurrence of *Gephyrocapsa* spp. C/D, which correlates with the Jaramillo (1.0 Ma) in middle to low latitudes, is placed between Samples 162-980A-8H-CC and 9H-1, 10 cm. Common to abundant *Gephyrocapsa* spp. A/B occur from Sample 162-980A-11H-3, 18 cm, downward. An age of 1.22 Ma can be assigned to this sample. The last occurrence of *Helicosphaera sellii,* which has a general age of

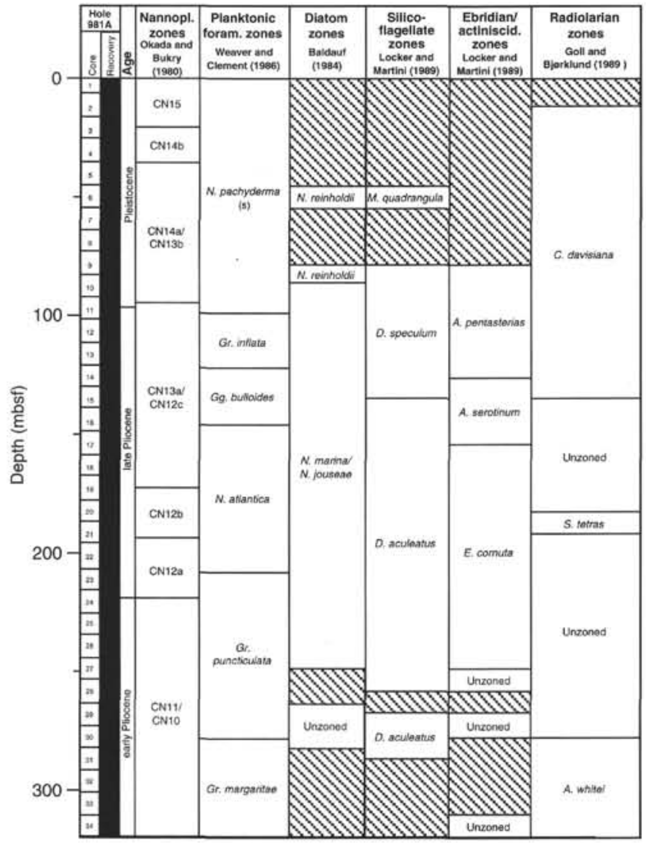

Figure 16. Biostratigraphic summary, Hole 981A. Hatched intervals indicate absence of fossils. The Pliocene/Pleistocene boundary is based on paleomagnetic data. The early Pliocene/late Pleistocene boundary is based on nannofossil biostratigraphy.

about 1.2 Ma, is located between Samples 162-980A-11H-5, 105 cm, and 11H-6, 105 cm. The oldest sediment recovered, Sample 162-980A-12H-CC, contains abundant *Gephyrocapsa* spp. A/B in the absence of *Calcidiscus macintyrei,* and is thus younger than about 1.5 Ma.

Site 981

Nannofossil zonal boundaries have also been determined between core sections in Hole 981A (see Table 8). The Pleistocene interval from this hole is similar to Hole 980A discussed above and contains generally abundant and well-preserved nannofossil assemblages.

Nannofossils are also abundant in the Pliocene. Zonal boundaries recognized for the Pliocene interval are summarized in Figure 16. Discoasters are generally rare at this high-latitude site; the CN12a/CN12b and CN12b/CN12c boundaries defined by the LO of *Discoaster tamalis* and *D. surculus,* respectively, are thus not precise.

Planktonic Foraminifers

Site 980

Planktonic foraminifers are abundant and well preserved throughout the early Pleistocene to Holocene sequence in Hole 980A. Planktonic foraminifers include common *Globigerina bulloides, Globorotalia inflata, Globorotalia scitula, Globigerinita glutinata,* and *Neoglobobquadrina pachyderma* (both left- and right-coiling varieties). Assemblage composition was dependent upon whether the core-catcher sample chanced to fall within an interglacial or glacial interval. Inferred glacial samples feature abundant *N. pachyderma* (sinistrally coiling), while inferred interglacial samples contain abundant *Gg. bulloides* and *Gr. inflata.* Subpolar paleoenvironmental conditions are indicated throughout the sequence, varying from warm subpolar to cool subpolar. The Hole 980A sequence lies entirely within the *N. pachyderma* (sinistrally coiling) Zone, which is Pleistocene in age (see "Explanatory Notes" chapter, this volume).

Site 981

Planktonic foraminifers are abundant and well preserved throughout the early Pliocene to Holocene sequence in Hole 981A. Quaternary planktonic foraminifers include *Globigerina bulloides, Globorotalia inflata, Globorotalia scitula, Globigerinita glutinata,* and *Neoglobobquadrina pachyderma* (both left- and right-coiling varieties). As in Hole 980A, assemblage composition was dependent upon whether the core-catcher sample chanced to fall within an interglacial or glacial interval. Inferred glacial samples feature abundant *N. pachyderma* (sinistrally coiling), while inferred interglacial samples contain abundant *Gg. bulloides* and *Gr. inflata.* Subpolar paleoenvironmental conditions are indicated throughout the Pleistocene, varying from warm subpolar to cool subpolar. The base of the Pleistocene is marked by the start of the acme zone of *N. pachyderma* (sinistrally coiling, encrusted, compact form) between Samples 162-981A-10H-CC and 11H-CC.

The Pliocene is subdivided into four zones, the uppermost Pliocene *Gr. inflata* Zone, the upper Pliocene *N. pachyderma* (dextrally coiling) Zone, the middle Pliocene *Gr. puncticulata/N. atlantica* Zone, and the lower Pliocene *Gr. margaritae* Zone (Fig. 16). Several planktonic foraminifer datums are found in the Pliocene. The FO of *Gr. inflata* is found between Samples 162-981A-13-CC and 14H-2, 49–51 cm. The LO of *N. atlantica* is found between Samples 162-981A-16H-2, 19–21 cm, and 16H-5, 19–21 cm. The LO of *Gr. puncticulata* is found between Samples 162-981A-16H-5, 19–21 cm, and 16H-CC. The LO of *Gr. crassula* is found between Samples 162-981A-22H-CC and 23H-2, 19–21 cm. Lastly, the FO of *Gr. puncticulata* is found between Samples 162-981A-29H-CC and 30H-CC.

Benthic Foraminifers

Site 980

Benthic foraminifers were present in all the core-catcher samples from this site, generally constituting less than 1%–2% of the total foraminiferal fauna from the >63-µm sieve fraction studied. Semiquantitative estimates of relative species abundance were made with counts of >100 individuals per sample. This provides a means of rapidly estimating the diversity and identifying the most abundant taxa present. However, rare species will tend to be missed and diversity underestimated, perhaps by about 25%, according to the species-specimen plot for DSDP Sample 85-573-4-CC (Thomas, 1985).

Diversity is variable, with up to about 40 species counted in some samples (162-980A-4H-CC and 8H-CC), but less than 25 species counted elsewhere (162-980A-5H-CC, 6H-CC, and 9H-CC). Preservation is good throughout, with rare, thin-walled miliolids showing no sign of damage and the aragonitic species *Hoeglundina elegans* present in Section 162-980A-8H-CC.

Relative abundances of the most common taxa exhibit considerable variability at this site, although the overall faunal composition does not change markedly downhole. There does not appear to be any clear relationship between benthic diversity and inferred glacial cycles. However, shore-based study of these sections will clarify any relationships that do exist. The most abundant taxa include *Cassidulina obtusa, Cassidulina laevigata, Cassidulina teretis, Epistominella exigua, Globocassidulina subglobosa, Melonis pomiloides,* *Melonis barleeanus, Nonionella* spp., *Stainforthia fusiformis, Stainforthia loeblichi,* and *Trifarina (Angulogerina) angulosa.* Thomas (1987) noted that the last appearance of *Stilostomella* spp. at Site 610 occurs below about 45 mbsf (less than 1 Ma), considerably younger than at deeper North Atlantic sites. At this site the last occurrence of *S. lepidula* occurs in Sample 162-980A-9H-CC (about 0.9 Ma).

Site 981

Benthic foraminifers were examined from 12 core-catcher samples at this site (162-981A-1H-CC, 6H-CC, 8H-CC, 10H-CC, 12H-CC, 14H-CC, 16H-CC, 18H-CC, 24H-CC, 26H-CC, 30H-CC, and 34H-CC). Diversity is highly variable, with a maximum 43 species (total number of specimens = 128) in Sample 162-981A-30H-CC and a minimum 16 species (total number of specimens = 77) in Sample 162-981A-14H-CC. Preservation is generally good to moderate.

The Quaternary is characterized by a diverse assemblage, with common taxa including *Cassidulina obtusa, Cibicidoides wuellerstorfi, Epistomella exigua, Globocassidulina subglobosa, Nonionella sp.,* and *Stainforthia fusiformis.* Decreased sedimentation rates during the Pleistocene at this site compared to nearby Site 980 may explain some of the observed differences in the foraminiferal assemblages. The last appearance of *Stilostomella lepidula* occurs between Samples 162-981A-6H-CC and 8H-CC (0.8–1.2 Ma), suggesting that the LO of this species may be a useful regional marker (see Site 980 discussion above).

The expanded Pliocene sequence (nearly 200 m) at this site is characterized by less variable faunal assemblages than those found in the Quaternary. However, some variation does occur, with the genera *Cassidulina, Bolivina,* or *Trifarina* generally dominating the assemblages older than about 1.2 Ma. Detailed shore-based study of these sections will clarify any relationships that may exist between the onset of glaciation and changes in the benthic foraminiferal assemblages during the Pliocene.

Bolboforma

Site 981

Specimens belonging to the genus *Bolboforma* were picked and examined in parallel with benthic foraminifers. No *Bolboforma* species were recorded from the Pleistocene succession of Site 980, but a number of specimens were recovered from the lower part of Site 981. The last occurrence of *Bolboforma* is in Sample 162-981A-19H-CC, where a single specimen of *B. laevis* is recorded. Numerous specimens are found in Sample 162-981A-20H-CC (younger than 2.78 Ma) and they probably represent the youngest reliable record of *Bolboforma* from the North Atlantic region. Species present within the sequence include *B. costairregularis, B. laevis, B. costata,* and *B. clodiusi.* Shore-based studies will concentrate on detailed zonation of *Bolboforma* through this interval.

Diatoms

Site 980

Diatoms from Hole 980A vary greatly in preservation and abundance. Generally, in intervals with large amounts of silt and clay, diatoms are absent, while in intervals with higher carbonate content, diatoms can be well-preserved and abundant. Most often, diatoms were rare and poorly preserved.

In core-catcher samples from Hole 980A, assemblages from Cores 162-980A-1H through 7H contain the diatom species *Pseudoeunotia doliolus* and *Thalassiosira oestrupii.* The absence of *Nitzschia reinholdii* in Cores 162-980A-1H through 7H suggests that these cores fall within the *P. doliolus* Zone of Baldauf (1984), with an age between 0.65 and 0 Ma. The last occurrence of *N. reinholdii,* which marks the top of the *N. reinholdii* Zone, is located between Samples 162-980A-7H-CC and 8H-CC. The presence of *P. doliolus* and *N. reinholdii* between Samples 162-980A-8H-CC and 12H-CC indicates an age within the N. reinholdii Zone, between 1.89 and 0.65 Ma. The last occurrence of *Nitzschia fossilis,* with an age of 0.92 Ma, is placed between Sections 162-980A-9H-CC and 10H-3.

Site 981

Diatom preservation is consistently poor throughout Cores 162-981A-1H through 8H. In intervals within these cores that are not barren, diatom assemblages contain rare, non-age-diagnostic species. The interval between Cores 162-981A-9H and 26H contains well-preserved, abundant diatoms. From Core 162-981A-27H to the base of the section, diatoms again become poorly preserved, rare, or absent.

The presence of *N. reinholdii* fragments in Sample 162-981A-6H-CC indicates that cores below this sample are older than 0.65 Ma. While many samples above 162-981A-9H-CC are barren, the presence of *N. fossilis* in Sample 162-981A-9H-CC indicates a minimum age of 0.92 Ma, which is within the *N. reinholdii* Zone of Baldauf (1984). Between Sections 162-981A-10H-2 and 10H-4, the first occurrence of the diatom *P. doliolus* marks the boundary between the *N. reinholdii* and *N. marina* Zones. The last occurrence of *Thalassiosira convexa,* which has an age of 2.19 Ma, occurs between Sections 162-981A-14H-CC and 14H-5. The sporadic occurrence of *N. jouseae,* whose range defines the *N. jouseae* Zone, makes it impossible to identify the boundary between the *N. marina* and the *N. jouseae* Zones. The occurrence of *T. convexa convexa* in Sample 162-981A-26H-CC indicates a maximum age of 3.85 Ma.

Radiolarians

Site 980

Radiolarians are poorly preserved throughout the section and are mainly present as fragments. The assemblages contain temperate and cool-water species, such as *Cornutella profunda, Lithomitra lineata, Lithostrobus botryocyrtis, Spongodiscus resurgens,* and *Spongotrochus glacialis.* The presence of *Cycladophora davisiana* in Samples 162-980A-1H-CC, 6H-CC, and 2H-CC indicates the high-latitude *Cycladophora davisiana* Zone (Goll and Bjørklund, 1989) of the Pleistocene.

Site 981

All core-catcher samples from Hole 981A were studied for radiolarians. The frequency of radiolarians varies from rare to abundant in the Pleistocene and from common to abundant in the Pliocene. The preservation of skeletons is poor in the uppermost Pleistocene and lower Pliocene, but moderate to good in all other parts of the section.

The uppermost Sample 162-981A-1H-CC is barren of radiolarians. From Samples 162-981A-2H-CC to 5H-CC, rare radiolarian assemblages are found which can be assigned to the *Cycladophora davisiana* Zone, due to the presence of the nominate species. Below, rich radiolarian assemblages are recorded between Samples 162-981A-6H-CC and 14H-CC. These assemblages can be also placed in the Pleistocene to upper Pliocene *Cycladophora davisiana* Zone. The most common species of this interval are spumellarians, such as *Lithelius spiralis, Spongodiscus resurgens,* and *Stylochlamydium venustum.*

The interval between Samples 162-981A-15H-CC and 19H-CC remains unzoned. In Sample 162-981A-20H-CC *Spongaster tetras* occurs, which indicates the upper Pliocene *Spongaster tetras* Zone. Samples 162-981A-21H-CC through 29H-CC are unzoned because distinct marker species could not be found. Samples 162-981A-30H-CC to 33H-CC can be assigned to the lower Pliocene *Antarctissa whitei* Zone, since the nominate species exhibits higher abundance in this interval. The most common species of the Pliocene interval are spumellarians, such as *Lithelius spiralis, Spongodiscus resurgens,* and *Stylochlamydium venustum. Druppatractus* cf. *universus* and *Lithomitra* ex gr. *lineata* also attain higher abundances in certain parts of the Pliocene section.

The lowermost Sample 162-981A-34H-CC raises some questions. Besides *Antarctissa whitei,* this sample contains three species which may indicate a late Miocene age. *Cyrtocapsella tetrapera,* present as two well-preserved skeletons, appears from the early to the middle Miocene in low latitudes, but the last appearance may be later in high latitudes (Nigrini and Sanfilippo, 1992). *Larcospira quadrangula,* found as one well-preserved skeleton, appears throughout the late Miocene in both tropical and temperate regions (Nigrini and Lombari, 1984). *Stichocorys delmontensis,* recorded only as a fragment, appears from the early to the late Miocene in low and middle latitudes, but may persist until the early Pliocene in higher middle latitudes (Nigrini and Sanfilippo, 1992).

Thus, the radiolarian study from Site 981 demonstrates that only the high-latitude zonation scheme of Goll and Bjørklund (1989) can be applied to the Quaternary through Pliocene section. This indicates relatively cool surface-water conditions in the northern North Atlantic, comparable to the eastern Norwegian-Greenland Sea during that time interval.

Siliceous Flagellates

Site 980

Siliceous flagellates (including silicoflagellates, ebridians, and actiniscidians) are very rare throughout the section. An exception is Sample 162-980A-12H-CC, which contains *Dictyocha calida, D. hessii, D. perlaevis,* and some other species. This assemblage is characteristic for the lower and middle Pleistocene.

Site 981

Siliceous flagellates (including silicoflagellates, ebridians, and actiniscidians) are continuously present between Samples 981A-9H-CC and 27H-CC. The abundance of these fossils varies from trace to common. Preservation of silicoflagellates is generally moderate, but may be also poor. Preservation of ebridians and actiniscidians is usually good.

Samples 981A-1H-CC to 8H-CC are barren of silicoflagellates, with the exception of Sample 6H-CC, where a single specimen of *Mesocena quadrangula* was found. The presence of this species suggests the *Mesocena quadrangula* Subzone of the lower Pleistocene, which ranges from Chron C1r.1n to the upper part of Chron C1r.1r.

Samples 981A-9H-CC to 14H-CC contain only a few nondiagnostic silicoflagellate species of the lower *Distephanus speculum* Zone. Samples 162-981A-15H-CC to 30H-CC are placed in the *Distephanus aculeatus* Zone, which is late to early Pliocene in age. *Paramesocena circulus circulus,* which occurs from Sample 981A-18H-CC to 26H-CC, clearly correlates with this zone.

Samples 162-981A-1H-CC to 8H-CC are barren of ebridians/actiniscidians. Samples 162-981A-9H-CC to 13H-CC belong to the *Actiniscus pentasterias* Zone of the Pleistocene. Samples 162-981A-14H-CC to 16H-CC can be placed in the Pliocene *Ammodochium serotinum* Zone, with an upper age of 2.00 Ma. Samples 162-981A-17H-CC to 26H-CC are assigned to the *Ebriopsis cornuta* Zone, with an upper age of 2.61 Ma. The lowermost Sample 162-981A-34H-CC contains *Parathranium clathratum,* which may suggest a stratigraphic position near the Miocene/Pliocene boundary.

PALEOMAGNETISM

Site 980

Archive halves of all cores from Holes 980A, 980B, and 980C were measured on the pass-through cryogenic magnetometer. Time constraints and the necessity to keep pace with core flow permitted only a single alternating-field (AF) demagnetization step for the majority of core sections. All cores from each hole at Site 980 were oriented using the Tensor tool.

For Hole 980A, a peak AF demagnetization of 15 mT was used on all sections, with additional demagnetization steps for a few sections (Table 9). Progressive AF demagnetization of discrete samples indicated that a very strong, steeply inclined drill-string magnetic (viscous) overprint was removed by alternating fields in the 15–30 mT range (Fig. 17). Based on these data, we increased the peak demagnetization field for Holes 980B and 980C to 25 mT, with some additional demagnetization steps as time allowed (Table 9).

Natural remanent magnetization (NRM) intensities at Site 980 average about 100 mA/m, with large variations coincident with changes in volume susceptibility. After demagnetization in peak fields of 15 mT, the magnetization intensities averaged about 10 mA/m, with large variations (~1–70 mA/m) in the Brunhes Chron (above 75 mbsf). No progressive decreases in magnetization intensity are apparent downhole.

The Brunhes/Matuyama boundary and the Jaramillo Subchron are well defined in all three holes (Fig. 18). Sub-bottom depths of polarity chron boundaries are given in Table 10. Several intervals of anomalously low inclination may be attributed to core deformation and/or authigenic growth of iron sulfides. In many cores, the upper 50% (at least) of Section 1 appears to have a high coercivity (drill-string) remagnetization which was not removed at peak alternating fields of 25 or 30 mT.

A thin interval within the Brunhes Chron of low negative inclinations, close to 35 mbsf, occurs in all three holes and may represent a magnetic excursion within the Brunhes Chron. The closer measurement spacing (5 cm) used for Hole 980A indicates progressive changes in inclination within the Brunhes Chron which may denote geomagnetic secular variation (Fig. 18).

Table 9. Summary of pass-through cryogenic magnetometer measurements at Sites 980 and 981.

Measurement	Core sections
	162-980A-
NRM	1H, 2H-1, 3H-2, 4H-2, 6H-1, 6H-6, 7H-1, 8H-1, 9H-1, 9H-3, 10H-1, 10H-3
15 mT	1H-1 through 12H-6
20 mT	5H-1, 9H-7
25 mT	11H-2, 12H-3 through 12H-6
	162-980B-
NRM	4H-5
15 mT	1H, 2H, 4H-5
25 mT	1H-1 through 13H-7
25 mT	162-980C-2H-2 through 14H-2
	162-981A-
NRM	29H-2, 29H-3
15 mT	28H-5, 28H-6, 29H, 30H, 31H
25 mT	1H-1 through 29H-4, 30H-2, 30H-5
30 mT	8H-3, 11H-1, 12H-5, 13H-2, 23H-6
	162-981B-
15 mT	18H-3, 18H-4
25 mT	1H-1 through 20H-3
30 mT	13H-2, 14H-1, 17H, 18H-2 through 18H-4

Site 981

At Site 981, archive halves of Holes 981A and 981B were measured using the pass-through cryogenic magnetometer. Demagnetization was carried out at peak AF fields of 25 mT for all cores. Additional demagnetization steps were made on some core sections, as time allowed (Table 9). Discrete-sample stepwise AF demagnetization indicates that the steeply inclined drill-string (viscous) magnetization was removed by demagnetization fields exceeding 10 mT (Fig. 17).

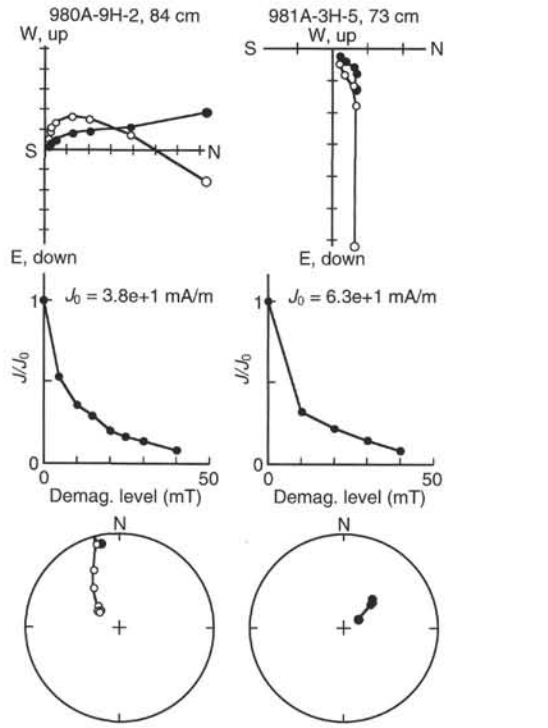

Figure 17. Stepwise AF demagnetization of two samples from Holes 980A and 981A. Top: orthogonal projection of end points of the magnetization vector. Open and solid symbols represent projection on the vertical and horizontal planes, respectively. Middle: change in magnetization intensity during AF demagnetization. Bottom: equal area projection of magnetization vector during demagnetization.

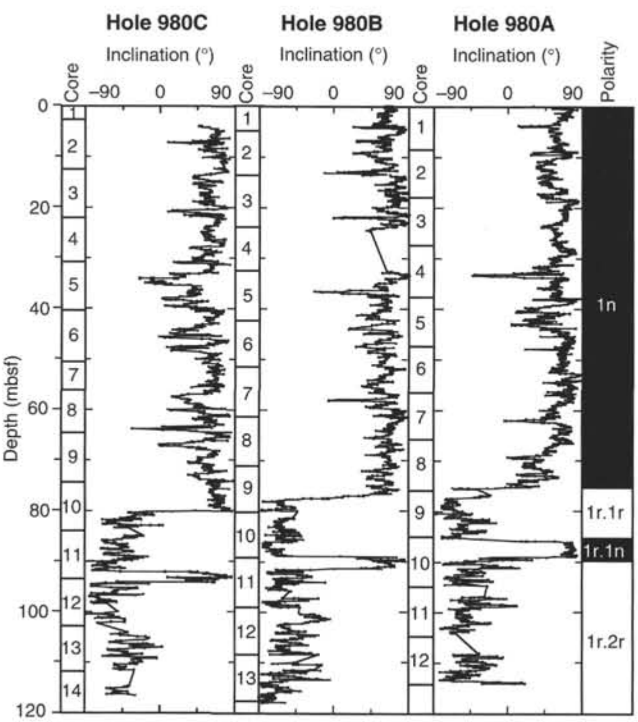

Figure 18. Inclination of the magnetization vector vs. depth (mbsf) for Site 980, after AF demagnetization at peak fields of 15 mT for Hole 980A and 25 mT for Holes 980B and 980C.

Table 10. Preliminary positions of polarity chron boundaries at Sites 980 and 981.

Core, section, interval (cm)	Depth (mbsf)	Interpreted boundary	Age (Ma)	Comments
162-980A-				
8H-6, 140	75.30	Brunhes/Matuyama	0.78	
10H-1, 0	85.50	Jaramillo (top)	0.99	Section break
10H-3, 110	89.50	Jaramillo (bottom)	1.07	
162-980B-				
9H-5, 65	77.35	Brunhes/Matuyama	0.78	
10H-6, 125	88.95	Jaramillo (top)	0.99	
11H-2, 25	91.45	Jaramillo (bottom)	1.07	
162-980C-				
10H-5, 15	80.25	Brunhes/Matuyama	0.78	
11H-6, 90	92.60	Jaramillo (top)	0.99	
12H-1, 100	94.10	Jaramillo (bottom)	1.07	
162-981A-				
6H-4, 20	49.20	Brunhes/Matuyama	0.78	
7H-4, 5	58.55	Jaramillo (top)	0.99	
7H-6, 5	61.55	Jaramillo (bottom)	1.07	
8H-3, 95	67.45	Cobb Mountain (?)	1.21	
11H-4, 25	96.75	Olduvai (top)	1.77	
12H-5, 0	107.50	Olduvai (bottom)	1.95	Section break
14H-1, 25	120.75	Reunion (top)	2.14	
14H-3, 75	124.25	Reunion (bottom)	2.15	
16H-7, 40	148.90	Matuyama/Gauss (1)	2.60	Poorly defined (see text)
18H-5, 65	165.10	Matuyama/Gauss (2)		
162-981B-				
6H-6, 10	48.00	Brunhes/Matuyama	0.78	
7H-6, 75	58.15	Jaramillo (top)	0.99	
8H-1, 80	60.20	Jaramillo (bottom)	1.07	
8H-4, 95	64.85	Cobb Mountain (?)	1.21	
11H-6, 145	96.85	Olduvai (top)	1.77	
13H-2, 0	109.90	Olduvai (bottom)	1.95	Section break
14H-5, 115	123.55	Reunion (top)	2.14	
14H-6, 135	125.25	Reunion (bottom)	2.15	
17H-4, 95	150.35	Matuyama/Gauss (1)	2.60	Poorly defined (see text)
18H-7, 40	163.80	Matuyama/Gauss (2)		

At Site 981, magnetic remanence intensities (after demagnetization at 25 mT) change abruptly at about 150 mbsf (Fig. 19). Above this level (approximately coincident with the Gauss/Matuyama boundary), the magnetic stratigraphy is well defined in both Holes 981A and 981B. Below this level, magnetization intensities are close to the noise level of the shipboard pass-through magnetometer. Measurements were discontinued below 200 mbsf due to low magnetization intensities and the resulting poor quality data from the pass-through magnetometer.

In Hole 981A, the magnetic polarity stratigraphy indicates the Brunhes/Matuyama boundary and the subchrons within the Matuyama Chron (Jaramillo, Cobb Mountain?, Olduvai, and Reunion) (Fig. 20; Table 10). The record from Hole 981B is less clear. Many intervals of low and/or positive inclination are observed in the Matuyama Chron (Fig. 20). Some of these may be attributed to core deformation and/or iron sulfide mineralization.

In both Holes 981A and 981B, the Gauss/Matuyama boundary is problematic. It is at this level that magnetization intensities fall by almost two orders of magnitude (Fig. 19). The interval 150–165 mbsf in both Holes 981A and 981B appears to be predominantly normal polarity; however, the quality of the data is poor in this interval and there is the possibility that this interval is remagnetized. The two options for the position of the Gauss/Matuyama boundary are listed in Table 10. The true position of this polarity chron boundary should be resolvable from shore-based studies.

Hole 981C was not measured using the shipboard pass-through magnetometer. Cores 981A-3H through 34H and Cores 981C-3H through 14H were oriented using the Tensor tool. Cores from Hole 981B were unoriented.

SEDIMENTATION RATES

Site 980

A sedimentary section about 120 m thick was recovered from three holes at Site 980, representing the interval from the middle Pleistocene to the Holocene. Sedimentation rates were determined on the basis of magnetostratigraphy and calcareous nannofossil biostratigraphy (Table 11; see "Paleomagnetism" and "Biostratigraphy" sections, this chapter). Sedimentation rate reconstructions were based primarily on data from Hole 980A, although the Site 980 composite depth section provided for the use of paleomagnetic events from all three holes in determining the depth of the Brunhes/Matuyama Chron boundary (see "Composite Depths" section, this chapter). To facilitate comparison between sites, sedimentation rates were estimated from age vs. depth plots by drawing straight-line segments (uniform sedimentation rate) between selected datums. These reconstructions confirm very high sedimentation rates for the middle Pleistocene to the Holocene, as indicated by the lithologic cycles observed in the multisensor track and reflectance data (see "Lithostratigraphy" section, this chapter) and seismic stratigraphy (see "Seismic Stratigraphy" section, this chapter).

Sedimentation rates were calculated for both the meters below seafloor (mbsf) depth scale and the meters composite depth (mcd) depth scale. Figure 21 presents sedimentation rates as a function of age and composite depth. Magnetic polarity age control points include the Brunhes/Matuyama Chron boundary and the Jaramillo Subchron. Calcareous nannofossil datums include the FO of *Emilianii huxleyi* at 0.26 Ma, the LO of *Pseudoemilianii lacunosa* at 0.46 Ma, and the LO *Gephyrocapsa* A/B at 1.23 Ma. These datums are considered synchronous from tropical through temperate zones. Two diatom datums (LO *Nitzschia reinholdii* and LO *Nitzschia fossilis*) fall just below the age-depth line, and two calcareous nannofossil datums (FO *Gephyrocapsa* C/D and LO *Helicosphaera sellii*) lie significantly off the age-depth line (Fig. 22). These deviations may be attributed

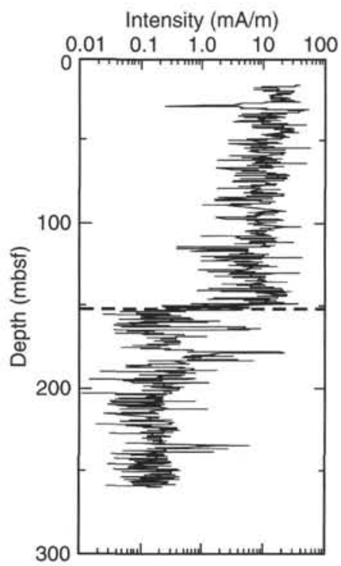

Figure 19. Magnetization intensity from Hole 981A after demagnetization in peak alternating fields of 25 mT. The shift in intensity at about 150 mbsf (dashed line) corresponds approximately to the Gauss/Matuyama polarity chron boundary.

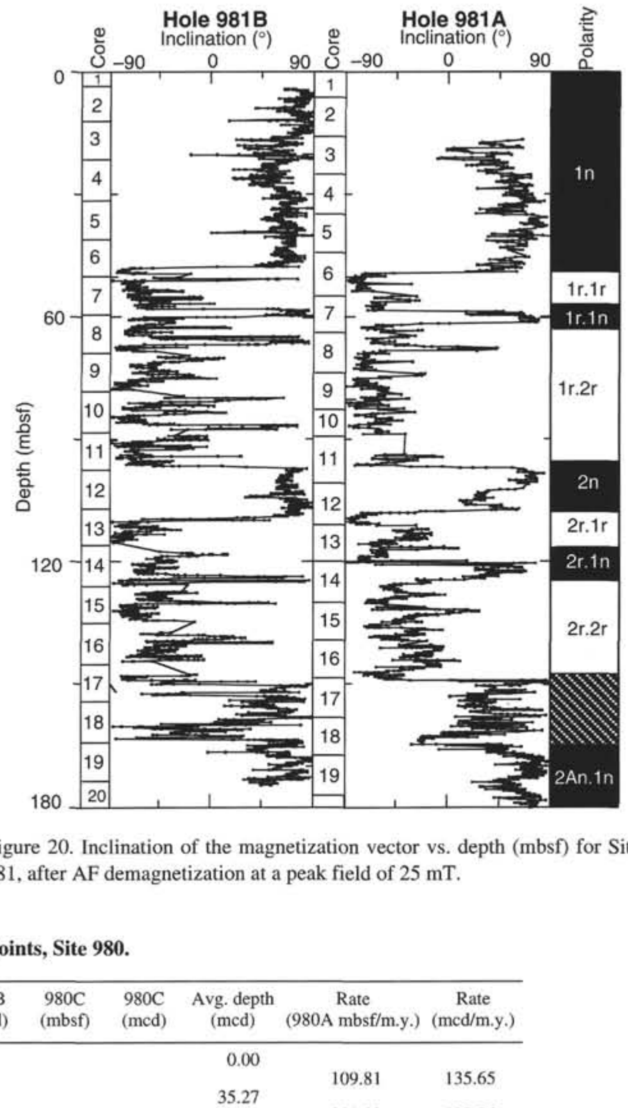

Figure 20. Inclination of the magnetization vector vs. depth (mbsf) for Site 981, after AF demagnetization at a peak field of 25 mT.

Table 11. Age control points, Site 980.

Event	Age (Ma)	980A (mbsf)	980A (mcd)	980B (mbsf)	980B (mcd)	980C (mbsf)	980C (mcd)	Avg. depth (mcd)	Rate (980A mbsf/m.y.)	Rate (mcd/m.y.)
Core top	0.00	0.00	0.00					0.00		
									109.81	135.65
FAD *E. huxleyi* (N)	0.26	28.55	35.27					35.27		
									121.00	137.75
LAD *P. lacunosa* (N)	0.46	52.75	62.82					62.82		
									70.47	76.66
Brunhes/Matuyama	0.78	75.30	87.61	77.35	87.05	80.25	87.40	87.35		
									48.57	61.90
Jaramillo top	0.99	85.50	99.73	88.95	100.38	92.60	100.93	100.35		
									50.00	42.13
Jaramillo bottom	1.07	89.50	103.73	91.45	103.74	94.10	103.69	103.72		
									50.56	48.31
LA *Gephyrocapsa* A/B (N)	1.23	97.59	111.46					111.46		

Notes: Ages are from Berggren et al. (1995). N = calcareous nannofossil.

to insufficient sampling resolution, differential preservation, and/or diachronous appearances (see "Biostratigraphy" section, this chapter).

Site 981

A sedimentary section about 327 m thick was recovered at Site 981, extending to the early Pliocene. Sedimentation rate reconstructions were based on magnetic polarity events from all three holes and calcareous nannofossil datums from Hole 981A (see "Paleomagnetism" and "Biostratigraphy" sections, this chapter). The Site 981 composite depth section (see "Composite Depths" section, this chapter) was used to relate events recorded in the multiple holes to a common depth scale. To facilitate comparison between sites, sedimentation rates were estimated from age vs. depth plots by drawing straight-line segments (uniform sedimentation rate) between selected datums.

Sedimentation rates were calculated for both the meters below seafloor (mbsf) depth scale and the meters composite depth (mcd) depth scale. Figure 23 presents sedimentation rates as a function of age and composite depth. Magnetic polarity age control points included are the Brunhes/Matuyama and Matuyama/Gauss Chron boundaries, and the Jaramillo, Olduvai, and Reunion Subchrons. Calcareous nannofossil datums include the FO of *Emilianii huxleyi* at 0.26 Ma, the LO of *Pseudoemilianii lacunosa* at 0.46 Ma, the FO of *P. lacunosa* at 3.7 Ma, and the LO of *Amaurolithus primus* at 4.7 Ma. These datums are considered synchronous from tropical through temperate zones. Two *Discoaster* datums lie significantly below the age-depth line (Fig. 24), but these tropical species may have disappeared early in this region (see "Biostratigraphy" section, this chapter). However, given the uncertain location of the Matuyama/Gauss Chron boundary (see "Paleomagnetism," this chapter), an alternative age model for the interval between 2 and 3 Ma may be indicated. Table 12 includes an alternative in which the Matuyama/Gauss Chron boundary is located deeper in the section. Sedimentation rates achieved using this alternate depth are displayed in Figure 23. Based on the shipboard stratigraphy alone, the correct age model for this interval cannot be confidently determined. Post-cruise stratigraphic studies incorporating oxygen isotopes should resolve the age vs. depth curve in this interval.

ORGANIC GEOCHEMISTRY

The shipboard organic geochemistry program at Sites 980 and 981 consisted of analyses of volatile hydrocarbons, determinations of inorganic carbon, total nitrogen, total carbon, and total sulfur, and pyrolysis measurements (for methods, see "Explanatory Notes" chapter, this volume).

Volatile Hydrocarbon

As part of the shipboard safety and pollution monitoring program, concentrations of methane (C_1) and ethane (C_2) were measured in every core using the standard ODP headspace-sampling technique. At Hole 980A, 12 sediment samples were collected between 7.5 and 111.9 mbsf in Quaternary sediments. Throughout the sediment sequence of Hole 980A, the methane content remained constantly low (4–10 ppm; Table 13; Fig. 25). Ethane was not detected. From Hole 981A, 34 sediment samples were collected between 4.5 and 314.1 mbsf and, throughout the sediment sequence, the methane content remained consistently low (2–7 ppm; Table 14; Fig. 26). Ethane was not detected.

Carbon, Nitrogen, and Sulfur Concentration

Determinations of inorganic carbon, carbonate, total carbon, total nitrogen, and total sulfur of Holes 980A and 981A are summarized in

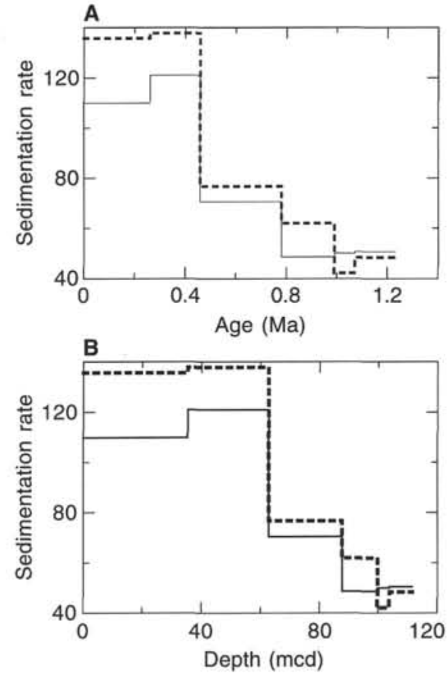

Figure 21. Site 980 sedimentation rates vs. age (**A**) and vs. composite depth (**B**). Dashed lines indicate rates in mbsf/m.y.; solid lines indicate rates in mcd/m.y.

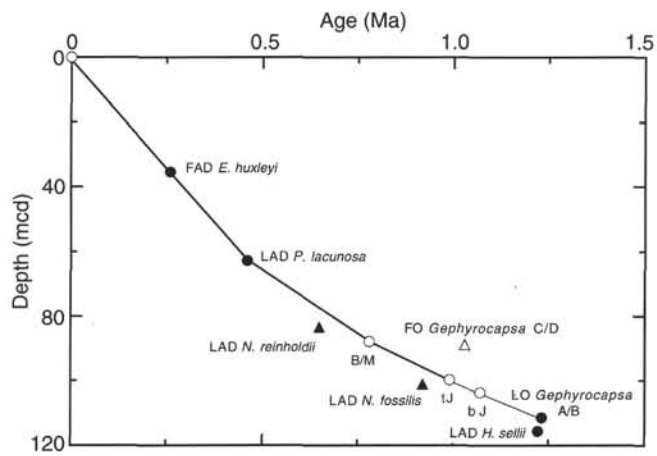

Figure 22. Site 980 age vs. depth (mcd) curve based on integrated magnetostratigraphic and biostratigraphic datums. Solid circles = nannofossils; open circles = diatoms; open triangles = magnetostratigraphic datums. B/M = Brunhes/Matuyama Chron boundary; tJ and bJ = Jaramillo Subchron (top and bottom).

Tables 15 and 16, respectively. According to the carbonate content data (calculated from the inorganic carbon content, assuming that all carbonate occurs as calcium carbonate), the sediment sequence of Hole 981A can be divided into three intervals (Fig. 26). The sediment sequence of Hole 980A and the upper interval (0–160 mbsf; Holocene to late Pliocene) of Hole 981A, which corresponds to lithostratigraphic Unit I (see "Lithostratigraphy" section, this chapter), are characterized by high amplitude variations of carbonate percentages ranging from 10% to 85% and from 1% to 85%, respectively (Figs. 25, 26). The concentration of carbonate in sediment is primarily controlled by dilution of biogenic carbonate by ice-rafted debris. These

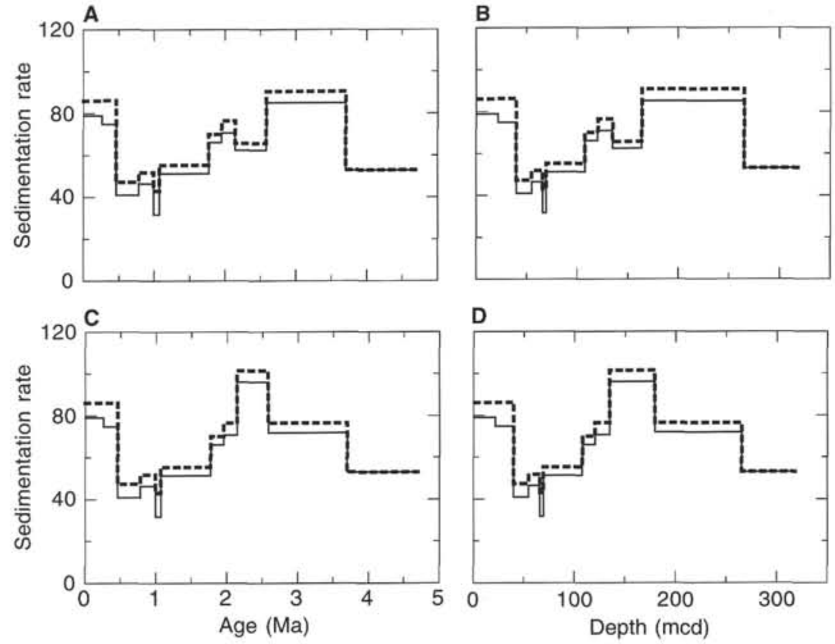

Figure 23. **A.** Site 981 sedimentation rates vs. age. **B.** Site 981 sedimentation rates vs. composite depth. **C, D.** Site 981 sedimentation rates, using the alternate depth of the Matuyama/Gauss Chron boundary (as discussed in "Paleomagnetism" section, this chapter). Solid lines indicate rates in mbsf/m.y.; dashed lines indicate rates in mcd/m.y.

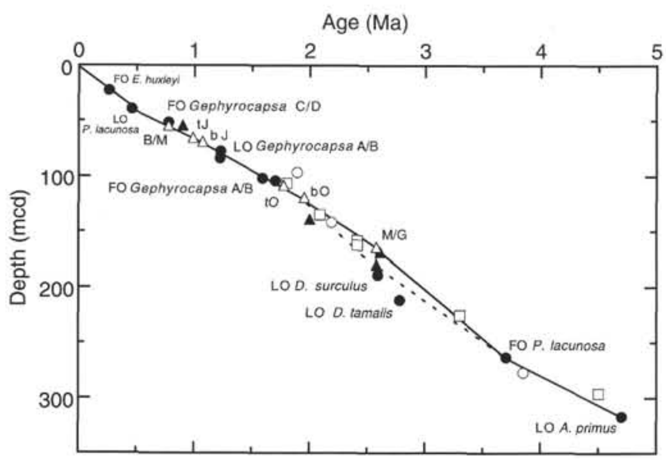

Figure 24. Site 981 age vs. depth (mcd) curve based on integrated magnetostratigraphic and biostratigraphic datums. The dashed line indicates the age vs. depth curve obtained using an alternate depth for the Matuyama/Gauss Chron boundary (see Table 12 and "Paleomagnetism" section, this chapter, for discussion). Solid circles = nannofossils; open circles = diatoms; open squares = foraminifers; solid triangles = siliceous flagellates; open triangles = magnetostratigraphic datums. B/M = Brunhes/Matuyama Chron boundary; M/G = Matuyama/Gauss Chron boundary; tJ and bJ = Jaramillo Subchron (top and bottom); tO and bO = Olduvai Subchron (top and bottom).

high amplitude variations are similar to those recorded and described in detail in DSDP Leg 94 sites (e.g., Ruddiman, Kidd, Thomas, et al., 1987) and in DSDP Hole 552A from the Hatton Drift in the North Atlantic (Zimmerman et al., 1984). The carbonate cycles at Sites 980 and 981 undoubtedly reflect glacial/interglacial fluctuations. The middle (160–195 mbsf) and lower (195–320 mbsf) intervals of Hole 981A correspond to lithostratigraphic Subunits IIA and IIB, respectively (see "Lithostratigraphy" section, this chapter). The carbonate content in both intervals is relatively higher, but the middle interval has slightly lower carbonate concentrations than the lower interval. These data suggest that input of ice-rafted debris did not occur in any significant amount in the lower interval, whereas terrigenous material was supplied in small quantities in the middle interval.

In Hole 980A, the total organic carbon (TOC) contents vary between 0.01% and 0.88% (Fig. 25), although low values (<0.4%) dominate the entire section of this hole. A maximum TOC value of 0.88% occurs in the upper part of the sedimentary record of Hole 980A (Sample 162-980A-3H-5, 25–26 cm; 25.15 mbsf). Total nitrogen contents are generally very low (Fig. 25; Table 15; 0.03%–0.11%). Total sulfur values vary between 0% and 0.77% (Fig. 25; Table 15). In Hole 981A, TOC contents vary between 0% and 0.87% (Fig. 26). TOC content values increase in the upper interval, compared to the lower. Total nitrogen contents are generally very low (Fig. 26; Table 16; 0.03%–0.12%). Total sulfur values vary between 0% and 0.63% (Fig. 26; Table 16).

Composition of Organic Matter

The type of organic matter in the sediments of Holes 980A and 981A has been characterized using organic carbon/nitrogen (C/N) ratios. The average C/N ratio of marine zoo- and phytoplankton is between 5 and 8, whereas higher land plants have ratios between 20 and 200 (Bordovskiy, 1965; Emerson and Hedges, 1988). Due to the organic carbon-poor nature of the sediments, pyrolysis analyses were not made (Katz, 1983; Peters, 1986). C/N ratios vary between 0.1 and 12 in the sediments of Hole 980A (Fig. 25; Table 15). In Hole 981A, they vary between 1.9 and 8.9 (Fig. 26; Table 16). These data suggest a mixture between marine and terrigenous organic carbon, with a dominance of marine material (Fig. 27). Further qualitative and quantitative organic geochemical data, such as detailed records of flux rates of terrigenous and marine organic carbon, as well as biomarker data, are required before a detailed paleoceanographic interpretation of the organic carbon data can be made.

INORGANIC GEOCHEMISTRY

Interstitial Water

Site 980

Site 980 on the Feni Drift is marked by rapidly deposited sediments of middle to late Pleistocene age, with rates as high as 25 cm/

Table 12. Age control points, Site 981.

Event	Age (Ma)	981A (mbsf)	981A (mcd)	981B (mbsf)	981B (mcd)	Avg. depth (mbsf)	Avg. depth (mcd)	Rate (981A mbsf/m.y.)	Rate (mcd/m.y.)
Core top	0.00	0.00	1.07			0.00	1.07		
								79.00	86.08
FAD *E. huxleyi* (N)	0.26	20.54	22.38			20.54	22.38		
								74.80	86.15
LAD *P. lacunosa* (N)	0.46	35.50	39.61			35.50	39.61		
								40.94	47.28
Brunhes/Matuyama	0.78	49.20	54.72	48.00	54.76	48.60	54.74		
								46.43	51.81
Jaramillo top	0.99	58.55	65.65	58.15	65.59	58.35	65.62		
								31.56	43.00
Jaramillo bottom	1.07	61.55	68.65	60.20	69.47	60.88	69.06		
								51.32	55.24
Olduvai top	1.77	96.75	108.31	96.85	107.15	96.80	107.73		
								66.11	69.97
Olduvai bottom	1.95	107.50	119.60	109.90	121.05	108.70	120.33		
								70.79	76.55
Reunion II top	2.14	120.75	134.77	123.55	134.97	122.15	134.87		
								62.44	65.61
								96.14	*101.39*
Matuyama/Gauss	2.58	148.90	163.96	150.35	163.52	149.63	163.74		
alt. Matuyama/Gauss	*2.58*	*165.10*	*180.88*	*163.80*	*178.08*	*164.45*	*179.48*		
								85.16	90.56
								71.92	*76.51*
FA *P. lacunosa* (N)	3.70	245.00	265.17			245.00	265.17		
								53.00	53.00
LA *A. primus* (N)	4.70	298.00	318.17			298.00	318.17		

Notes: Ages are from Berggren et al. (1995). N = calcareous nannofossil.

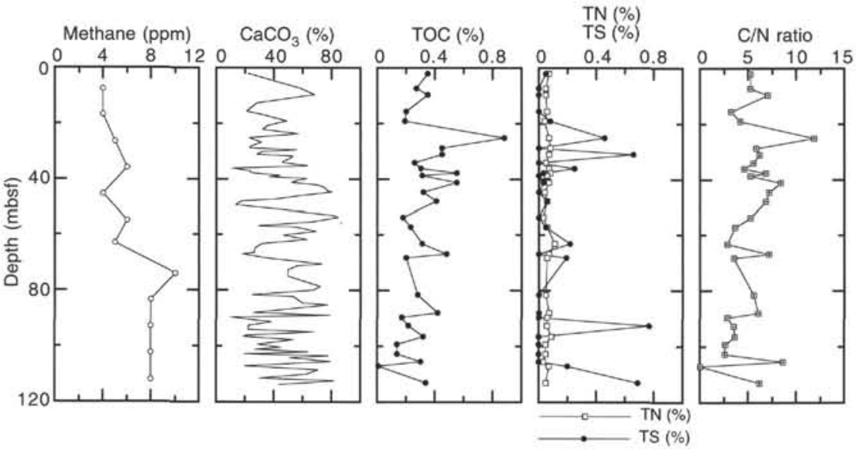

Figure 25. Methane concentration, calcium carbonate ($CaCO_3$), total organic carbon (TOC), total nitrogen (TN), and total sulfur (TS) contents, and TOC/TN (C/N) ratio in Hole 980A.

k.y. in interglacial intervals (See "Sedimentation Rates" section, this chapter). Diagenesis of organic matter in these rapidly deposited sediments has led to the depletion of dissolved sulfate in interstitial waters by the reaction of sulfate reduction:

$$53SO_4^{2-} + C_{106}H_{263}O_{110}N_{16}P = 39CO_2^- + 67HCO_3^- + 16NH_4^+ + 53HS^- + 39H_2O + HPO_4^{2-} \quad (1)$$

In this process, sulfate is consumed and alkalinity (i.e., HCO_3^-), ammonium, and phosphate are byproducts. The hydrogen sulfide so produced can react with iron to form iron sulfide minerals (e.g., FeS and FeS_2), which are ubiquitous components of the sediments (see "Lithostratigraphy" section, this chapter). Sulfate concentrations are near seawater values at the top of the section and decrease to a minimum of about 9.6 mM in Core 162-980A-9H (~85 m) (Fig. 28A; Table 17), indicating that complete sulfate consumption has not occurred. This observation is consistent with relatively low methane in headspace samples (see "Organic Geochemistry" section, this

Table 13. Results of headspace gas analyses of Hole 980A samples using the Hewlett Packard Series II 5890 gas chromatograph.

Core, section, interval (cm)	Depth (mbsf)	C_1 (ppm)
162-980A-		
1H-6, 0–5	7.53	4
2H-6, 0–5	16.93	4
3H-6, 0–5	26.43	5
4H-6, 0–5	35.93	6
5H-6, 0–5	45.43	4
6H-6, 0–5	54.93	6
7H-5, 0–5	62.93	5
8H-6, 0–5	73.93	10
9H-6, 0–5	83.43	8
10H-6, 0–5	92.93	8
11H-6, 0–5	102.43	8
12H-6, 0–5	111.93	8

Note: C_1 = methane

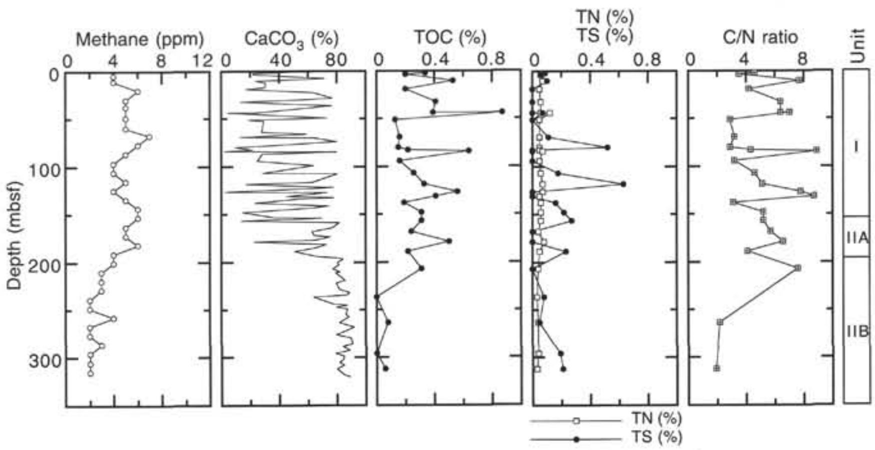

Figure 26. Methane concentration, calcium carbonate ($CaCO_3$), total organic carbon (TOC), total nitrogen (TN), and total sulfur (TS) contents, TOC/TN (C/N) ratio, and lithostratigraphic unit in Hole 981A.

Table 14. Results of headspace gas analyses of Hole 981A samples using the Hewlett Packard Series II 5890 gas chromatograph.

Core, section, interval (cm)	Depth (mbsf)	C_1 (ppm)
162-981A-		
1H-4, 0–5	4.53	4
2H-4, 0–5	11.03	4
3H-4, 0–5	20.53	6
4H-4, 0–5	30.03	5
5H-3, 0–5	38.03	5
6H-4, 0–5	49.03	5
7H-5, 0–5	60.03	5
8H-4, 0–5	68.03	7
9H-4, 0–5	77.53	6
10H-4, 0–5	87.03	5
11H-4, 0–5	96.53	4
12H-4, 0–5	106.03	4
13H-4, 0–5	115.53	5
14H-4, 0–5	125.03	4
15H-4, 0–5	134.53	5
16H-4, 0–5	144.03	6
17H-4, 0–5	153.53	6
18H-4, 0–5	163.03	5
19H-4, 0–5	172.53	5
20H-4, 0–5	182.03	6
21H-4, 0–5	191.53	4
22H-4, 0–5	201.03	4
23H-4, 0–5	210.53	3
24H-4, 0–5	220.03	3
25H-4, 0–5	229.53	3
26H-4, 0–5	239.03	2
27H-4, 0–5	248.53	2
28H-4, 0–5	258.03	4
29H-4, 0–5	267.53	2
30H-4, 0–5	277.03	2
31H-4, 0–5	286.53	3
32H-4, 0–5	296.03	2
33H-4, 0–5	305.53	2
34H-4, 0–5	314.16	2

Note: C_1 = methane

chapter), suggesting that methanogenesis is not an important process in these sediments. As a result of sulfate reduction, pore-water profiles of ammonium, phosphate, and alkalinity increase downcore (Fig. 28B–D; Table 17). Ammonium shows a strong inverse relationship with sulfate, increasing to a maximum 1.8 mM at about 55 mbsf (Fig. 28B). Dissolved phosphate is released during sulfate reduction and reaches a maximum of 47 µM at about 25 mbsf (Fig. 28C). Alkalinity increases from the top of the core to a maximum of 11 mM at about 55 mbsf (Fig. 28D).

Magnesium concentrations decrease downcore from 51 to 43 mM (Fig. 28E; Table 17). This depletion can be explained either by diffusion and chemical alteration of oceanic crust below, or by in situ alteration of volcanic material in the sediments to form clays (this point is discussed in more detail in the "Site 981" section below). Dissolved calcium shows a pattern that is typical of sediments in which sulfate reduction occurs. Calcium decreases from the top of the core to 55 mbsf, and then increases below this level (Fig. 28F; Table 17). In the zone of sulfate reduction, release of HCO_3^- can cause supersaturation of interstitial waters and precipitation of calcite, which decreases calcium concentrations. Below this level, calcium increases are probably due to the release and diffusion of calcium from the alteration of oceanic crust below. Silica increases downcore, possibly reflecting dissolution of siliceous microfossils and/or alteration of volcanic material (Fig. 28G; Table 17). Potassium generally shows little variation except for a weak minimum at 55 mbsf (Fig. 28H; Table 17).

Sodium and chloride concentrations do not show any significant trends downcore (Table 17; Fig. 28I). Salinity decreases downcore due to the removal of dissolved sulfate from the interstitial waters during sulfate reduction (Fig. 28J; Table 17; Gieskes, 1974).

Dissolved lithium increases from quite high values near the surface (45 µM) to a minimum of 25 µM at 50 mbsf, and then increases again toward the base of the core (Fig. 28K; Table 17). The lithium profile bears a strong resemblance to the calcium profile at this site (Fig. 28F). The minimum in both calcium and lithium is probably due to uptake of lithium during authigenic calcite precipitation. The increase in calcium and lithium below about 60 mbsf is related to diffusive exchange with underlying basement.

The profile of dissolved strontium concentration increases from about 100 µM near to the surface to about 350 µM at 120 mbsf (Fig. 28L; Table 17). This increase reflects the dissolution of biogenic calcite and reprecipitation of authigenic calcite, which results in a net source of strontium to pore waters because of the difference in distribution coefficients between biogenic and authigenic calcite. The moderate increase in dissolved strontium with depth reflects, therefore, the extent of calcite recrystallization in these young sediments (Baker et al., 1982).

Site 981

Site 981 has lower sedimentation rates, and a longer record was drilled at this site. Interstitial water samples were taken in every section in the top hundred meters for shore-based oxygen isotope analyses, followed by samples taken every third core to the bottom of the hole. A subset of 30 of these samples was chosen for shipboard analyses.

As at Site 980, the primary process affecting pore-water profiles of sulfate, ammonia, and alkalinity is sulfate reduction. At Site 981, sulfate has a maximal value of 25 mM near the surface and decreases to a constant 6 mM by 150 m depth (Table 18; Fig. 29A). Ammonia

Table 15. Summary of organic geochemical analyses of Hole 980A samples.

Core, section, interval (cm)	Depth (mbsf)	IC (%)	$CaCO_3$ (%)	TC (%)	TOC (%)	TN (%)	TS (%)	C/N
162-980A-								
1H-2, 70–71	2.20	2.67	22.24	3.02	0.35	0.07	0.05	5.3
1H-5, 141–142	7.41	6.98	58.14	7.25	0.27	0.05	0.00	5.3
2H-1, 39–40	9.79	8.19	68.22	8.54	0.35	0.05	0.00	7.1
2H-3, 39–40	12.79	3.37	28.07					
2H-5, 39–40	15.79	2.53	21.07	2.73	0.20	0.06	0.00	3.3
2H-5, 120–121	16.60	3.58	29.82					
3H-1, 25–26	19.15	5.89	49.06	6.08	0.19	0.04	0.08	4.2
3H-2, 25–26	20.65	4.26	35.49					
3H-3, 25–26	22.15	3.87	32.24					
3H-4, 25–26	23.65	6.81	56.73					
3H-5, 25–26	25.15	2.72	22.66	3.60	0.88	0.07	0.46	11.9
3H-6, 25–26	26.65	3.75	31.24					
3H-7, 25–26	28.15	2.87	23.91					
4H-1, 31–32	28.71	2.80	23.32	3.25	0.45	0.08	0.00	5.9
4H-1, 114–115	29.54	6.70	55.81					
4H-2, 37–38	30.27	3.80	31.65					
4H-2, 117–118	31.07	3.39	28.24	3.84	0.45	0.07	0.66	6.2
4H-3, 35–36	31.75	6.36	52.98					
4H-3, 118–119	32.58	6.20	51.65					
4H-4, 74–75	33.64	5.58	46.48					
4H-4, 120–121	34.10	5.52	45.98	5.78	0.26	0.05	0.00	5.5
4H-5, 10–11	34.50	6.36	52.98					
4H-5, 83–84	35.23	7.58	63.14					
4H-6, 36–37	36.26	1.32	11.00	1.62	0.30	0.07	0.25	4.6
4H-6, 125–126	37.15	2.76	22.99					
4H-7, 40–41	37.80	2.93	24.41	3.48	0.55	0.08	0.03	6.9
5H-1, 77–78	38.67	5.28	43.98	5.59	0.31	0.06	0.00	5.3
5H-1, 123–124	39.13	4.36	36.32					
5H-2, 55–56	39.95	7.51	62.56					
5H-2, 118–119	40.58	6.71	55.89					
5H-3, 36–37	41.26	6.25	52.06	6.80	0.55	0.07	0.03	8.4
5H-3, 127–128	42.17	8.41	70.06					
5H-4, 79–80	43.19	9.02	75.14					
5H-5, 37–38	44.27	9.26	77.14					
5H-5, 86–87	44.76	9.60	79.97	9.92	0.32	0.04	0.00	7.2
5H-6, 75–76	46.15	6.88	57.31					
5H-7, 37–38	47.27	4.97	41.40					
6H-1, 44–45	47.84	2.11	17.58	2.52	0.41	0.06	0.06	6.9
6H-2, 34–35	49.24	1.62	13.49					
6H-3, 34–35	50.74	4.90	40.82					
6H-4, 113–114	53.03	9.72	80.97					
6H-5, 37–38	53.77	10.15	84.55	10.33	0.18	0.03	0.00	5.3
6H-6, 44–45	55.34	7.95	66.22					
6H-7, 34–35	56.74	3.54	29.49					
7H-1, 34–35	57.24	6.54	54.48	6.77	0.23	0.06	0.05	3.7
7H-2, 34–35	58.74	8.29	69.06					
7H-3, 34–35	60.24	5.59	46.56					
7H-4, 34–35	61.74	7.52	62.64					
7H-5, 34–35	63.24	3.78	31.49	4.09	0.31	0.11	0.22	2.9
7H-6, 39–40	64.79	3.21	26.74					
7H-7, 39–40	66.29	3.13	26.07					
8H-1, 38–39	66.78	2.13	17.74	2.61	0.48	0.07	0.00	7.2
8H-2, 28–29	68.18	4.02	33.49	4.22	0.20	0.06	0.19	3.5
8H-3, 113–114	70.53	8.73	72.72					
8H-4, 28–29	71.18	6.73	56.06					
8H-5, 28–29	72.68	5.99	49.90					
8H-6, 99–100	74.89	5.96	49.65					
9H-2, 124–125	78.64	8.64	71.97					
9H-3, 113–114	80.03	8.09	67.39					
9H-4, 113–114	81.53	2.99	24.91	3.27	0.28	0.05	0.00	5.6
9H-5, 44–45	82.34	6.44	53.65					
9H-6, 118–119	84.58	7.13	59.39					
9H-7, 44–45	85.34	9.30	77.47					
10H-2, 118–119	88.08	3.12	25.99	3.54	0.42	0.07	0.00	6.1
10H-3, 62–63	89.02	9.45	78.72					
10H-3, 133–134	89.73	1.18	9.83	1.35	0.17	0.06	0.00	2.9
10H-4, 126–127	91.16	4.57	38.07					
10H-5, 122–123	92.62	2.67	22.24	2.89	0.22	0.06	0.77	3.5
10H-6, 118–119	94.08	2.65	22.07					
10H-7, 48–49	94.88	8.17	68.06					
11H-1, 18–119	96.08	2.62	21.82					
11H-2, 7–28	96.67	2.25	18.74	2.57	0.32	0.09	0.00	3.7
11H-2, 122–123	97.62	6.47	53.90					
11H-3, 132–133	99.22	3.47	28.91	3.61	0.14	0.05	0.00	2.7
11H-4, 117–118	100.57	5.42	45.15					
11H-5, 35–36	101.25	3.20	26.66					
11H-5, 118–119	102.08	7.62	63.47					
11H-6, 47–48	102.87	2.36	19.66	2.50	0.14	0.05	0.00	2.6
11H-6, 117–118	103.57	9.36	77.97					
11H-7, 23–24	104.13	6.14	51.15					
12H-1, 115–116	105.55	9.51	79.22	9.81	0.30	0.03	0.00	8.7
12H-2, 115–116	107.05	2.41	20.08	2.42	0.01	0.07	0.20	0.1
12H-3, 115–116	108.55	8.47	70.56					

Table 15 (continued).

Core, section, interval (cm)	Depth (mbsf)	IC (%)	$CaCO_3$ (%)	TC (%)	TOC (%)	TN (%)	TS (%)	C/N
12H-4, 115–116	110.05	7.49	62.39					
12H-5, 115–116	111.55	3.56	29.65					
12H-6, 66–67	112.56	9.82	81.80					
12H-6, 115–116	113.05	7.69	64.06	8.03	0.34	0.05	0.69	6.2
12H-7, 41–42	113.81	5.22	43.48					

Notes: IC = inorganic carbon, $CaCO_3$ = calcium carbonate, TC = total carbon, TOC = total organic carbon, TN = total nitrogen, TS = total sulfur, and C/N = total organic carbon/total nitrogen ratio.

Table 16. Summary of organic geochemical analyses of Hole 981A samples.

Core, section, interval (cm)	Depth (mbsf)	IC (%)	$CaCO_3$ (%)	TC (%)	TOC (%)	TN (%)	TS (%)	C/N
162-981A-								
1H-1, 79–80	0.79	5.80	48.3					
1H-2, 75–76	2.25	2.59	21.6	2.93	0.34	0.07	0.09	4.6
1H-3, 20–21	3.20	2.73	22.7	2.93	0.20	0.06	0.06	3.5
2H-1, 103–104	7.53	8.61	71.7					
2H-3, 34–35	9.84	2.81	23.4	3.34	0.53	0.07	0.10	7.7
2H-4, 114–115	12.14	3.68	30.7					
3H-1, 114–115	17.14	3.65	30.4					
3H-2, 104–105	18.54	2.09	17.4	2.29	0.20	0.05	0.00	4.2
3H-5, 46–47	22.46	7.64	63.6					
4H-2, 100–101	28.00	9.22	76.8					
4H-3, 104–105	29.54	7.25	60.4					
4H-5, 100–101	32.50	1.61	13.4	2.02	0.41	0.06	0.00	6.4
5H-1, 107–108	36.07	9.18	76.5					
5H-6, 107–108	42.54	2.70	22.5	3.09	0.39	0.06	0.00	6.4
5H-6, 144–145	42.91	0.56	4.7	1.43	0.87	0.12	0.07	7.0
6H-4, 34–35	49.34	8.81	73.4					
6H-5, 34–35	50.84	2.31	19.2	2.44	0.13	0.05	0.00	2.9
6H-6, 34–35	52.34	3.50	29.2					
8H-1, 33–34	63.83	3.38	28.2					
8H-2, 90–91	65.90	7.04	58.6					
8H-4, 103–104	69.03	1.58	13.2	1.74	0.16	0.05	0.11	3.2
8H-5, 33–34	69.83	7.67	63.9					
9H-1, 117–118	74.17	9.60	80.0					
9H-5, 67–68	79.67	1.19	9.9	1.34	0.15	0.05	0.52	2.9
9H-7, 40–41	82.40	2.59	21.6	2.81	0.22	0.05	0.00	4.3
10H-1, 138–139	83.88	0.28	2.3	0.92	0.64	0.07	0.00	8.9
10H-2, 103–104	85.03	9.60	80.0					
10H-3, 102–103	86.52	3.40	28.3					
11H-2, 94–95	94.44	3.00	25.0	3.16	0.16	0.05	0.00	3.2
11H-5, 58–59	98.58	7.69	64.1					
12H-4, 103–104	107.03	3.41	28.4	3.67	0.26	0.06	0.18	4.6
12H-4, 130–131	107.30	9.68	80.6					
13H-4, 108–109	116.58	7.57	63.1					
13H-5, 108–109	118.08	2.10	17.5	2.43	0.33	0.07	0.63	5.1
14H-1, 91–92	121.41	9.32	77.6					
14H-4, 112–113	126.12	0.30	2.5	0.86	0.56	0.07	0.00	7.8
14H-5, 60–61	127.10	8.84	73.6					
15H-1, 131–132	131.31	5.38	44.8	5.79	0.41	0.05	0.00	8.7
15H-2, 84–85	132.34	9.34	77.8					
15H-3, 90–91	133.90	6.30	52.5					
15H-6, 50–51	138.00	2.81	23.4	3.00	0.19	0.06	0.16	3.1
16H-2, 51–52	141.51	8.98	74.8					
16H-3, 59–60	143.09	7.53	62.7					
16H-6, 86–87	147.86	1.80	15.0	2.11	0.31	0.06	0.22	5.2
17H-3, 93–94	152.93	4.44	37.0					
17H-4, 76–77	154.26	8.38	69.8					
17H-6, 11–12	156.61	1.68	14.0	1.99	0.31	0.06	0.27	5.2
18H-1, 39–40	158.89	9.81	81.7					
18H-4, 101–102	164.01	9.24	77.0					
18H-7, 35–36	167.85	7.50	62.5	7.74	0.24	0.04	0.00	5.7
19H-3, 93–94	171.93	7.73	64.4					
19H-4, 114–115	173.64	9.05	75.4					
19H-6, 116–117	176.66	7.89	65.7					
20H-1, 111–112	178.61	2.73	22.7	3.23	0.50	0.08	0.00	6.6
20H-3, 104–105	181.54	8.74	72.8					
20H-5, 114–115	184.64	7.87	65.6					
21H-2, 59–69	189.09	6.08	50.6	6.30	0.22	0.05	0.23	4.1
21H-5, 110–111	194.10	8.06	67.1					
21H-6, 106–107	195.56	9.70	80.8					
22H-1, 70–21	197.20	10.17	84.7					
22H-3, 70–71	200.20	9.65	80.4					
22H-5, 70–71	203.20	9.77	81.4					
23H-1, 116–117	207.16	9.28	77.3	9.59	0.31	0.04	0.00	7.6
23H-3, 116–117	210.16	9.87	82.2					
23H-4, 58–59	211.08	9.52	79.3					
24H-3, 59–60	219.09	10.32	86.0					
24H-5, 59–60	222.09	9.54	79.5					
25H-3, 58–59	228.58	9.80	81.6					
25H-5, 58–59	231.58	10.68	89.0					
26H-1, 36–37	234.86	10.39	86.5					

Table 16 (continued).

Core, section, interval (cm)	Depth (mbsf)	IC (%)	$CaCO_3$ (%)	TC (%)	TOC (%)	TN (%)	TS (%)	C/N
26H-2, 58–59	236.58	7.68	64.0	7.65	0.00	0.03	0.08	0.0
26H-7, 32–33	243.82	9.32	77.6					
27H-1, 105–106	245.05	10.47	87.2					
27H-3, 58–59	247.58	9.61	80.1					
27H-4, 116–117	249.66	10.51	87.5					
28H-1, 113–114	254.63	10.36	86.3					
28H-3, 113–114	257.63	10.65	88.7					
29H-1, 60–61	263.60	9.82	81.8	9.90	0.08	0.04	0.05	2.2
29H-4, 101–102	268.51	11.06	92.1					
29H-7, 10–11	272.10	10.37	86.4					
30H-3, 113–114	276.63	9.53	79.4					
30H-5, 109–110	279.59	10.78	89.8					
31H-3, 62–63	285.62	10.95	91.2					
31H-5, 60–61	288.60	10.08	84.0					
32H-1, 95–96	292.45	10.67	88.9					
32H-3, 98–99	295.48	9.50	79.1	9.47	0.00	0.04	0.19	0.0
32H-5, 116–117	298.66	10.21	85.0					
33H-1, 92–93	301.92	10.17	84.7					
33H-3, 93–94	304.93	9.81	81.7					
33H-5, 112–113	308.12	10.21	85.0					
34H-1, 120–121	311.70	9.59	79.9	9.65	0.06	0.03	0.21	1.9
34H-5, 117–118	316.80	10.21	85.0					
34H-7, 80–81	319.43	10.69	89.0					

Notes: IC = inorganic carbon, $CaCO_3$ = calcium carbonate, TC = total carbon, TOC = total organic carbon, TN = total nitrogen, TS = total sulfur, and C/N = total organic carbon/total nitrogen ratio.

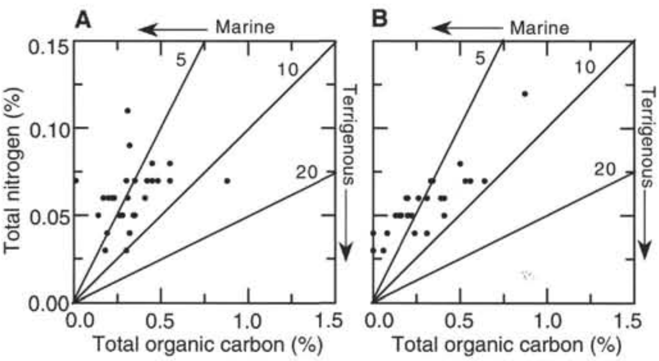

Figure 27. Total organic carbon vs. total nitrogen in (A) Hole 980A and (B) Hole 981A. Lines show C/N ratios of 5, 10, and 20.

has a minimum near the surface of 216 µM and increases to a level of 2007 µM by 220 m (Fig. 29C; Table 17). Alkalinity increases linearly with depth from 4.7 to 10.9 mM at the bottom of the hole, perhaps indicating some other source of alkalinity below the region of major sulfate reduction (Fig. 29D; Table 17). As at Site 980, the occurrence of sulfide minerals accompanies sulfate reduction (see "Lithostratigraphy" section, this chapter). The formation of iron sulfide minerals in the zone of sulfate reduction also effects the magnetic properties of the sediments (see "Paleomagnetism" section, this chapter).

Similar to Site 980, magnesium concentrations decrease rapidly in the top 150 m of core at Site 981 (Fig. 29B; Table 17), and then remain relatively constant at 33 mM. Decreasing magnesium concentrations is a common feature of deep-sea pore-water profiles and can be attributed to either chemical alteration of oceanic crust or to the alteration of volcanic material in the sediments. We suggest that the latter is the more important of the two processes at Site 981 for reasons outlined below. First, the nature of basement underlying the Feni Drift is uncertain, although Site 117 on the Rockall Plateau (1038 m water depth) recovered altered olivine basalt at 311 mbsf that may represent shallow-water extrusion (Sabine, 1972). Second, if the magnesium simply reflected a diffusive gradient with oceanic crust some 1 to 5 km below, we would not expect to find such a sharp drop in the upper 150 m followed by relatively constant values from 150 to 280 mbsf. Third, the magnesium profile bears a remarkable resemblance to sulfate (Fig. 29B), suggesting that the decline in magnesium may be linked to the process of sulfate reduction. Lastly, the decrease in magnesium in the upper 150 m corresponds with a rise in the abundance of smectite and chlorite (see "Lithostratigraphy" section, this chapter).

We suggest, therefore, that the rapid decline in magnesium is due to magnesium uptake during the chemical alteration of volcanic material to smectite in the sediments. A notable increase in the abundance of ash and volcanic debris occurs in the upper 160 m because it is delivered to Site 981 by ice rafting, which increased markedly following the intensification of Northern Hemisphere glaciation in the late Pliocene. This event is marked by an increase in magnetic susceptibility at about 160 m (see "Physical Properties" section, this chapter). A puzzling question, however, is why the magnesium profile bears such a strong resemblance to sulfate. Drever (1971) suggested that the nearly perfect parallelism between magnesium and sulfate may be explained by reaction of hydrogen sulfide with iron in chlorite or other clays to produce iron sulfides. This reaction is accompanied by replacement of magnesium for iron in the clay minerals. A similar relationship between sulfate and magnesium was observed in pore-water profiles from DSDP Site 116 on the Rockall Plateau (Manheim et al., 1972).

Calcium values show a depletion in the upper 90 m from 9.3 mM at the surface to a 4.2-mM minima (Fig. 29E; Table 18), suggesting that sulfate reduction has led to carbonate saturation and the precipitation of inorganic calcite. Below 100 m, calcium values increase again, reaching a maximum value of 11 mM at the bottom of the hole. It is likely that this reflects the release of calcium during alteration of basaltic basement below.

Dissolved silica increases with depth from 466 µM at the surface to 1132 µM at the bottom (Fig. 29F; Table 18). As at Site 980, this probably reflects alteration of volcanic ash and/or dissolution of siliceous microfossils. However, unlike Site 980, phosphate concentrations are highest at the surface (18.5 µM) and generally decrease with depth to minimum values of 5.42 µM (Fig. 29G; Table 18). The brief excursion in Cores 162-981C-2X and 3X is reproducible and appears to be a real feature. Phosphate is released during sulfate reduction (Equation 1), which implies that phosphate must be removed by mineral precipitation (e.g., $Ca_3[PO_4]_2$, $Fe_3[PO_4]_3$, or $MgNH_4PO_4$) to explain the decrease with depth (Gieskes, 1983). Potassium shows a slight decrease from 13 to 11.5 mM at 50 mbsf and then remains vari-

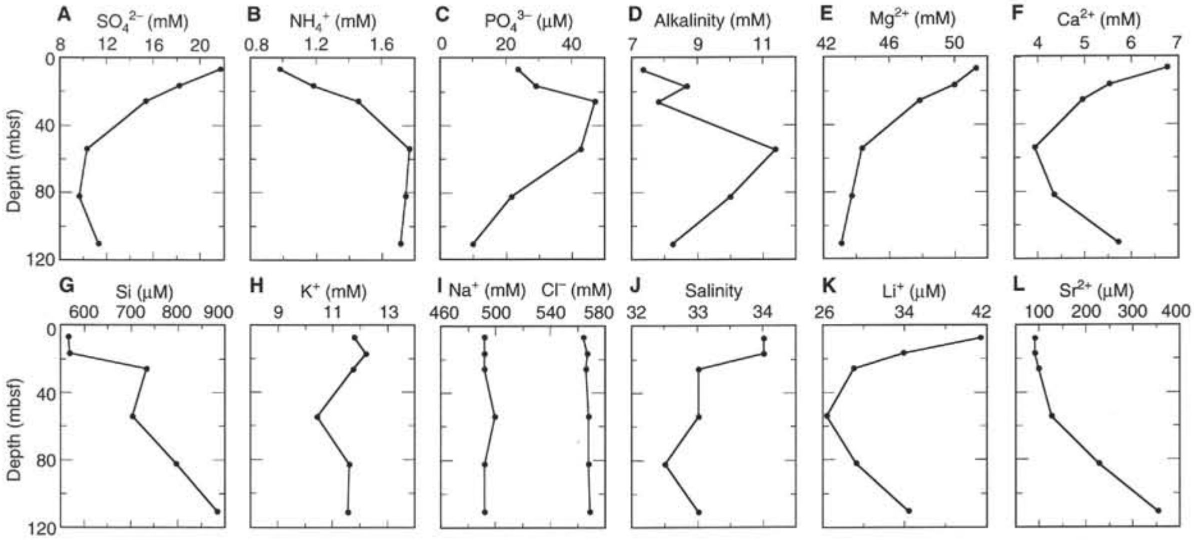

Figure 28. Vertical profiles of interstitial sulfate (**A**), ammonium (**B**), phosphate (**C**), alkalinity (**D**), magnesium (**E**), calcium (**F**), silica (**G**), potassium (**H**), sodium and chloride (**I**), salinity (**J**), lithium (**K**), and strontium (**L**) concentrations in Hole 980A.

Table 17. Composition of interstitial waters in Hole 980A.

Core, section, interval (cm)	Depth (mbsf)	Na (mM)	K (mM)	Li (μM)	Mg (mM)	Ca (mM)	Sr (μM)	Cl (mM)	SO_4 (mM)	NH_4 (μM)	Si (μM)	PO_4 (μM)	pH	Alkalinity (mM)	Salinity
162-980A-															
1H-5, 145–150	7.45	487	11.8	41.3	51.3	6.8	90	564	21.6	971	563	23.6	7.80	7.296	34.0
2H-5, 145–150	16.85	488	12.2	33.8	49.9	5.5	89	566	18.2	1174	567	29.2	7.44	8.649	34.0
3H-5, 145–150	26.35	486	11.7	28.9	47.8	4.9	97	565	15.2	1447	730	47.1	7.54	7.764	33.0
6H-5, 145–150	54.85	492	10.4	26.2	44.3	3.9	126	567	10.2	1765	700	42.8	7.62	11.369	33.0
9H-5, 145–150	83.35	489	11.6	29.2	43.6	4.3	227	567	9.6	1741	795	21.5	7.82	9.965	32.5
12H-5, 145–150	111.85	490	11.5	34.3	43.0	5.7	353	568	11.2	1708	883	9.76	7.49	8.192	33.0

Table 18. Composition of interstitial waters in Hole 981C.

Core, section, interval (cm)	Depth (mbsf)	Na (mM)	K (mM)	Li (μM)	Mg (mM)	Ca (mM)	Sr (μM)	Cl (mM)	SO_4 (mM)	NH_4 (μM)	Si (μM)	PO_4 (μM)	pH	Alkalinity (mM)	Salinity
162-981C-															
1H-4, 140–145	5.95	473	13.2	33.0	53.2	9.3	94	561	25.00	216	466	18.50	7.58	4.670	34.5
2H-4, 140–145	11.65	476	13.2	30.2	50.7	7.9	104	558	24.10	462	480	12.30	7.78	5.380	34.5
3H-4, 140–145	21.15	478	12.4	27.5	47.9	6.3	118	558	20.20	765	625	10.50	7.77	5.780	34.0
4H-4, 140–145	30.65	478	12.8	26.2	47.2	6.1	141	561	18.10	794	680	17.30	7.90	5.970	34.0
5H-4, 140–145	40.15	471	13.3	26.5	46.4	5.1	159	557	15.20	1068	662	12.90	7.90	6.340	34.0
6H-4, 140–145	49.65	474	12.8	26.6	45.3	4.8	190	559	14.30	1213	536	12.90	7.82	5.599	34.0
7H-4, 140–145	59.15	470	11.6	26.9	44.0	5.1	194	556	11.90	1278	636	12.30	7.93	6.948	34.0
8H-4, 140–145	68.65	473	11.2	27.8	42.5	5.2	256	557	11.30	1112	695	12.60	7.85	7.439	33.0
9H-4, 140–145	78.15	480	11.5	28.5	41.0	5.0	285	563	10.20	1343	753	12.00	7.91	7.317	32.2
10H-4, 140–145	87.65	480	12.1	28.7	38.7	4.2	311	560	9.06	1480	736	10.20	7.96	6.330	32.2
11H-4, 140–145	97.15	479	11.5	30.4	38.4	5.2	378	560	8.61	1372	777	9.58	7.90	7.550	32.2
12H-4, 140–145	106.65	477	12.1	32.5	38.6	5.6	440	562	7.77	1545	815	8.39	7.89	7.430	32.2
13H-6, 140–145	119.15	477	11.5	35.1	36.4	5.5	507	558	7.03	1646	875	11.10	7.80	7.840	32.2
14H-5, 140–145	127.15	479	11.4	36.3	35.7	5.8	572	560	6.71	1653	815	7.80	7.90	7.930	32.2
15H-5, 140–145	136.65	479	11.9	40.2	34.3	5.7	638	557	6.86	1494	892	8.10	7.82	7.710	32.2
16H-4, 140–145	144.65	479	11.1	41.5	35.0	6.2	687	561	5.99	1523	878	8.10	7.78	8.390	32.2
17H-4, 140–145	154.15	478	11.7	44.7	34.3	6.2	724	558	6.07	1827	851	8.99	7.70	8.189	32.2
18H-4, 140–145	163.65	481	11.3	47.4	33.2	6.0	779	559	6.03	1624	950	8.39	7.52	8.170	32.2
19H-4, 140–145	173.15	476	12.1	50.4	34.1	6.4	826	557	5.88	1956	987	9.58	7.41	8.640	32.2
20H-4, 140–145	182.65	477	12.1	54.4	33.6	6.6	924	558	5.65	1458	974	7.20	7.68	9.040	32.2
21H-4, 140–145	192.15	476	12.0	58.8	34.1	6.9	962	559	5.34	1971	991	6.61	7.72	8.940	32.2
22H-4, 140–145	201.65	478	11.9	62.0	33.0	7.3	1046	559	5.53	1956	949	6.61	7.73	9.630	32.2
23H-4, 140–145	211.15	475	11.5	71.6	33.2	8.0	1232	559	5.03	2007	973	6.91	7.72	10.220	32.2
24H-4, 140–145	220.65	477	12.2	66.3	33.1	7.4	1130	559	5.61	1956	979	8.10	7.70	9.600	32.2
25H-4, 140–145	230.15	472	12.6	78.1	34.5	8.5	1294	560	5.54	1863	1032	6.01	7.75	9.830	32.2
26H-4, 140–145	239.65	476	11.9		33.8	9.0	1304	562	6.00	1855	1025	6.91	7.62	10.480	32.2
27H-4, 140–145	249.15	471	11.8	95.9	34.7	10.0	1422	562	5.73		1006	5.42	7.30	10.510	32.2
28H-4, 140–145	258.65	476	11.7	109.7	32.7	9.7	1470	561	6.00	1581	1029	5.42	7.77	10.210	32.2
29H-5, 140–145	269.65	475	11.5	127.8	32.5	11.0	1516	562	5.51	1819	1062	6.01	7.59	10.560	32.2
30H-4, 140–145	277.65	471	12.2	148.5	33.6	11.0	1558	561	6.09	1725	1132	5.42	7.78	10.940	32.2

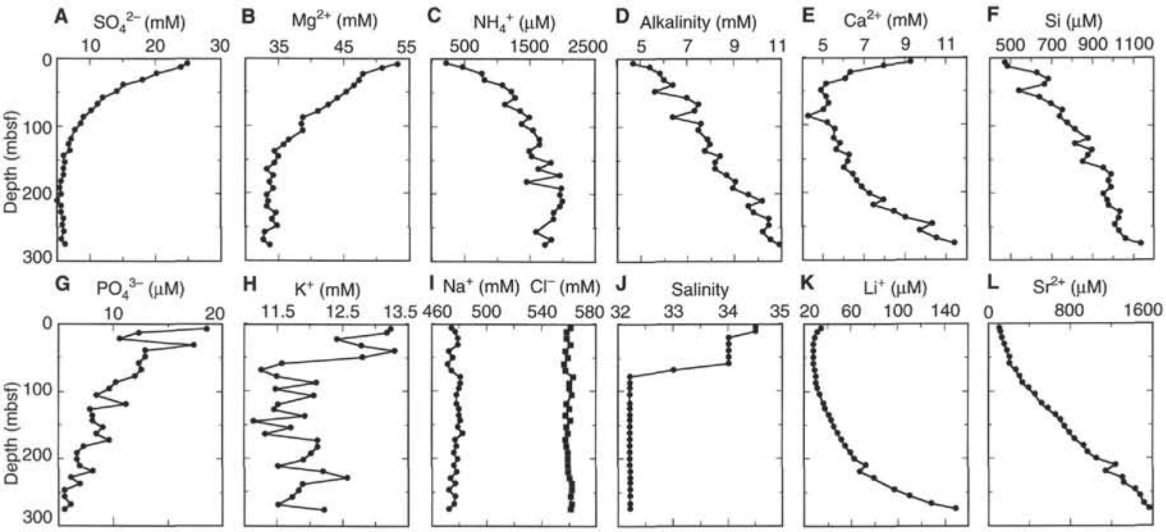

Figure 29. Vertical profiles of interstitial sulfate (**A**), magnesium (**B**), ammonium (**C**), alkalinity (**D**), calcium (**E**), silica (**F**), phosphate (**G**), potassium (**H**), sodium and chloride (**I**), salinity (**J**), lithium (**K**), and strontium (**L**) concentrations in Hole 981C.

able, but with no distinct trends, to the bottom of the hole (Fig. 29H; Table 18).

The profiles of sodium and chloride are essentially unchanged downcore (Fig. 29I; Table 18), although salinity decreases from 34.5 to 32.2 in the top 80 m of the hole (Fig. 29J; Table 18), primarily reflecting the rapid removal of sulfate in the zone of sulfate reduction. Lithium generally increases with depth, suggesting a diffusive gradient with basalt below (Fig. 29K; Table 18). Strontium increases from a value of about 100 μM near the top of the hole to >1400 μM at the bottom (Fig. 29L; Table 18). The increase in strontium with depth primarily reflects the recrystallization of biogenic calcite.

PHYSICAL PROPERTIES

The shipboard physical properties program at Site 980 and 981 included nondestructive continuous measurements of bulk density, bulk magnetic susceptibility, compressional wave (*P*-wave) velocity, and natural gamma radiation on whole sections of all cores from Sites 980 and 981 using the multisensor track (MST). Thermal conductivity, *P*-wave velocity, and undrained shear strength measurements were made, on average, at one per section. Index properties measurements were made at an average of two samples per working section in all cores of Hole 980A and in the upper four cores of Hole 980C. In Hole 981A, sampling frequency was reduced to one per section below 24 mbsf and one per two sections below 200 mbsf because of the very homogeneous nature of the sediments (nannofossil ooze; see "Lithostratigraphy" section, this chapter). Samples were generally taken at intervals where thermal conductivity measurements were made and where lithologic changes occurred. Methodology is discussed in the "Explanatory Notes" chapter (this volume).

Density and Related Properties

A high-resolution record of GRAPE wet bulk density and index properties data are presented in Tables 19 and 20 and Figures 30 and 31. Values determined from Method B (using wet sediment volume) were unreliable. The methodological differences between Methods B and C are discussed in the "Explanatory Notes" chapter (this volume). In Holes 980A and 981A, the gravimetric bulk density values are consistently higher than the GRAPE density by 0.2 g/cm^3, except where porosity is more than 70% in Hole 980A (see Fig. 30). This discrepancy between GRAPE and gravimetric bulk density values was observed throughout Leg 162 and is discussed in the "Explanatory Notes" chapter (this volume).

Magnetic Susceptibility

Magnetic susceptibility signals at Sites 980 and 981 show lower frequency variations in the upper 80 and 50 mbsf, respectively, and higher frequency variations below (see Figs. 30 and 31), most likely corresponding to varying terrigenous input from the continents surrounding the North Atlantic; high magnetic susceptibility and natural gamma radiation values show a positive correlation with clay-rich zones, while the amount of carbonate correlates inversely with magnetic susceptibility (see "Lithostratigraphy" section, this chapter).

Compressional Velocity

The sonic transducer pair T1 (*z*-direction) of the digital sound velocimeter (DSV) for split cores, was used to a depth of approximately 60 mbsf in cores from Hole 980A, and to a depth of approximately 30 mbsf in cores from Hole 981A. Sediment became too consolidated below these depths to use the DSV. Below these depths the Hamilton Frame velocimeter was used for sonic measurements in the *x* direction while the core was still in the liner. *P*-wave velocities ranged from 1500 to 1680 m/s, with an average of 1560 m/s in Hole 980A (see Table 21), and from 1500 to 1690 m/s, with an average of 1570 m/s in Hole 981A (see Table 22). Below about 80 mbsf at Site 980, the sediments were markedly more fractured, which may account for the increased scatter in the data. In the upper 45 m the velocity is relatively constant, with an average value of 1530 m/s. Between 45 to 80 m, velocities show an increase with depth after which the values remain relatively constant at an average value of about 1600 m/s (Fig. 30). In Figures 30 and 31 the velocities measured discretely and with the PWL are superimposed; the two sets of values coincide well.

A gradual downhole increase in velocities is observed to 80 mbsf at Site 980 which corresponds to the base of seismic Unit FE-I (Fig. 30). An increase in velocity is not as readily apparent at the correlative depth (50 mbsf) at Site 981 (Fig. 31). However, a small increase in velocity is seen just above 160 mbsf, corresponding with seismic Reflector R2. At about 278 mbsf velocities increase abruptly, corre-

Table 19. Index properties of samples from Holes 980A and 980C.

Core, section, interval (cm)	Depth (mbsf)	Water content (wet%)	Water content (dry%)	Bulk density Method B (g/cm³)	Bulk density Method C (g/cm³)	Grain density Method B (g/cm³)	Grain density Method C (g/cm³)	Dry density Method B (g/cm³)	Dry density Method C (g/cm³)	Porosity Method B (g/cm³)	Porosity Method C (g/cm³)	Void ratio Method B	Void ratio Method C
162-980A-													
1H-1, 75–77	0.75	49.264	97.099		1.500		2.731		0.761		72.130		2.588
1H-2, 75–77	2.25	48.119	92.751		1.521		2.761		0.789		71.426		2.500
1H-3, 35–37	3.35	34.898	53.605		1.725		2.721		1.123		58.745		1.424
1H-3, 115–117	4.15	52.880	112.223		1.448		2.701		0.682		74.741		2.959
1H-4, 75–77	5.25	43.663	77.504		1.583		2.740		0.892		67.460		2.073
1H-5, 35–37	6.35	41.113	69.816		1.641		2.829		0.966		65.845		1.928
1H-5, 115–117	7.15	52.907	112.345		1.461		2.802		0.688		75.446		3.073
1H-6, 75–77	8.25	52.695	111.396		1.449		2.690		0.685		74.523		2.925
1H-7, 12–14	9.12	42.504	73.926		1.592		2.697		0.915		66.060		1.946
2H-1, 35–37	9.75	48.616	94.612		1.520		2.804		0.781		72.140		2.589

Only part of this table is reproduced here. The entire table appears on the CD-ROM (back pocket).

Table 20. Index properties of samples from Hole 981A.

Core, section, interval (cm)	Depth (mbsf)	Water content (wet%)	Water content (dry%)	Bulk density Method B (g/cm³)	Bulk density Method C (g/cm³)	Grain density Method B (g/cm³)	Grain density Method C (g/cm³)	Dry density Method B (g/cm³)	Dry density Method C (g/cm³)	Porosity Method B (g/cm³)	Porosity Method C (g/cm³)	Void ratio Method B	Void ratio Method C
162-981A-													
1H-1, 103–105	1.03	46.861	88.185	1.556	1.537	2.869	2.748	0.827	0.817	71.178	70.284	2.470	2.365
1H-2, 38–40	1.88	43.842	78.068	1.591	1.582	2.798	2.750	0.893	0.888	68.075	67.695	2.132	2.095
1H-2, 118–120	2.68	40.800	68.918	1.632	1.599	2.759	2.607	0.966	0.947	64.989	63.688	1.856	1.754
1H-3, 115–117	4.15	36.729	58.049	1.665	1.669	2.614	2.630	1.054	1.056	59.698	59.842	1.481	1.490
1H-4, 36–38	4.86	34.726	53.200	1.674	1.680	2.527	2.547	1.093	1.097	56.756	56.948	1.312	1.323
1H-4, 123–125	5.73	36.966	58.644	1.648	1.638	2.561	2.523	1.038	1.032	59.446	59.085	1.466	1.444
2H-1, 35–37	6.85	41.811	71.853	1.680	1.606	3.107	2.712	0.977	0.934	68.544	65.540	2.179	1.902
2H-1, 115–117	7.65	47.636	90.971	1.440	1.448	2.281	2.320	0.754	0.758	66.945	67.321	2.025	2.060
2H-2, 35–37	8.35	47.321	89.829	1.555	1.546	2.906	2.848	0.819	0.814	71.813	71.406	2.548	2.497
2H-2, 115–117	9.15	32.938	49.115	1.675	1.667	2.433	2.410	1.123	1.118	53.839	53.601	1.166	1.155

Only part of this table is reproduced here. The entire table appears on the CD-ROM (back pocket).

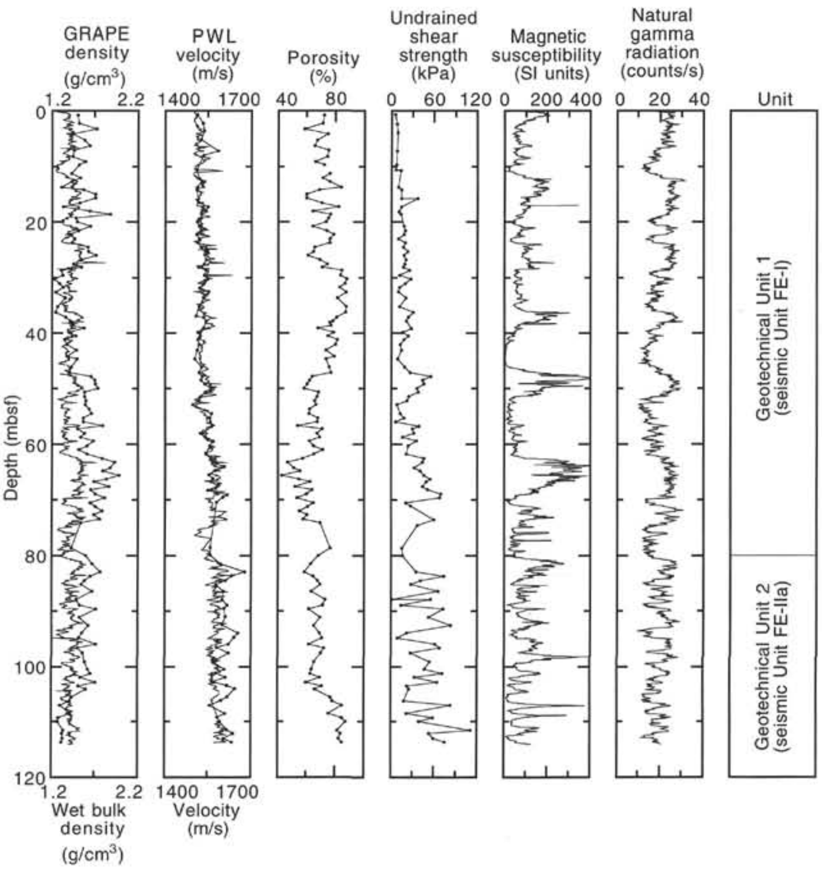

Figure 30. Data from Hole 980A: GRAPE bulk density (thin line) and gravimetric bulk density (Method C; line with dots), PWL velocity (thin line) and split-core velocity (line with dots), porosity, undrained shear strength, magnetic susceptibility, and natural gamma radiation.

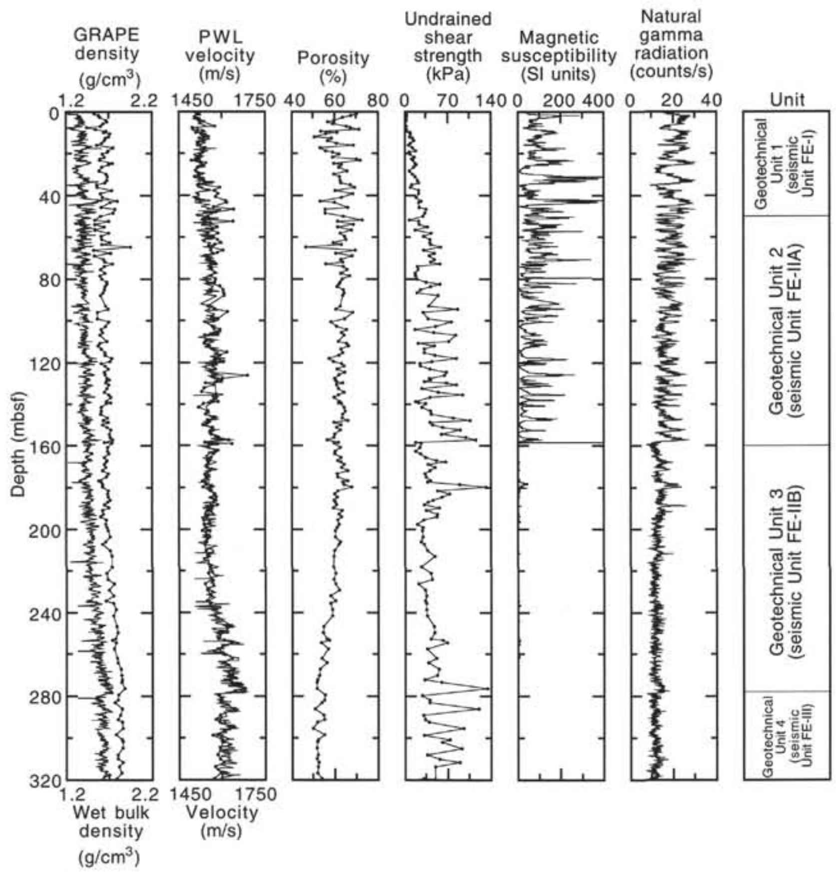

Figure 31. Data from Site 981: GRAPE bulk density (thin line) and discrete bulk density (Method C; line with dots), PWL velocity (thin line) and discrete velocity (thick line with dots), porosity, undrained shear strength, magnetic susceptibility, and natural gamma radiation.

Table 21. Compressional-wave velocity measurements from Hole 980A.

Core, section, interval (cm)	Depth (mbsf)	Velocity (m/s)	Temperature (°C)	Direction
162-980A-				
1H-1, 68–75	0.68	1512	22.0	z
1H-2, 68–75	2.18	1532	21.3	z
1H-3, 56–63	3.56	1537	21.2	z
1H-4, 63–70	5.13	1525	21.6	z
1H-5, 125–132	7.25	1585	21.3	z
1H-6, 46–53	7.96	1533	21.5	z
2H-1, 116–123	10.56	1510	22.3	z
2H-2, 129–136	12.19	1520	22.2	z
2H-3, 30–37	12.70	1528	22.3	z

Note: For explanation of measurement directions, see "Explanatory Notes" chapter (this volume).

Only part of this table is reproduced here. The entire table appears on the CD-ROM (back pocket).

Table 22. Compressional-wave velocity measurements from Hole 981A.

Core, section, interval (cm)	Depth (mbsf)	Velocity (m/s)	Temperature (°C)	Direction
162-981A-				
1H-1, 102–109	1.02	1513	19.9	z
1H-2, 119–125	2.69	1506	19.9	z
1H-3, 115–122	4.15	1522	19.7	z
1H-3, 35–42	3.35	1522	20.2	z
1H-3, 122–129	4.22	1527	20.1	z
2H-1, 35–42	6.85	1577	20.1	z
2H-1, 115–122	7.65	1497	20.0	z
2H-2, 34–41	8.34	1502	19.5	z
2H-2, 115–122	9.15	1517	19.6	z

Note: For explanation of measurement directions, see "Explanatory Notes" chapter (this volume).

Only part of this table is reproduced here. The entire table appears on the CD-ROM (back pocket).

sponding with seismic Reflector R3 (see "Seismic Stratigraphy" section, this chapter).

Natural Gamma Radiation

The natural gamma radiation record shows periodic increases (see Figs. 30 and 31) and, like magnetic susceptibility, the cyclic patterns appear to correspond to variations in input of terrigenous material (see "Lithostratigraphy" section, this chapter), with lower frequency variations above 50 mbsf and higher frequency variations between 50 and 160 mbsf at Site 981. Below 160 mbsf, activity shows less scatter about a lower mean with a small jump in values centered around 278 mbsf.

Shear Strength

In the upper 45 m of Hole 980A, shear strength increases mildly with depth with very little scatter (Table 23; Fig. 30). Between 45 and 80 m the strength shows more variability with peaks, correlating well with high magnetic susceptibility and natural gamma radiation values. In Hole 981A there is a general increase in strength downhole (Table 24; Fig. 31). Between 50 and 160 mbsf, more variability in the strength is observed which corresponds with seismic Unit FE-IIa (see "Seismic Stratigraphy" section, this chapter). Below this, strength is relatively constant with the downsection transition into relatively pure nannofossil ooze (see "Lithostratigraphy" section, this chapter). Below about 275 mbsf, the top of seismic Unit FE-III, strength values again become more variable.

Heat Flow

Fifteen downhole temperature measurements with the APC temperature tool were taken in Hole 981C between 25 mbsf and 186 mbsf. In addition, thermal conductivity was measured in the sediment cores of Holes 981A and 981C at intervals of 2–3 m. The objective was to investigate the potential geothermal response to Holocene changes in bottom-water temperature, and to establish the local heat flow.

Thermal conductivity measurements (Table 25) from Holes 981A and 981C were normalized for three different needle probes, using the control measurements taken in the red rubber standard for each run (see "Explanatory Notes" chapter, this volume). Data from Holes 981A and 981C were then combined into a single data set using the meters composite depth (mcd) scale (Fig. 32A). The spliced data, compared with GRAPE density data from Hole 981C, also in composite depth, illustrates that thermal conductivity is mainly controlled by bulk density variations (Fig. 32A). In order to match the depth below seafloor of thermal conductivity data measured in cores with downhole temperature measurements, the spliced thermal conductivity data were depth-corrected (see "Explanatory Notes" chapter, this volume).

The APC temperature tool yielded no useful results above 70 mbsf (Cores 156-981C-3H through 7H; Fig. 33A) because the extremely soft nature of the sediment allowed movement of the tool and associated frictional heat disturbances. Of the 10 measurements between 72 and 186 mbsf, four measurements were of poor quality (Cores 162-981C-8H, 9H, 11H, and 12H), three were of acceptable quality (Cores 162-981C-10H, 13H, and 14H), and three were of good quality (Cores 162-981C-16H, 18H, and 20H). The thermal conductivity data required for the temperature evaluation were taken from the corrected data in Figure 32B. The measurements between 72 and 186 mbsf yielded a thermal gradient of 5.1°C/100 m (Fig. 34). The estimated errors vary between 0.5° and 0.1°C and decrease downhole. Depth errors are in the order of ±0.5 m.

We measured bottom-water temperatures 10 times during five runs (Cores 981C-3H, 4H, 9H, 10H, and 16H), leaving the tool about 20 m above the seafloor for approximately 10 min before and after piston coring. Equilibration curves yielded apparent bottom-water temperatures between 2.90° and 3.23°C (Table 26). The four best bottom-water records, considered most reliable and representative, are illustrated in Figure 33L and 33M. Bottom-water temperatures are assumed to be the lowest temperatures in the sediment-water column system. Convection or circulation within the drill string from downhole or from the ship pumps, respectively, would mix the bottom water with warmer water. The data therefore suggest a bottom-water temperature of 2.9° ± 0.1°C.

Geotechnical Stratigraphy

At Sites 980 and 981, intervals of high magnetic susceptibility and natural gamma radiation values represent higher abundances of magnetic minerals and higher clay concentration in the sediments. Therefore, the peaks suggest periods with increased terrigenous input from the continents surrounding the North Atlantic vs. pelagic carbonate-rich sedimentation (see "Lithostratigraphy" section, this chapter). The frequency and amplitude changes at 80 and 50 mbsf at Sites 980 and 981, respectively, occur at around 0.9 Ma (see "Biostratigraphy" and "Paleomagnetism" sections, this chapter). These changes probably reflect changes in the character of glaciation with smaller terrigenous input but more frequent glacial/interglacial cycles prior to 0.9 Ma, and greater terrigenous input but long frequency glacial/interglacial cycles after 0.9 Ma. These climatic changes generate the fluctuations in sedimentation and physical properties that give rise to the seismic reflectors.

The different physical property trends define three geotechnical units (Figs. 30, 31). Geotechnical Unit G1 (0–80 mbsf at Site 980; 0–50 mbsf at Site 981) is represented by longer period variations in magnetic susceptibility and natural gamma radiation, and lower, constant values in sediment strength and velocity, while porosity and bulk density show more fluctuations. Geotechnical Unit G2 (below 80 mbsf at Site 980; 50–160 mbsf at Site 981) is represented by shorter period variations in magnetic susceptibility and natural gamma radiation, increased values of velocity, and a marked scatter in strength. Porosity and density values show less scatter. Geotechnical Units G1

Table 23. Shear strength measurements from Hole 980A.

Core, section, interval (cm)	Depth (mbsf)	Peak strength (kPa)	Residual (kPa)	Spring no.
162-980A-				
1H-1, 69–70	0.69	5.9	3.4	1
1H-2, 85–86	2.35	8.7	5.1	1
1H-3, 89–90	3.89	9.2		1
1H-5, 128–129	7.28	8.5	3.2	1
2H-1, 36–37	9.76	8.0	5.3	1
2H-1, 120–121	10.60	6.8	3.1	1
2H-1, 132–133	10.72	13.8	10.2	1
2H-3, 136–137	13.76	10.1	6.4	1
2H-4, 36–37	14.26	14.2	10.4	1

Only part of this table is reproduced here. The entire table appears on the CD-ROM (back pocket).

Table 24. Strength measurements from Hole 981A.

Core, section, interval (cm)	Depth (mbsf)	Peak strength (kPa)	Spring no.
162-981A-			
1H-1, 103	1.03	2.3	1
1H-2, 37	1.87	3.5	1
1H-2, 119	2.69	2.1	1
1H-3, 115	4.15	2.0	1
1H-3, 36	3.36	2.7	1
1H-3, 123	4.23	2.8	1
2H-1, 35	6.85	2.7	1
2H-1, 115	7.65	1.3	1
2H-2, 35	8.35	2.5	1

Only part of this table is reproduced here. The entire table appears on the CD-ROM (back pocket).

Table 25. Thermal conductivity measurements (corrected for drift) from Holes 980A, 981A, and 981C.

Core, section, interval (cm)	Depth (mbsf)	Thermal conductivity (W/[m·K])	Standard error (W/[m·K])
162-980A-			
1H-1, 75	0.75	1.172	0.00283
1H-2, 75	2.25	1.027	0.00396
1H-4, 75	5.25	1.056	0.00388
3H-1, 35	19.25	1.068	0.00209
3H-5, 35	25.25	1.159	0.00290
3H-7, 20	28.10	1.178	0.01044
4H-1, 35	28.75	1.067	0.00339
4H-3, 35	31.75	1.128	0.00360
4H-5, 35	34.75	1.095	0.00348

Only part of this table is reproduced here. The entire table appears on the CD-ROM (back pocket).

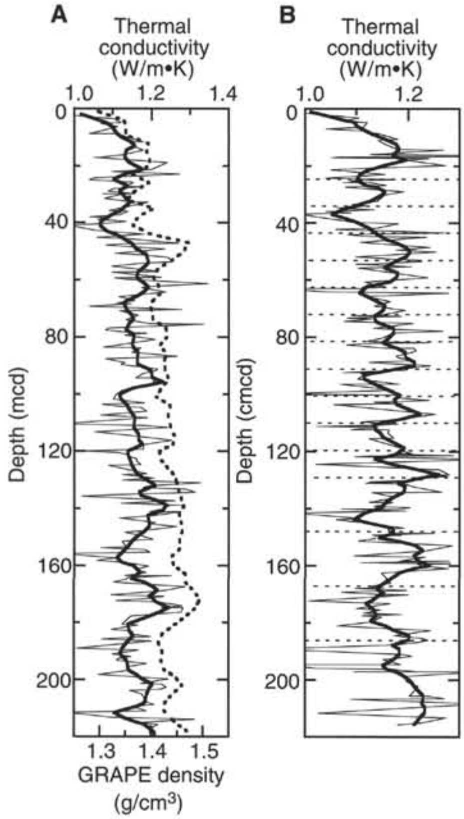

Figure 32. Thermal conductivity results combined from Holes 981A and 981C: (**A**) plotted with GRAPE bulk density data (dashed line) at meters composite depth (mcd) scale to illustrate the controlling density component, and (**B**) plotted at corrected meters composite depth (cmcd) to illustrate relationship to drilling depth and temperature measurement stations (dashed horizontal lines). GRAPE density (dashed line) and thermal conductivity (thick line) are locally weighted least-squares fit to original data (thin lines for thermal conductivity) to emphasize general trends.

and G2 coincide with seismic Units FE-I and FE-IIa (see "Seismic Stratigraphy" section, this chapter). Geotechnical Unit G3 is defined at Site 981 where the magnetic susceptibility and natural gamma radiation values drop significantly downhole and the other physical properties curves flatten out. This transition marks the change to nannofossil ooze (see "Lithostratigraphy" section, this chapter). Geotechnical Unit G4 begins at about 280 mbsf, reflecting a drop in velocity, increased scatter in peak strength values, and a slight change in character of density and natural gamma-ray curves. This level coincides with seismic Reflector R3.

SEISMIC STRATIGRAPHY

The first site survey during Leg 162 covered both Sites 980 and 981 (Fig. 35). Because an exact positioning of the sites was critical to meet the scientific objectives, and the originally submitted site survey data did not include crossing lines over the sites, a relatively detailed grid of seismic lines was run in the area of the two proposed sites. The survey lasted for approximately 5.5 hr, and seismic data were acquired along seven lines (S1–S7 (Fig. 35), using the 80-in.^{3} water gun as a source (see "Underway Geophysics" section, "Explanatory Notes" chapter, this volume). In addition, the 3.5-kHz and 12-Hz PDR systems were run throughout the entire survey. Total survey length was approximately 30 nmi. Line intersections were placed at the proposed sites FENI-1 and FENI-2, and the first line was run as close as possible to Line 87-5 of the pre-cruise survey. The survey resulted in a relocation of both sites. Site 980 was moved approximately 1 nmi southward from FENI-1, along Line S7 to SP2981, while Site 981 was moved 0.8 nmi northeastward from FENI-2 to SP2265, along Line S5 (Fig. 35). Figure 36 shows a composite plot of the parts of the two seismic lines which tie the sites together.

Description of Seismic Stratigraphic Units

Four seismic units, Unit FE-I to FE-IV, have been defined between acoustic basement and the seafloor in the surveyed area, based on difference in internal acoustic character as well as relationships between the bounding Reflectors R1 to R4 (Figs. 36, 37). Drilling at Sites 980 and 981 recovered sediments from the upper three units. Interval velocities used to calculate reflector depths (Fig. 37) are average velocities over adequate intervals from the shipboard *P*-wave velocity measurements (see "Physical Properties" section, this chapter).

The two lower units (FE-III and FE-IV) are characterized by high-amplitude, discontinuous internal reflections, resulting in a disturbed seismic character. Internal structures are often seen as bands of reflections and diffraction hyperbolae are frequent. Reflector R4, separating these two lower units, also appears as a band of reflections.

In the upper part of the drilled section, Unit FE-I shows a series of high-amplitude internal reflectors while Unit FE-II generally displays lower amplitude internal reflectors (Fig. 36). Unit FE-II internal reflectors onlap on Reflector R3, which locally shows truncation of underlying layers. Internal reflectors in both upper units are generally well defined and continuous over the length of the survey lines. The prominent Reflector R2 in the lower part of Unit FE-II, however, divides Unit FE-II into two subunits (FE-IIA and FE-IIB). Subunit FE-IIB differs from the upper Subunit FE-IIA in that it has only very weak, internal reflections, whereas Subunit FE-IIA displays continuous, high-amplitude internal reflectors. Due to the thinning of Unit FE-II northwestward, Subunit FE-IIB is best defined in the southeastern part of the survey area, and was penetrated by drilling at Site 981.

Two of the high-amplitude reflectors within Unit FE-I have been identified in the 3.5-kHz PDR records. The upper reflector, which can be followed continuously in the PDR records, is partly hidden in the seafloor reflection of the lower-resolution seismic records.

Units FE-I and FE-II thicken toward the northwest and east-southeast, respectively (Figs. 38, 39). The thickness variation between the two units is also obvious in the composite plot of the two seismic lines connecting the drill sites (Fig. 36). Unit FE-II thickens gradually east-southeastward, and apparently has its maximum thickness near Site 981. Unit FE-I, on the other hand, has a northeast-southwest-trending depocenter to the north of Site 980. Both units thin a short distance to the northwest of the surveyed area, where the seafloor slopes steeply up to the Rockall Bank (van Weering and de Rijk, 1991).

Relation to Core Data

Drilling at Sites 980 and 981 recovered Pleistocene and Pliocene-Pleistocene sedimentary sections, respectively (see "Lithostratigraphy" and "Biostratigraphy" sections, this chapter). The upper Pleistocene, approximately the last 0.9 m.y., is recorded down to approximately 80 and 50 mbsf at Sites 980 and 981, respectively. This corresponds to seismic Unit FE-I (Fig. 37). This core interval is characterized by pronounced variations in lithology, as well as associated variations in spectral reflectance (see "Lithostratigraphy" section, this chapter) and physical properties (see "Physical Properties" section, this chapter), which cause the distinct acoustic stratification in Unit FE-I. The sediments from the interval below approximately 80 mbsf at Site 980, and between approximately 50 and 163 mbsf at Site 981 (seismic Subunit FE-IIA, lower part of lithostratigraphic Unit I), show less distinct variations, as well as a change in the cyclicity of most measured parameters (see "Physical Properties" section,

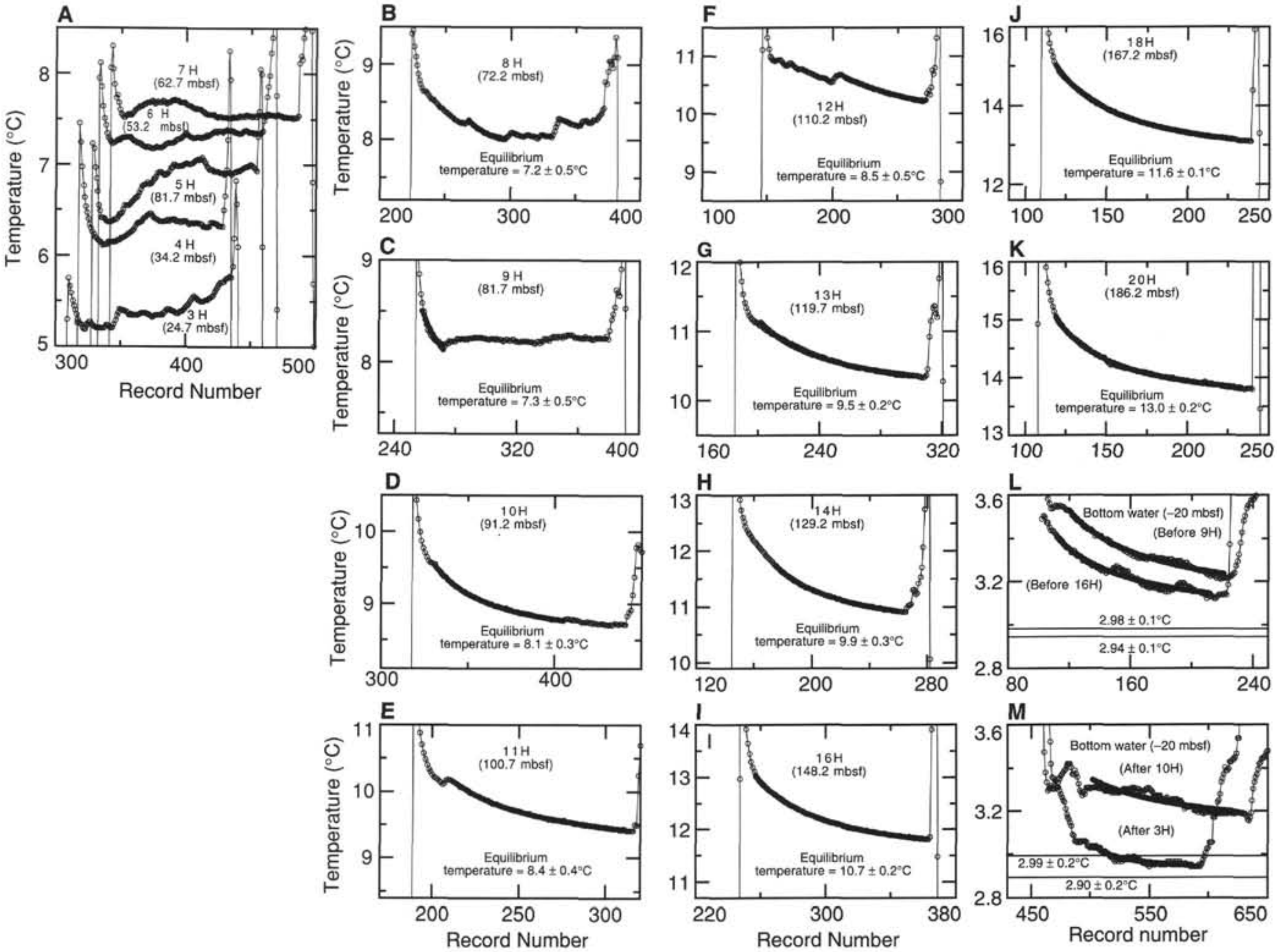

Figure 33. Hole 981C downhole temperature measurements: Open circles are original temperature measurements. Solid circles are calculated temperatures based on least-squares fits for the time interval (record number) chosen by the data analyzed. Horizontal lines are calculated equilibrium temperatures based on least-squares fits. **A.** Unsuccessful measurements due to soft sediment. **B–K.** Downhole sediment temperature records and calculated equilibrium temperatures. **L.** Two bottom-water measurement records taken before Cores 162-981C-9H and 16H were shot. **M.** Two bottom-water measurement records taken after Cores 162-981C-3H and 10H were shot.

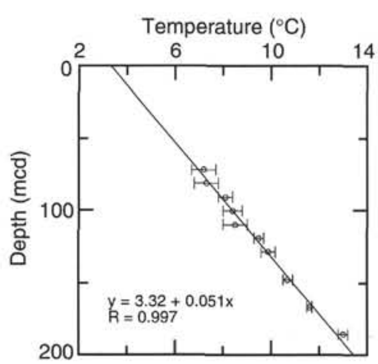

Figure 34. Downhole temperature gradient in Hole 981C.

Table 26. Calculated equilibration temperatures for bottom-water measurements from Hole 981C.

Core	Before coring (°C)	After coring (°C)
162-981C-		
3H	3.23	2.90
4H	3.16	3.08
9H	2.98	3.02
10H	3.01	2.99
16H	2.94	3.16

this chapter). This is also reflected in the apparently small, but more frequent, lithological variations between clay-bearing intervals and almost pure nannofossil ooze (see "Lithostratigraphy" section, this chapter). As a result, Subunit FE-IIA is characterized by lower amplitude acoustic stratification. Based on paleomagnetic and biostratigraphic age control (see "Paleomagnetism" and "Biostratigraphy" sections, this chapter), the base of Subunit FE-IIA at Site 981 has an age of approximately 2.7 Ma.

Below 160 mbsf at Site 981, the sediments are classified as nannofossil oozes, with carbonate content between 67% and 89% (lithostratigraphic Unit II, see "Lithostratigraphy" and "Inorganic Geochemistry" sections, this chapter). Physical properties in this subunit show low-amplitude, steady downhole trends of increasing compaction (geotechnical Unit G3; see "Physical Properties" section, this chapter). In the seismic records this interval corresponds to the more transparent, featureless Subunit FE-IIB.

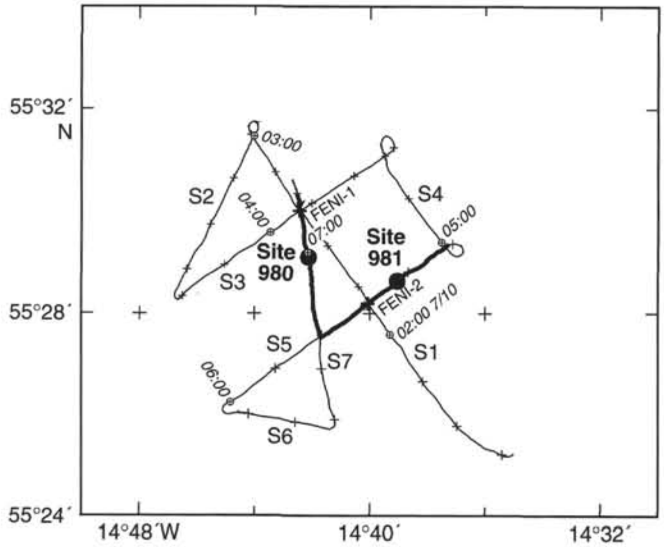

Figure 35. Map showing Leg 162 site survey track lines. Heavy parts of Lines S5 and S7 mark the seismic section shown in Figure 36. The originally proposed sites FENI-1 and FENI-2 are marked.

At Site 981, Reflector R3 was penetrated at approximately 271 mbsf, and sediments were recovered from seismic Unit FE-III, characterized by high-amplitude reflections which are less continuous than those observed in the above units. Reflector R3 forms an unconformity which locally truncates underlying strata, and apparently forms the base of the Feni Drift sediments proper. Lithostratigraphically, this interval cannot visually be distinguished from the nannofossil oozes above. However, slump structures can be observed at about 250 and 275 mbsf (see "Lithostratigraphy" section, this chapter). Relatively distinct changes in physical properties trends, as well as smaller changes in color reflectance and in natural gamma radiation, indicate that a facies change occurs at about 270–275 mbsf. Both bulk density and *P*-wave velocity drops, while undrained shear strength shows large variations below 275 mbsf. At this stage, any detailed interpretation of these changes would remain speculative, but they do suggest a subtle lithological change. Based on the general lithology of the cored sediments, this would imply changes in the relative abundance of carbonate and clay minerals. This, combined with an apparent unconformity in the seismic records, could explain the existence of Reflector R3, the seismic character of Unit FE-III, and the change in spectral reflectance and physical properties. The slump structures recorded in the lower parts of Holes 981A and 981C (see "Lithostratigraphy" section, this chapter) could also be related to the unconformity, and would be a reason for the high variation in undrained shear strength values (see "Physical Properties" section, this chapter). The relatively low resolution of the seismic data collected during Leg 162, in addition to uncertainties in determining interval velocities from physical properties data (see "Explanatory Notes" chapter, this volume), prevents accurate determination of the reflector depth.

In summary, the seismic data acquired during the survey at Sites 980 and 981 show that, given a seismic acquisition system of adequate resolution, the distribution of sediments deposited during periods of varying climatic conditions can be mapped seismically. At Sites 980 and 981 and in the adjacent area of the Feni Drift, the mid-Pleistocene shift in climatic cyclicity can be mapped as a boundary between continuous high-amplitude reflectors above and lower amplitude reflectors below. The transi-

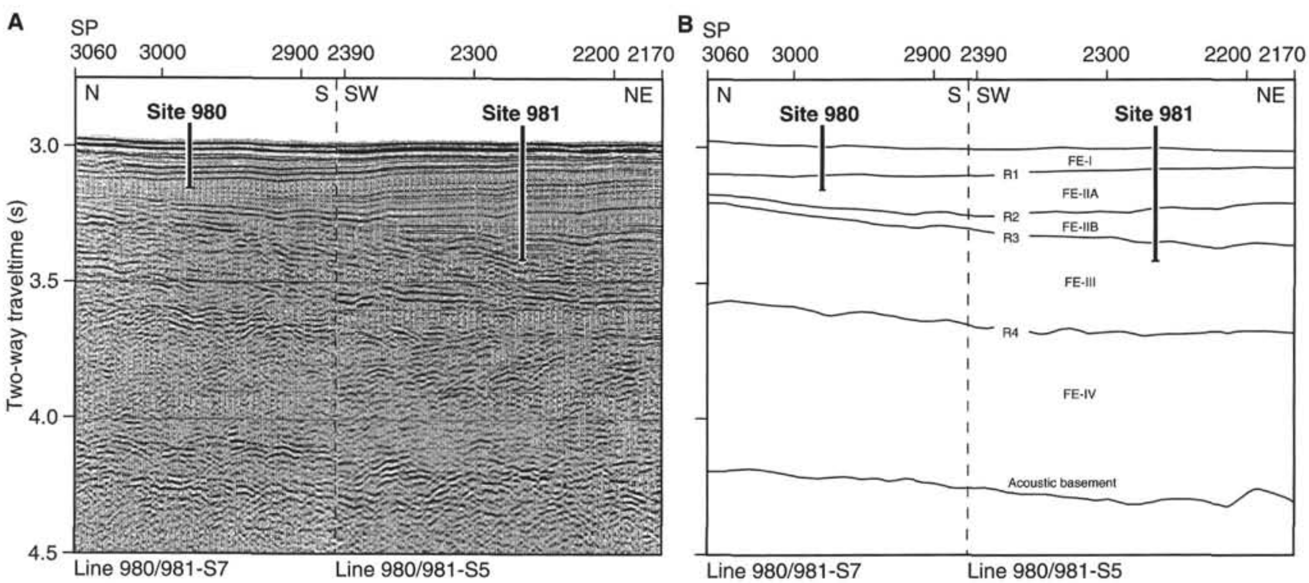

Figure 36. **A.** Composite plot of parts of seismic Lines S5 and S7, on which Sites 980 and 981 were identified. **B.** Interpretation of the seismic data shown in (A), with seismic reflectors and units shown. See Figure 35 for location.

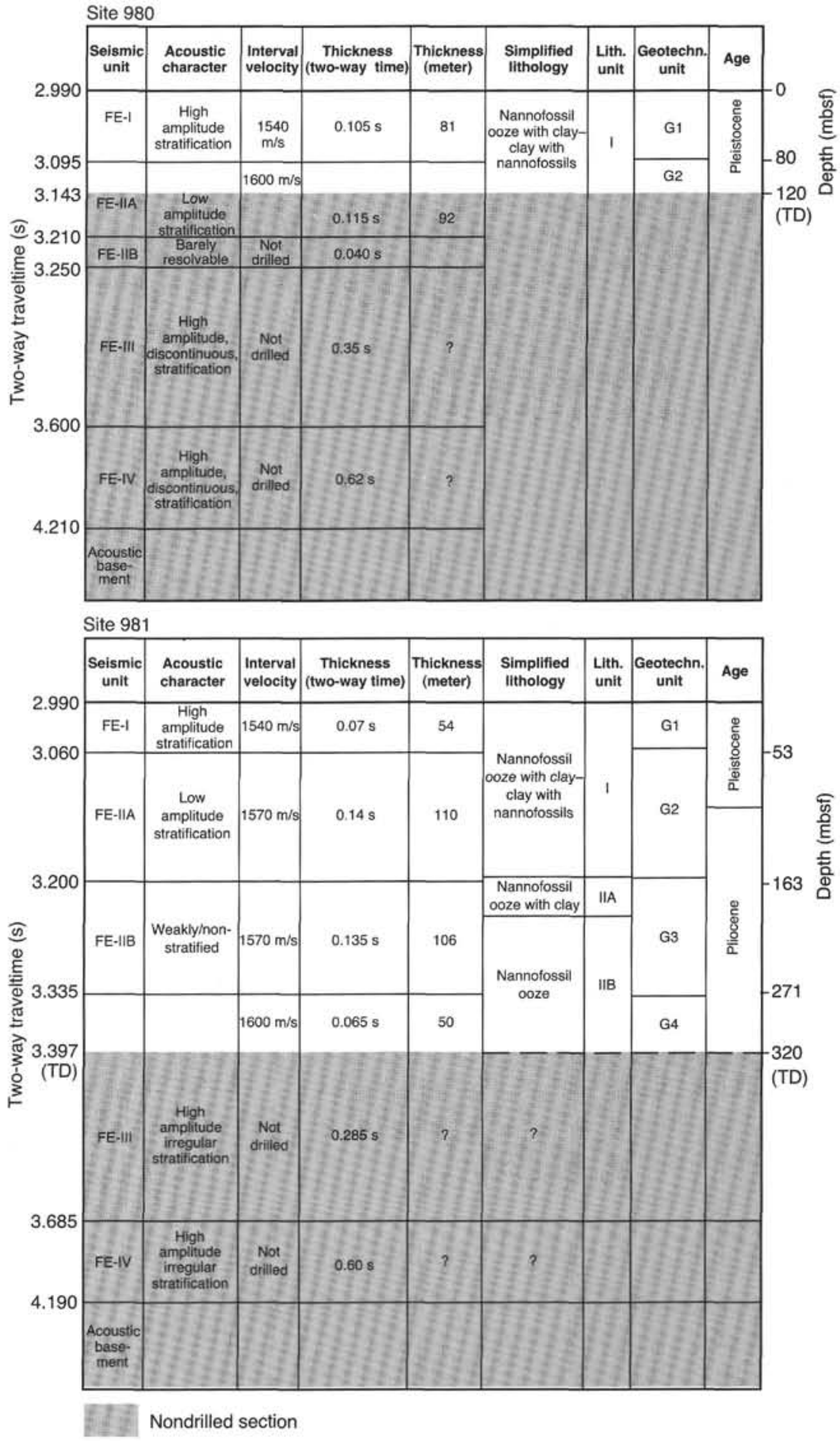

Figure 37. Diagram showing the seismic stratigraphy and its relation to lithostratigraphy and geotechnical units at Sites 980 and 981. Note that the time scale (seconds) is linear within the drilled depths.

tion from preglacial carbonate-rich oozes to glacially influenced sediments with varying clay content is seen as a change in seismic character from essentially homogeneous, acoustically transparent to various degrees of acoustic stratification. In the surveyed Feni Drift area, the late Pleistocene deposits are thickest near the northwestern boundary of the drift, toward the Rockall Bank, while the Pliocene–early Pleistocene deposits thicken east-southeastward. Reflector R3 seems to mark the onset of the main Feni Drift accumulation, which then started in the early Pliocene in the region at Sites 980 and 981.

REFERENCES

Baker, P.A., Gieskes, J.M., and Elderfield, H., 1982. Diagenesis of carbonates in deep-sea sediments: evidence from Sr^{2+}/Ca^{2+} ratios and interstitial dissolved Sr^{2+} data. *J. Sediment. Petrol.,* 52:71–82.

Baldauf, J.G., 1984. Cenozoic diatom biostratigraphy and paleoceanography of the Rockall Plateau region, North Atlantic, Deep Sea Drilling Project Leg 81. *In* Roberts, D.G., Schnitker, D., et al., *Init. Repts. DSDP,* 81: Washington (U.S. Govt. Printing Office), 439–478.

Berggren, W.A., Hilgen, F.J., Langereis, C.G., Kent, D.V., Obradovich, J.D., Raffi, I., Raymo, M.E., and Shackleton, N.J., 1995. Late Neogene chronology: new perspectives in high-resolution stratigraphy. *Geol. Soc. Am. Bull.*, 107:1272–1287.

Bond, G., Broecker, W., Johnsen, S., McManus, J., Labeyrie, L., Jouzel, J., and Bonani, G., 1993. Correlations between climate records from the North Atlantic sediments and Greenland ice. *Nature*, 365:143–147.

Bond, G., Heinrich, H., Broecker, W., Labeyrie, L., McManus, J., Andrews, J., Huon, S., Janitschik, R., Clasen, S., Simet, C., Tedesco, K., Klas, M., Bonani, G., and Ivy, S., 1992. Evidence for massive discharge of icebergs into the North Atlantic ocean during the last glacial period. *Nature*, 360:245–249.

Bond, G.C., and Lotti, R., 1995. Iceberg discharges into the North Atlantic on millennial time scales during the last glaciation. *Science*, 276:1005–1010.

Bordovskiy, O.K., 1965. Accumulation and transformation of organic substances in marine sediment, 2. Sources of organic matter in marine basins. *Mar. Geol.*, 3:5–31.

Boyle, E.A., and Keigwin, L.D., 1987. North Atlantic thermohaline circulation during the past 20,000 years linked to high-latitude surface temperature. *Nature*, 330:35–40.

Broecker, W.S., 1994. Massive iceberg discharges as triggers for global climate change. *Nature*, 372:421–424.

Drever, J.I., 1971. Magnesium-iron replacement in clay minerals in anoxic marine sediments. *Science*, 172:1334–1336.

Emerson, S., and Hedges, J.I., 1988. Processes controlling the organic carbon content of open ocean sediments. *Paleoceanography*, 3:621–634.

Fronval, T., Jansen, E., Bloemendal, J., and Johnsen, S., 1995. Oceanic evidence for coherent fluctuations in Fennoscandian and Laurentide ice sheets on millennium timescales. *Nature*, 374:443–446.

Gieskes, J.M., 1983. The chemistry of interstitial waters of deep-sea sediments: interpretation of deep-sea drilling data. *In* Riley, J.P., and Chester, R. (Eds.), *Chemical Oceanography* (Vol. 8): London (Academic), 222–269.

————, 1974. Interstitial water studies, Leg 25. *In* Simpson, E.S.W., Schlich, R., et al., *Init. Repts. DSDP*, 25: Washington (U.S. Govt. Printing Office), 361–394.

Goll, R.M., and Bjørklund, K.R., 1989. A new radiolarian biostratigraphy for the Neogene of the Norwegian Sea: ODP Leg 104. *In* Eldholm, O., Thiede, J., Taylor, E., et al., *Proc. ODP, Sci. Results*, 104: College Station, TX (Ocean Drilling Program), 697–737.

Heinrich, H., 1988. Origin and consequences of cyclic ice rafting in the northeast Atlantic Ocean during the past 130,000 years. *Quat. Res.*, 29:142–152.

Imbrie, J., Boyle, E.A., Clemens, S.C., Duffy, A., Howard, W.R., Kukla, G., Kutzbach, J., Martinson, D.G., McIntyre, A., Mix, A.C., Molfino, B., Morley, J.J., Peterson, L.C., Pisias, N.G., Prell, W.L., Raymo, M.E., Shackleton, N.J., and Toggweiler, J.R., 1992. On the structure and origin of major glaciation cycles, 1. Linear responses to Milankovitch forcing. *Paleoceanography*, 7:701–738.

————, 1993. On the structure and origin of major glaciation cycles, 2. The 100,000-year cycle. *Paleoceanography*, 8:699–736.

Katz, B.J., 1983. Limitations of "Rock-Eval" pyrolysis for typing organic matter. *Org. Geochem.*, 4:195–199.

Locker, S., and Martini, E., 1989. Cenozoic silicoflagellates, ebridians, and actiniscidians from the Vøring Plateau (ODP Leg 104). *In* Eldholm, O., Thiede, J., Taylor, E., et al., *Proc. ODP, Sci. Results*, 104: College Station, TX (Ocean Drilling Program), 543–585.

MacAyeal, D., 1993. Binge/purge oscillations of the Laurentide ice sheet as a cause of the North Atlantic's Heinrich events. *Paleoceanography*, 8:775–795.

Manheim, F.T., Sayles, F.L., and Waterman, L.S., 1972. Interstitial water studies on small core samples. *In* Laughton, A.S., Berggren, W.A., et al., *Init. Repts. DSDP*, 12: Washington (U.S. Govt. Printing Office), 1193–1200.

Manighetti, B., and McCave, I., 1995. Late glacial and Holocene palaeocurrents around Rockall Bank, NE Atlantic Ocean. *Paleoceanography*, 10:611–625.

McCave, I.N., Manighetti, B., and Robinson, S., 1995. Sortable silt and fine sediment size/composition slicing: parameters for palaeocurrent speed and palaeoceanography. *Paleoceanography*, 10:593–609.

Nigrini, C., and Sanfilippo, A., 1992. Cenozoic radiolarian stratigraphy for low and middle latitudes. Catalogue compiled for ODP. [Unpublished]

Nigrini, C., and Lombari, G., 1984. *A Guide to Miocene Radiolaria*. Spec. Publ. Cushman Found. Foraminiferal Res., 22.

Okada, H., and Bukry, D., 1980. Supplementary modification and introduction of code numbers to the low-latitude coccolith biostratigraphic zonation (Bukry, 1973; 1975). *Mar. Micropaleontol.*, 5:321–325.

Oppo, D.W., and Lehman, S.J., 1993. Mid-depth circulation of the subpolar North Atlantic during the last glacial maximum. *Science*, 259:1148–1152.

————, 1995. Suborbital timescale variability of North Atlantic deep water during the past 200,000 years. *Paleoceanography*, 10:901–910.

Peters, K.E., 1986. Guidelines for evaluating petroleum source rock using programmed pyrolysis. *AAPG Bull.*, 70:318–329.

Rahmstorf, S., 1994. Rapid climate transitions in a coupled ocean-atmosphere model. *Nature*, 372:82–85.

Raymo, M.E., Ruddiman, W.F., Shackleton, N.J., and Oppo, D.W., 1990. Evolution of Atlantic-Pacific $\delta^{13}C$ gradients over the last 2.5 m.y. *Earth Planet. Sci. Lett.*, 97:353–368.

Robinson, S., and McCave, I., 1994. Orbital forcing of bottom-current enhanced sedimentation on Feni Drift, NE Atlantic, during the mid-Pleistocene. *Paleoceanography*, 9:943–971.

Ruddiman, W.F., Kidd, R.B., Thomas, E., et al., 1987. *Init. Repts. DSDP*, 94 (Pts. 1 and 2): Washington (U.S. Govt. Printing Office).

Sabine, P.A., 1972. Preliminary report on the basalt [Sites 116 and 117]. *In* Laughton, A.S., Berggren, W.A., et al., *Init. Repts. DSDP*, 12: Washington (U.S. Govt. Printing Office), 407–410.

Saltzman, B., and Verbitsky, M., 1994. Late Pleistocene climatic trajectory in the phase space of global ice, ocean state, and CO_2: observations and theory. *Paleoceanography*, 9:767–779.

Thomas, E., 1985. Late Eocene to Recent deep-sea benthic foraminifers from the central equatorial Pacific Ocean. *In* Mayer, L., Theyer, F., Thomas, E., et al., *Init. Repts. DSDP*, 85: Washington (U.S. Govt. Printing Office), 655–694.

————, 1987. Late Oligocene to Recent foraminifers from Deep Sea Drilling Project Sites 608 and 610, northeastern North Atlantic. *In* Ruddiman, W.F., Kidd, R.B., Thomas, E., et al., *Init. Repts. DSDP*, 94: Washington (U.S. Govt. Printing Office), 997–1031.

van Weering, T.C.E., and de Rijk, S., 1991. Sedimentation and climate-induced sediments on Feni Ridge, Northeast Atlantic Ocean. *Mar. Geol.*, 101:49–69.

Weaver, A.J., and Hughes, T.M.C., 1994. Rapid interglacial climate fluctuations driven by North Atlantic ocean circulation. *Nature*, 367:447–450.

Weaver, P.P.E., and Clement, B.M., 1986. Synchroneity of Pliocene planktonic foraminiferal datums in the North Atlantic. *Mar. Micropaleontol.*, 10:295–307.

Zimmerman, H.B., Shackleton, N.J., Backman, J., Kent, D.V., Baldauf, J.G., Kaltenback, A.J., and Morton, A.C., 1984. History of Plio-Pleistocene climate in the northeastern Atlantic, Deep Sea Drilling Project Hole 552A. *In* Roberts, D.G., Schnitker, D., et al., *Init. Repts. DSDP*, 81: Washington (U.S. Govt. Printing Office), 861–875.

Ms 162IR-103

Note: For all sites drilled, core description forms ("barrel sheets") and core photographs can be found in Section 3, beginning on page 391. Forms containing smear slide data can be found in Section 4, beginning on page 1147. Also on the CD-ROM are all tables from this chapter (including an extended coring summary table) and shipboard measurements (files containing GRAPE density, *P*-wave velocity, natural gamma radiation, magnetic susceptibility, index properties, and spectral reflectance data).

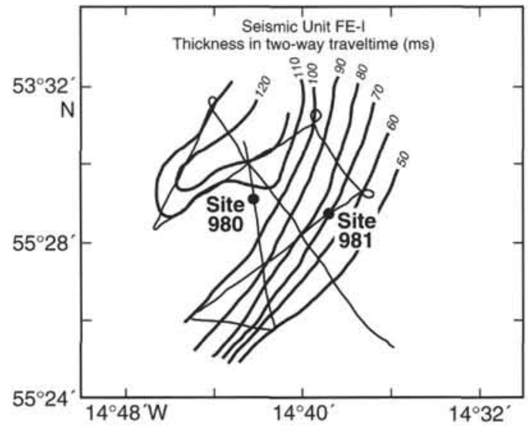

Figure 38. Isopach map of the upper seismic Unit FE-I.

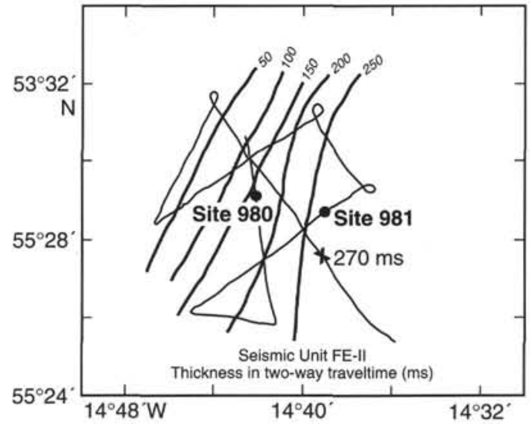

Figure 39. Isopach map of seismic Unit FE-II.